PhD Program in Biomolecular Sciences

Department of Cellular, Computational and Integrative Biology – CIBIO

35th Cycle

PLK1 promotes the mitotic surveillance pathway by controlling cytosolic 53BP1 availability.

Ph.D. Thesis of

Vincenza VIGORITO

Advisor

Luca FAVA

Tutor

Graziano LOLLI

Academic Year 2022/2023

DECLARATION

I, Vincenza Vigorito, confirm that this is my own work and that the use of all materials from other sources has been properly and fully acknowledged

.

ABSTRACT

Mitosis is a highly regulated process leading to the formation of two genetically identical cells. The main events defining mitotic duration are Cyclin B/CDK1 activation and the activation of the anaphase-promoting complex/cyclosome (APC/C), with the former essential for mitotic entry and the latter responsible for mitotic exit. There are a lot of control mechanisms ensuring mitotic fidelity, among them, the spindle assembly checkpoint (SAC) delays the anaphase onset until all chromosomes are bi-oriented on the mitotic spindle. However, this arrest cannot last indefinitely, and SAC activity might not suffice to preserve mitotic fidelity. Indeed, an additional fail-safe mechanism was revealed: the mitotic surveillance pathway (MSP). This mechanism monitors the duration of cell division, inducing p53-dependent cell cycle arrest when a critical time threshold is exceeded. 53BP1, a protein playing a central role in bridging DNA repair and the p53-mediated stress response, functions as a key component of the mitotic surveillance pathway. 53BP1 has been reported to be associated with mitotic kinetochores. Furthermore, the interaction between 53BP1 and kinetochores seems to rely on mitotic duration, regardless of the SAC activation status. Whether the temporary binding and release of 53BP1 at kinetochores play a role in MSP activation was not clear.

Herein, I present evidence demonstrating that Polo-like kinase 1 (PLK1) activity is vital for the time-dependent release of 53BP1 from kinetochores. Indeed, in prolonged mitosis, the inhibition of PLK1 results in forcing 53BP1 at the kinetochore. This leads to a reduction in the interaction with p53 in the cytosol, diminishing MSP efficiency. In addition, I show that the fibrous corona protein CENP-F directly interacts with 53BP1 and it is crucial for recruiting 53BP1 to kinetochores (KT). Using gene editing, I introduced a single amino acid substitution engineering the endogenous *CENPF* locus in human cells. Taking advantage of this mutant, I present evidence supporting the notion that the localization of 53BP1 at KTs is not essential for the functionality of the MSP as neither an unscheduled activation nor an inactivation of the pathway occur when 53BP1 recruitment at the KT is hindered.

However, in contrast with the findings in WT cells, our CENP-F mutant cells show that cytosolic 53BP1 can still bind to p53 and support MSP activation, even in the absence of PLK1 activity. Collectively, these results suggest that PLK1 supports the MSP by generating a cytosolic pool of 53BP1. Although this is a step forward in the understanding

of this pathway, the measurement of mitotic timing relies on an unknown cytosolic mechanism.

TABLE OF CONTENTS

INTRODUCTION

The cell cycle: an overview

The cell cycle is an evolutionarily conserved process in which a series of tightly regulated events occur, leading to the division of one cell into two daughter cells (Harper & Brooks, 2005). In eukaryotic cells, it is divided into two main phases: interphase and mitosis. This facilitates the separation between the duplication of cellular content and its segregation into two identical daughter cells.

The interphase is the longest part of the cell cycle, and it is made up of three steps: two gap phases, G_1 and G_2, during which the cell grows and synthetizes RNA, proteins and organelles, and the S phase in which the DNA is replicated. The Mitotic (M) phase involves distinct stages leading to the generation of two identical daughter cells. Not all cells are constantly dividing and some of them are defined as quiescent. These cells exit G_1 and enter G_0 being metabolically active without preparing to divide. This dormant state can be permanent for some cells, while others, in the presence of external factors such as mitogens, can re-enter the cell cycle **(Figure 1)**.

The cell cycle starts with the G_1 phase, which is marked by cell growth that is finely tuned by extracellular growth factors. During this phase, the cell readies itself for DNA duplication and when the growth conditions are optimal, the cells progress beyond the checkpoint. The S phase derives its name from DNA synthesis, as this stage is dedicated to the replication of genetic material but also centrioles. These duplications happen just once per cell cycle and are co-regulated (Nigg & Holland, 2018). The intra-S-checkpoint identifies errors in DNA replication and postpones mitosis until replication is successfully finished. During G_2, the cell undergoes rapid growth and prepares itself for the transition into mitosis.

The G_2/M transition represents a critical point of the cell cycle (Rieder, 2011) To complete this transition successfully, various kinases and phosphatases play essential roles: among these, the most well-studied and crucial is the cyclin B1/cyclin-dependent kinase (CDK1) complex. In the eukaryotic cell cycle, the accumulation of cyclin B to a certain threshold level represents a necessary yet not sufficient condition to trigger the G_2-M transition. In fact, despite of cyclin B1 levels, CDK1 remains inactive due to the actions of tyrosine kinase Wee1. As cells approach the M phase, it is believed that the coordinated interplay of Aurora A kinase and its cofactor Bora activates Polo-like kinase 1 (PLK1). This,

in turn, triggers the activation of the cell division cycle 25 (cdc25) phosphatase that unleashes CDK1 activity. This cascade of events establishes a feedback amplification loop, efficiently driving the cell into mitosis (Domingo-Sananes et al., 2011).

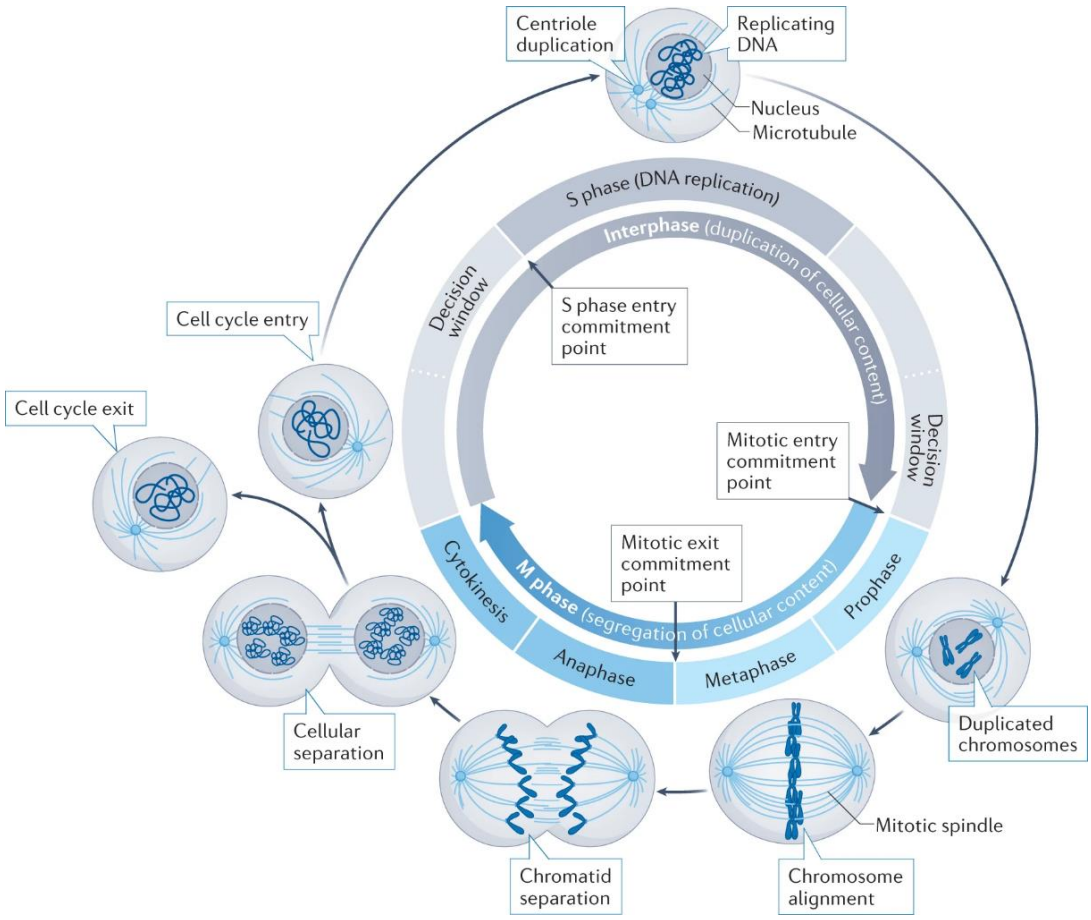

Figure 1. The eukaryotic cell cycle. The eukaryotic cell cycle is a coordinated process governing cell growth and division. It is divided into two main stages: the interphase and the mitosis. The interphase consists of G_1, where the cell grows and prepares for DNA replication; the S phase (S), where DNA synthesis occurs; and G_2, where the cell continues to grow in readiness for mitosis. The Mitotic (M) phase involves distinct stages leading to the generation of two identical daughter cells. Regulatory checkpoints ensure the accuracy of the cell cycle by monitoring DNA integrity and cellular conditions. These checkpoints allow for error correction or trigger programmed cell death if irreparable damage occurs. Image from (Matthews et al., 2022).

During the cell cycle, core regulatory proteins ensure that key events take place in the right order: the most important are cyclins. There is a specific cyclin associated with a determined phase of the cell cycle and the concentrations of different cyclins fluctuate

significantly throughout this process: typically, a cyclin is maintained at low levels for most of the cycle but experiences a substantial increase precisely at the stage when it is required. Cyclins trigger the events of the cell cycle by forming complexes with a group of enzymes known as cyclin-dependent kinases (CDKs). Without a cyclin partner, CDKs remain inactive, but, when associated with the right cyclin and in the presence of the appropriate set of post translational modifications, they turn into functional enzymes capable of modifying target proteins (Basu et al., 2022).

Mammalian cells were traditionally believed to rely on the sequential activation of at least four distinct cyclin-dependent kinases: CDK4, and CDK6, followed by CDK2 to facilitate the progression through interphase, as well as Cdk1 for the transition into mitosis. However, the ablation of individual CDKs in mice demonstrated that CDK1 is the only essential cell cycle CDK (Santamaría et al., 2007).

An additional layer of regulation for these cyclin-CDK complexes comes from their interaction with CDK inhibitors (CKIs) which can be described as brakes, halting the progression of the cell cycle when unfavourable conditions arise (Grana & Reddy, 1995). This ensures that cell cycle progression is both sequential and unidirectional. Due to these characteristics, once a cell is committed to start the cell cycle this cannot be reverted.

Mitosis

Mitosis is the process by which cells are able to replicate their chromosomes and segregate them into two identical daughter cells. It was described for the first time in 1882 by Walter Flemming who gave it the name mitosis from the Greek word μίτωσις highlighting the threadlike appearance of chromosomes in a dividing cell. Mitosis is divided into six stages namely prophase, prometaphase, metaphase, anaphase, telophase and cytokinesis (Mitchison & Salmon, 2001) **(Figure 2)**.

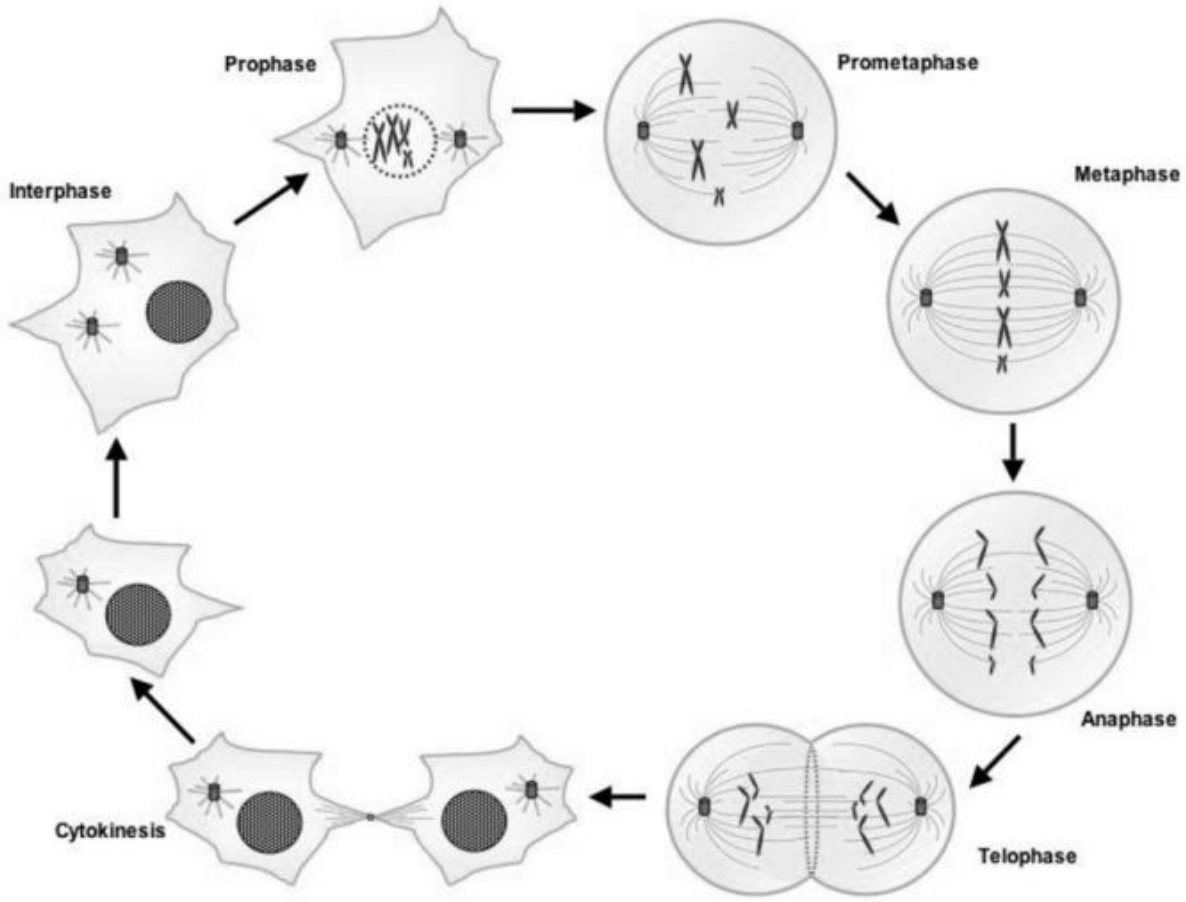

Figure 2. Stages of mitosis. Schematic of mitosis stages. Mitosis involves distinct phases: Prophase in which chromatin condenses into visible chromosomes, the nuclear envelope disassembles, and spindle fibers form; Prometaphase, a transition period during which the spindle continues growing; Metaphase in which chromosomes align along the cell's equatorial plane, guaranteeing precise positioning for chromatid separation; Anaphase during which sister chromatids, connected at the centromere, are pulled toward opposite poles by spindle fibers, ensuring equal distribution of genetic material; Telophase in which chromatids reach opposite poles, and the nuclear envelope reassembles. Then, cytokinesis is the last stage resulting into the division of two genetically identical daughter cells. Image from (Salaun P et al., 2008).

During prophase, nuclear and cytoplasmic changes take place. Chromosome condensation depends on the phosphorylation of histones and non-histone proteins and begins within isolated patches of chromatin located at the nuclear periphery. This leads to the formation of condensed regions which in turn fuse to adjacent areas, forming two threads termed sister chromatids. Moreover, in this phase, the mitotic spindle starts to form, and the nucleolus disappears. In the late prophase, another crucial event occurs: the nuclear envelope breakdown (NEBD) (Richard McIntosh, 2016). This is due to the disassembly of the nuclear

lamina after lamin hyperphosphorylation by kinases such as cyclin-dependent kinase 1 (CDK1), Aurora kinases, Polo-like kinase 1 (PLK1), Protein kinase C (PKC) and Never in mitosis gene a (NIMA)-related kinases.

The subsequent phase, namely prometaphase, is a transition period in which the mitotic spindle continues growing and the microtubules of the spindle can attach to the kinetochores (KTs) of sister chromatids positioned on the opposite sides of chromosomes. The microtubules that do not bind to kinetochores (named central spindle or non-kinetochores microtubules) have the function of stabilizing the spindle.

Metaphase is a critical stage characterized by the alignment of chromosomes along the equatorial plane of the cell. During metaphase, the spindle apparatus orchestrates the precise positioning of chromosomes, ensuring that each sister chromatid is attached to spindle fibers from opposite poles. Pinpointing the exact beginning of metaphase can be challenging because most chromosomes do not remain static at the equator; instead, they oscillate along the spindle axis. The transition from metaphase to anaphase is controlled by a multiprotein complex named spindle assembly checkpoint (SAC) which is able to delay anaphase onset until all kinetochores are attached to microtubules (Orr et al., 2021). Experiments performed on mammalian cells demonstrated that the time from the last chromosome attachment and anaphase onset is around 20 minutes (Rieder et al., 1995).

The separation of sister chromatids during anaphase represents one of the most striking events in the entire cell cycle. In this phase, sister chromatids migrate towards opposite spindle poles (Anaphase A) and the spindle poles themselves move apart (Anaphase B). Additionally, anaphase is the point at which the mitotic spindle becomes engaged in stimulating the cell cortex, laying the groundwork for the subsequent process of cytokinesis.

In telophase, the nuclear envelope reconstitutes itself around the separated sister chromatids, which are usually near the spindle poles. Cytokinesis is the process that divides a mitotic cell into two daughter cells. This phase relies on signalling to determine the cleavage plane, the assembly and contraction of the contractile apparatus, specific modifications of the cell membrane, and the separation, also known as abscission, of the two daughter cells. In animals, protozoa, and most fungi, the separation of daughter cells at the end of mitosis is guided by a contractile ring composed of actin filaments and myosin-II (Oliferenko et al., 2009).

Cell cycle checkpoints

The mammalian cell cycle is regulated by checkpoints able to decide whether a cell can move forward through this cycle or not. Indeed, specific criteria must be satisfied to guarantee cell division progression (the 'go' decision). Failure to meet these criteria results in temporary or permanent cell cycle arrest (the 'stop' decision) (Panagopoulos & Altmeyer, 2021). The first checkpoint is also known as the restriction (R) point: this layer of control monitors the presence of an appropriate amount of nutrients ensuring that cells are no longer dependent on growth factors for completing the cell cycle. Moreover, to maintain cell size, cells must double their contents before division: for this reason, control of cell size occurs in G_1 and G_2 (Barnum & O'Connell, 2014). Early signs of these checkpoints arose from observations indicating that the size of newly produced daughter cells following mitosis impacts the progression of the cell cycle. Specifically, larger daughter cells tend to accelerate the transition through G_1 and/or G_2 phases, while smaller daughter cells tend to postpone their exit from these growth phases (D. Killander & A. Zetterberg, 1965).

Another layer of regulation is represented by the G_2/M checkpoint also known as the DNA damage checkpoint (Uzbekov & Prigent, 2022). This mechanism ensures that cells entering mitosis have undamaged DNA and allows the cell to repair DNA before resuming the cell cycle.

Also, during mitosis cells are continuously subjected to controls: in this phase, the SAC monitors the kinetochores-microtubules attachment, while the cytokinesis checkpoint controls whether there are chromosome bridges at the cleavage plane to avoid chromosome breakage (Strohacker LK et al., 2021) **(Figure 3).**

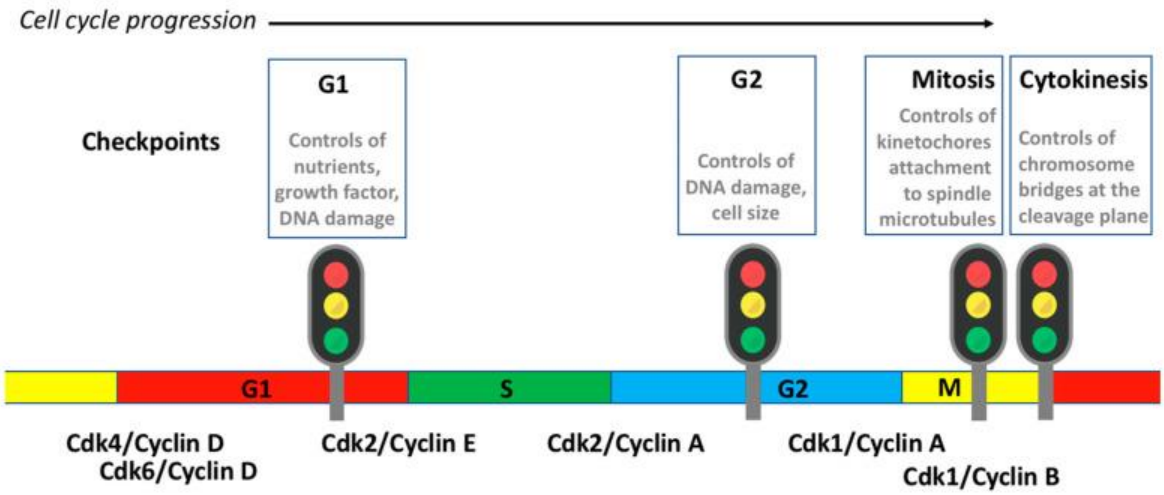

Figure 3. Cell cycle checkpoints. Cell cycle checkpoints act as molecular control points, monitoring critical events to ensure accurate cell division. The key control steps are**:** G1 Checkpoint (Restriction Point) with the task of evaluating cellular conditions for division and assessing DNA integrity; G2 Checkpoint which controls the completion of DNA replication and the proper cellular growth; Spindle Assembly checkpoint able to delay anaphase onset until all kinetochores are properly bi-oriented to spindle microtubules; Cytokinesis checkpoint in which cells control the presence of chromosome bridges at the cleavage plane. Image adapted from (Uzbekov & Prigent, 2022).

The consequences of checkpoint dysfunction vary depending on the severity of the cell cycle defect. They can range from cell death to the reprogramming of the cell cycle, which may ultimately contribute to the development of cancer. Genetic analysis of human cancers has uncovered that proteins associated with the G_1/S checkpoint are often inactivated. Moreover, changes in the DNA damage checkpoint are likely responsible for the resistance of tumor cells to chemotherapy or radiation. In contrast, alterations to the G_2/M checkpoint are less frequently observed in cancer (Molinari, 2000).

The kinetochore

The kinetochore is a proteinaceous multi-subunit assembly that forms at the centromeric region of each sister chromatid. It acts as a dynamic linker between the chromosome and the mitotic spindle apparatus, facilitating the distribution of the duplicated

genome from a mother cell to its daughters (Nagpal & Fukagawa, 2016). The kinetochore acts as a dynamic linker between the chromosome and the mitotic spindle apparatus (Pesenti et al., 2016) (**Figure 4**). In addition to mediating interactions with spindle microtubules, kinetochores also are involved in the spindle assembly checkpoint (SAC), also referred to as the metaphase checkpoint (Foley & Kapoor, 2013) (Lara-Gonzalez et al., 2021). This checkpoint acts as a feedback system, essential for synchronizing the onset of mitotic exit with the achievement of sister chromatid biorientation (Santaguida & Musacchio, 2009).

Electron microscopic analysis of vertebrate cells revealed the structure of the kinetochore (Brinkley & Stubblefield, 1966). The kinetochore is a button-like structure with three layers of proteins: the inner plate, an electron-dense layer that anchors the kinetochore to centromeric heterochromatin and recruits other kinetochore components; the interzone, an electron-lucent portion containing proteins that participate in tension sensing and signalling; the outer plate, an electron-dense layer connecting with numerous microtubules, housing microtubule-associated proteins, kinesins, and structural units that regulate spindle dynamics and checkpoint signalling. The outer plate is surrounded by a fibrous corona seen clearly when microtubules are absent (Fukagawa & De Wulf, 2009). The corona contains kinetochore components involved in recruiting spindle checkpoint proteins, establishing kinetochore-microtubule attachment and regulating microtubule dynamics for accurate chromosome segregation (Maiato & Silva, 2023).

The kinetochore of vertebrate cells consists of over 100 distinct proteins, with each protein present in multiple copies per kinetochore (Cheeseman et al., 2004). These proteins can be classified into three primary groups based on their relative spatial localization and functions: Inner Kinetochore Proteins, Outer Kinetochore Proteins and Regulatory Proteins responsible for monitoring and controlling the activities of the kinetochore to ensure accurate chromosome segregation (Cheeseman, 2014).

The kinetochore plays several essential roles during cell division: first of all, the inner kinetochore provides a robust connection to centromeric chromatin; then, the outer kinetochore facilitates the binding to microtubules (Navarro & Cheeseman, 2021). Moreover, the kinetochore is equipped with a guardian known as the spindle assembly checkpoint (SAC), a control mechanism that supervises the status of kinetochore-microtubule attachments to regulate the advancement of the cell cycle; finally, the kinetochore distinguishes between proper and improper attachments, inhibiting the

stabilization of the latter while permitting the selective reinforcement of the former (Cheeseman, 2014).

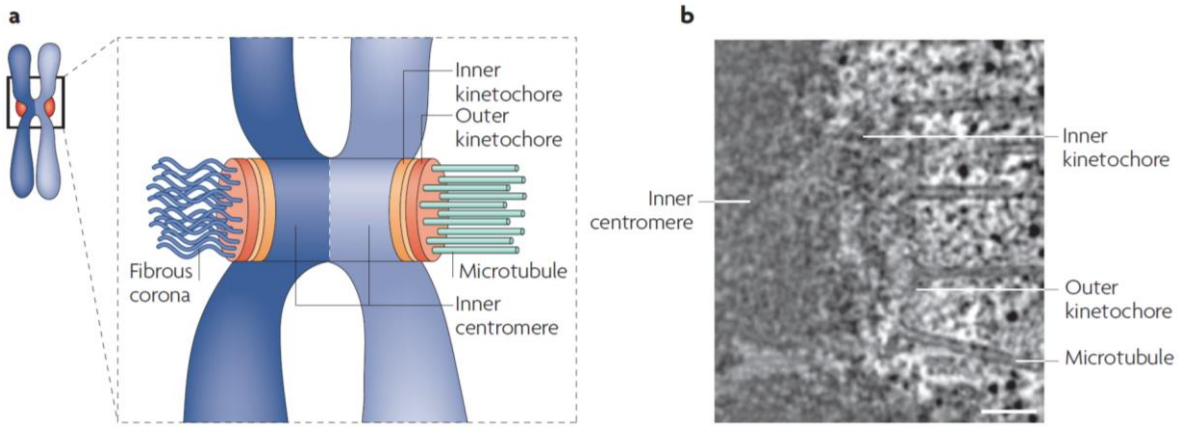

Figure 4. Kinetochore structure. (A) Representation of a mitotic chromosome with paired sister chromatids. The centromere, centrally positioned on the chromosome, serves as the attachment site for spindle fibers during cell division. The kinetochore, a complex protein structure at the centromere, is the point of attachment for microtubules from the mitotic spindle. It can be divided into different parts: the outer kinetochore, interacting with microtubules and facilitating chromosome movement; the inner kinetochore connecting with centromeric DNA to ensure proper chromosome segregation; and the fibrous corona, essential for the nucleation of kinetochore-derived microtubules. (B) Electron micrograph of a human kinetochore. Scale bar: 100 nm. Images from (Cheeseman I A & Desai A, 2008).

As specific DNA sequences are occasionally linked to the centromere, it was initially thought that the centromere positioning should be determined by a specific DNA sequence (Ariyoshi & Fukagawa, 2023). However, centromere analysis revealed that centromere positioning is epigenetically determined rather than depending on a primary DNA sequence. A central component in this process is the histone H3 variant, CENP-A. CENP-A forms specialized nucleosomes exclusively present at the centromeres. While there has been an ongoing debate regarding the precise composition of these centromeric nucleosomes, it is commonly accepted that CENP-A plays a crucial role in specifying centromere identity. CENP-A is involved in localizing all known kinetochore proteins in vertebrate cells, as well as in most other eukaryotes. Moreover, CENP-A forms a stable association with centromeres. Live-cell studies in different organisms have provided insights into the initial stages of kinetochore assembly: the deposition of CENP-A onto centromeric DNA is among

the earliest events in this process (Blower M D & Karpen G H, 2001) (Oegema K et al., 2001) (Régnier V et al., 2005). However, it's essential to note that the presence of CENP-A alone does not suffice to initiate kinetochore formation. After determining the site for kinetochore assembly on each chromosome, the subsequent crucial task is to create the assembly of this complex made up of multiple proteins capable of interacting with dynamic microtubule polymers.

Kinetochore assembly is a highly regulated and intricate process that occurs during cell division (Musacchio & Desai, 2017) (**Figure 5**). In detail, we can identify six different steps, each with its set of key proteins and specific timing:

- Step 1: Centromere Establishment and CENP-A Deposition (Early Interphase): the process begins with the establishment of centromeres, special regions on chromosomes. This happens during interphase, providing the basis for kinetochore assembly. An essential event at this stage is the deposition of CENP-A, a centromere-specific histone variant. CENP-A takes the place of conventional histone H3 within centromeric nucleosomes, ensuring centromere identity and function (McKinley & Cheeseman, 2016).
- Step 2: Inner Kinetochore Formation (Early to Mid-Interphase): CENP-C is a pivotal protein that binds to the centromere, bridging the connection between centromeric DNA and the kinetochore. Then, CENP-T and CENP-N coordinate the formation of the inner kinetochore, preparing it for the subsequent attachment of microtubules.
- Step 3: Development of the KNL-1/Mis12 complex/Ndc80 complex (KMN) Network (Mid-Interphase): KNL1, serving as a bridge between the inner and outer kinetochore layers, plays a pivotal role. MIS12 is essential for microtubule attachment. NDC80, another component of the KMN network, directly binds to spindle microtubules, making it a key player in ensuring the precise attachment of kinetochores to microtubules, facilitating chromosome segregation during cell division (DeLuca & Musacchio, 2012).
- Step 4: Maturation of the Kinetochore (Late Interphase): During this process, key protein complexes, notably the NDC80 complex, become fully functional.
- Step 5: Tension Sensing and Regulation (Metaphase): during metaphase, tension-sensing proteins such as Ska1 and Dam1 complexes monitor the tension and the attachment of microtubules to the kinetochore. When proper tension is achieved, this

acts as a signal for the cell to proceed to anaphase, triggering chromosome separation (Tanaka, 2010).

- Step 6: Spindle Checkpoint Activation (Metaphase): Regulatory proteins, including those associated with the SAC, monitor and control kinetochore activities. SAC activation ensures the proper kinetochore-microtubules attachment before allowing the cell to progress to anaphase, thus safeguarding against aneuploidy.

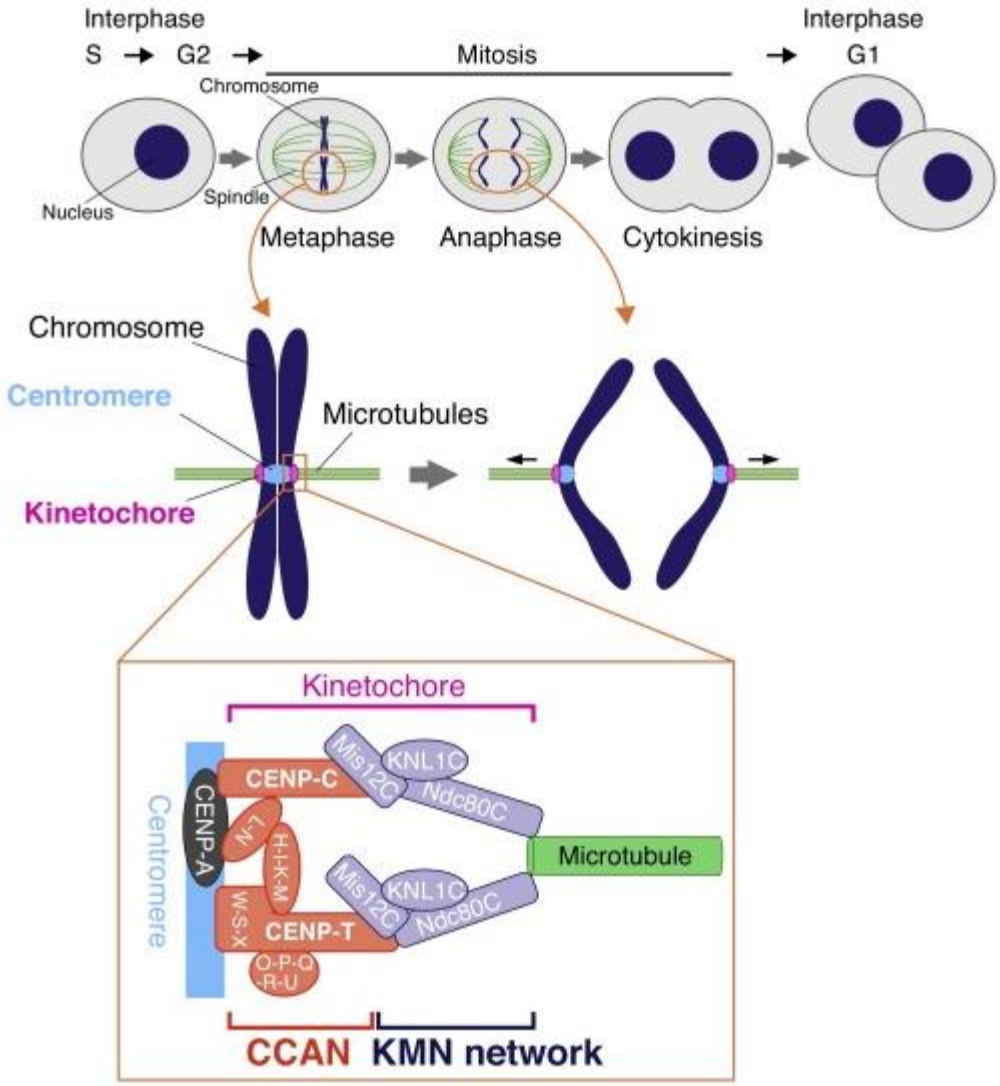

Figure 5. Kinetochore assembly is finely regulated during the cell cycle. The steps of kinetochore assembly are: 1. Centromere Establishment (Early Interphase): Formation of centromeres and deposition of CENP-A; 2. Inner Kinetochore Formation (Early to Mid-Interphase): CENP-C connects centromeric DNA to the kinetochore, with CENP-T and CENP-N preparing for microtubule attachment; 3. KMN Network Development (Mid-Interphase): KNL1 bridges inner and outer kinetochore layers; 4. Kinetochore Maturation (Late Interphase): Key complexes, especially NDC80, become fully functional. 5. Tension Sensing

(Metaphase): Proteins like Ska1 monitor microtubule attachment, signalling proper tension for anaphase and chromosome separation; 6. Spindle Checkpoint Activation (Metaphase): SAC ensures proper kinetochore-microtubule attachment, preventing aneuploidy. Image from (Hara & Fukagawa, 2018).

The kinetochore plays a pivotal role in facilitating chromosome segregation thus preserving cells from errors. Chromosome segregation errors can lead to cell death or result in aneuploidy, a condition prevalent in tumour cells (Levine & Holland, 2018). Since the kinetochore is indispensable for actively dividing cells, it offers an attractive target for anti-mitotic chemotherapy. Indeed, inhibitors of key proteins like Aurora kinases, PLK1 and CENP-E demonstrated promising antitumour effects in pre-clinical studies but failed in clinical trials and for this reason no small molecule has been approved for clinical use. Therefore, the use of preclinical models, such as patient-derived 3D tumours, could help in better investigating the effects of these drugs (Novais et al., 2021). However, additional research is needed to unravel the intricate molecular mechanisms governing kinetochore proteins' collaboration in facilitating chromosome segregation (Cheeseman I A & Desai A, 2008).

The Spindle Assembly Checkpoint (SAC)

The ultimate aim of mitosis is to ensure that each daughter cell inherits an identical copy of the genome: to do so, biorientation is essential. Biorientation means that each sister chromatid must be attached to microtubules from opposite ends of the spindle. Sister chromatids that attach to the spindle but fail to properly align or chromatids that don't attach to the spindle at all, are at risk of being mis-segregated. Mistakes in the segregation of chromosomes are associated with the development of human cancers and are more prevalent in cancer cells compared to non-cancerous cells (Foley & Kapoor, 2013).

Regulatory proteins located at the kinetochore play a crucial role in preventing erroneous segregation by acting in two ways: first, they selectively stabilize attachments on properly aligned kinetochore pairs, while configurations with incorrect attachments are destabilized and removed, providing a chance for re-alignment; second, unattached kinetochores serve as activating platforms for the spindle assembly checkpoint, a

surveillance mechanism able to delay the anaphase onset until proper spindle attachment is ensured (**Figure 6**).

The spindle assembly checkpoint was initially discovered through genetic screens in the budding yeast *Saccharomyces cerevisiae* (Hoyt et al., 1991) (R. Li & Murray, 1991). Initially, it was unclear what the SAC was monitoring, but experiments in higher eukaryotic cells, particularly through laser ablation, brought attention to kinetochores (X. Li & Nicklas, 1995). These experiments suggested that unattached kinetochores generated an inhibitory signal that delayed the onset of anaphase (Rieder et al., 1995). Subsequently, experiments performed using frog egg extracts and murine cells lead to the discovery of SAC components in vertebrates revealing that they all localized to kinetochores (Chen RH et al., 1996) (Taylor SS & McKeon F, 1997). Therefore, it is now widely accepted that the SAC "on" signal is exclusively generated by events at kinetochores.

Two critical events, both under the regulation of the SAC, have the potential to influence the mitotic timing. First is the period required to satisfy the SAC by establishing proper kinetochore-microtubule attachments and chromosome biorientation (Gorbsky et al., 1998; Hauf et al., 2003; Mogilner and Craig, 2010; Foley and Kapoor, 2013; Sacristan and Kops, 2015). This process characterizes the prometaphase stage of mitosis, during which SAC signalling remains active. Second is the duration needed for the SAC to be silenced once complete chromosome alignment at the metaphase plate has been achieved (Rieder et al., 1994, 1995; Howell et al., 2000; Shah et al., 2004; Pereira and Maiato, 2012). This period would define the length of the metaphase.

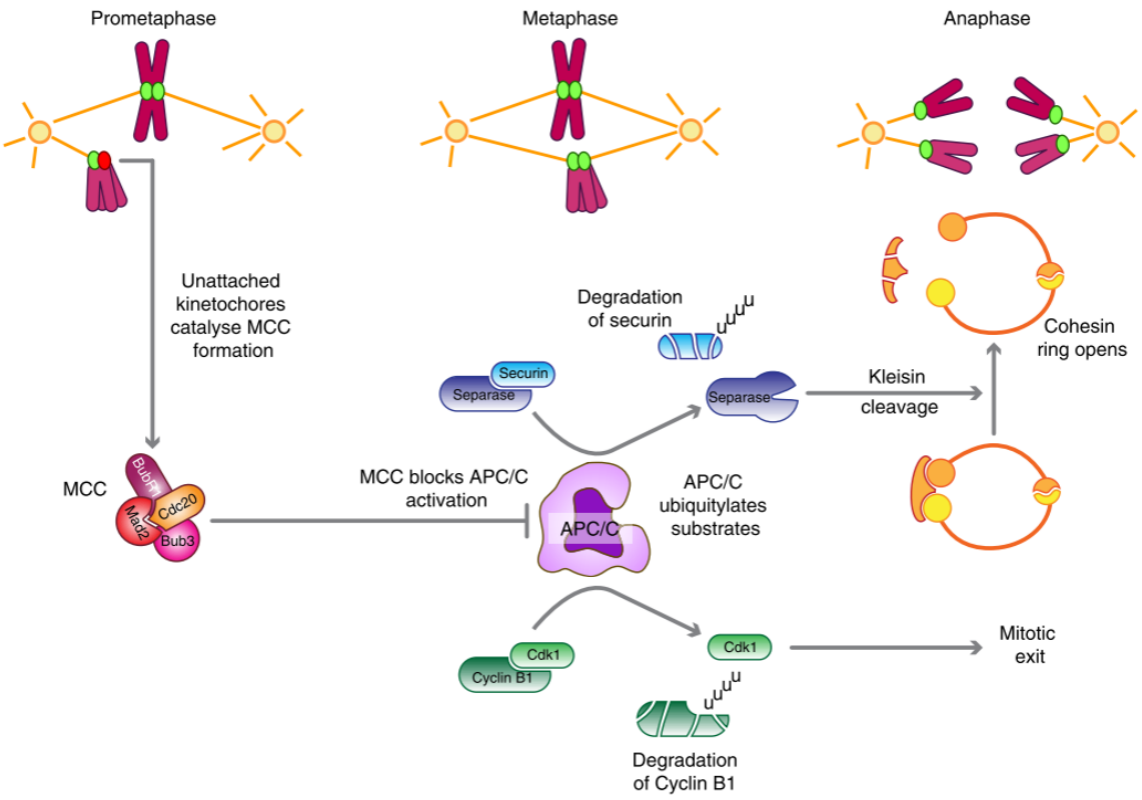

Figure 6. Spindle Assembly Checkpoint activation. Schematic of SAC activation. Unattached kinetochores trigger the formation of the mitotic checkpoint complex able to inhibit APC/C activation. This event pauses the anaphase onset until all kinetochores are attached to spindle microtubules. When the SAC is satisfied APC/C is no longer inhibited and can ubiquitylates securin and Cyclin B activating separase leading to mitotic exit. Image from (Lara-Gonzalez et al., 2012).

During metaphase, when biorientation of the chromosomes is achieved, the Anaphase-Promoting Complex/Cyclosome (APC/C) is phosphorylated by CDK1 and able to associate with its co-activators CDC20 and Cdh1. Then, active APC/C adds polyubiquitin chains to two critical substrates, securin and cyclin B. This tagging targets them for degradation by the 26S proteasome. The degradation of securin activates separase which leads to the separation of sister chromatids. Simultaneously, the destruction of B-type cyclins initiates a pathway for mitotic exit by suppressing the activity of CDK1.

Surprisingly, one unattached kinetochore is sufficient to trigger this “anaphase-wait” signal leading to the inhibition of CDC20 from activating APC/C (Rieder et al., 1995). The precise nature of this inhibitor is not known, but genetic, biochemical, and structural studies demonstrated that all SAC proteins localize at kinetochores and identified all the components

of this molecular complex: mitotic arrest deficient 1 (MAD1), mitotic arrest deficient 2 (MAD2), BUB1-related kinase (BUBR1), budding uninhibited by benzimidazoles 1 (BUB1) and budding uninhibited by benzimidazoles 3 (BUB3) but also the kinase monopolar spindle 1 (MPS1). The crucial role of kinetochores is to promote the creation of a complex between MAD2 and CDC20 (Lara-Gonzalez et al., 2021). Once formed, the MAD2-CDC20 complex quickly associates with BUBR1 and BUB3 in the cytosol, leading to the formation of the mitotic checkpoint complex (MCC), which inhibits APC/C activity. The formation of this complex depends on MAD2's ability to adopt two distinct conformational states: an open, unbound state (O-MAD2), and a closed ligand-bound state (C-MAD2) (Fava et al., 2011) (Mapelli et al., 2007). The difference between the two conformers relies on the orientation of a C-terminal beta-sheet, which, in the closed configuration, interferes with the interaction with MAD2 partners (Sironi et al., 2002). The best-characterized partners of MAD2 are MAD1 and CDC20. The MAD1-MAD2 complex is present throughout the cell cycle, whereas the assembly of MAD2 onto CDC20 is a process that is kinetically less favoured and needs the catalytic activity of unattached kinetochores. In detail, a stable complex formed by MAD1 and C-MAD2, anchored to kinetochores, recruits a conformer of O-MAD2 from the cytoplasm through an asymmetric dimerization process. Subsequently, this O-MAD2 is connected to CDC20 **(Figure 7)**.

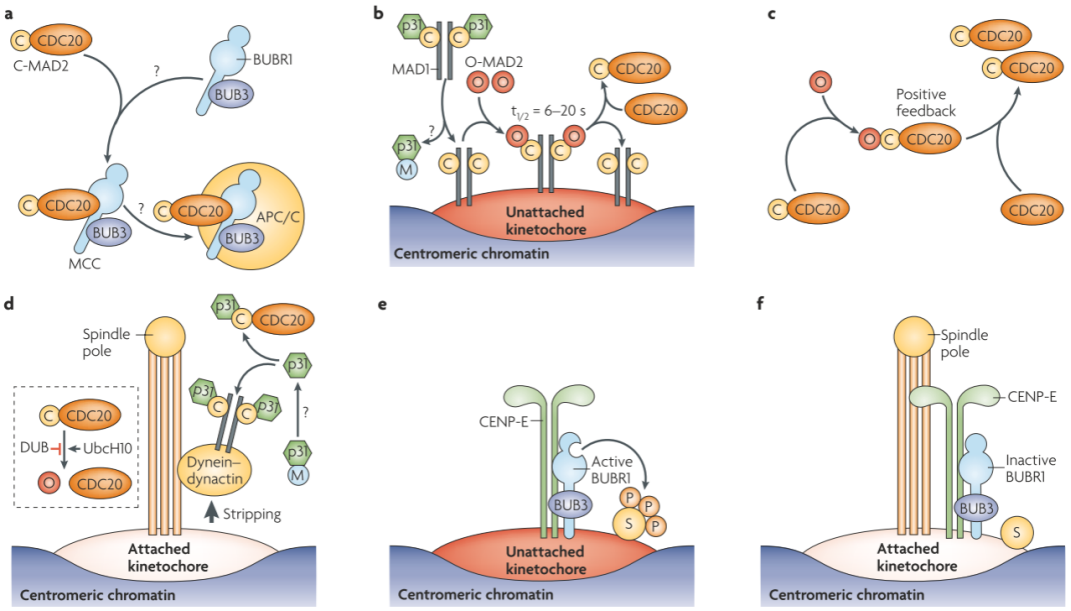

Figure 7. Molecular view of SAC activation. (A) The mitotic checkpoint complex (MCC) is composed of c-MAD2-CDC20 and BUBR- BUB3 subcomplexes. (B) The MAD2 template model contemplates that unattached kinetochores bind to MAD1-CMAD2-p31comet. P31 is released and MAD1-CMAD2 recruits O-MAD2 to kinetochores leading to the conversion into CMAD2 and the creation of a structural copy of MAD1-CMAD2. (C) CMAD2-CDC20 are involved in a cytosolic auto-amplification reaction. (D) The disappearance of unattached kinetochores reactivates p31comet, inhibiting C-MAD2–O-MAD2 interaction, and preventing SAC signal amplification. Non-degradative ubiquitylation of CDC20 accelerates C-MAD2–CDC20 dissociation, while the dynein–dynactin complex limits new C-MAD2–CDC20 complexes during kinetochore microtubule formation. (E) In prometaphase, CENP-E activates BUBR1 kinase activity at unattached kinetochores. (F) On microtubule attachment, BUBR1 activity is switched off. Image from (Musacchio & Salmon, 2007).

Furthermore, phospho-regulation is also involved in this mechanism with contributions from the MPS1 kinase: first of all, upon mitotic entry, MPS1 activity is needed for the recruitment of MAD1-C-MAD2 to the kinetochore; then, MPS1 activity is also an ongoing requirement throughout mitosis to facilitate its detachment from kinetochores (Musacchio & Desai, 2017) (Saurin, 2018). This detachment, in turn, enables the recruitment of O-MAD2 to the MAD1-C-MAD2 complex. An interesting observation is that after the attachment of the last unattached kinetochore, anaphase and mitotic exit happen only a few minutes later: this means that the inactivation of the SAC is fast, and the timing of mitotic exit seems to be largely dependent on the rate of CDC20 turnover. The precise mechanism of SAC silencing is not perfectly clarified, nevertheless, there is a sort of multi-step regulation. Three regulatory factors seem to promote the dissociation of C-MAD2–CDC20 at anaphase. First, as unattached kinetochores disappear, $p31^{comet}$ is able to prevent C-MAD2 from interacting with O-MAD2 and inhibiting SAC signal amplification. Second, non-degradative ubiquitylation of CDC20 speeds up C-MAD2–CDC20 separation. Third, when kinetochore microtubules form, the dynein-dynactin complex removes via stripping MAD1-C-MAD2 and other proteins from kinetochores, reducing the ability to form new complexes. (Musacchio & Salmon, 2007). Finally, although SAC activation and silencing have been studied hard over time there are still open questions to be investigated.

p53 activation after prolonged prometaphase

The mitotic checkpoint serves as a guardian of genomic stability, its primary role is to prevent the transition from metaphase to anaphase until all kinetochores have successfully attached to spindle microtubules. However, it's important to note that certain defects can elude detection by this control mechanism. In cases where microtubule-targeting agents are administered at low concentrations, the checkpoint may eventually be satisfied. Nevertheless, this could lead to the formation of shorter or multipolar spindle structures compromising the fidelity of mitosis (Rieder & Maiato, 2004). It was also commonly thought that once the checkpoint is fulfilled and cells proceed to divide, the resulting daughter cells will keep proliferating regardless of how long the prometaphase lasts (Uetake & Sluder, 2010).

Work by Uetake and Sluder, in 2010, clarified the relationship between prometaphase duration and the proliferative capacity of daughter cells becoming a milestone in the mitosis field. Indeed, they used four different triggers for prolonging prometaphase (nocodazole, monastrol, taxol, and MG132) obtaining the same results: a daughter cell of a mother that spent more than a certain time in prometaphase arrests in G_1 (Uetake & Sluder, 2010) (**Figure 8**). The threshold was measured as 1,5 h in human retinal pigment epithelial-1 (hTERT-RPE1) cells and 2 h in primary fibroblasts. This was accompanied by an increase in p53 and p21 levels but they also identified a contribution by p38 in this G_1 arrest.

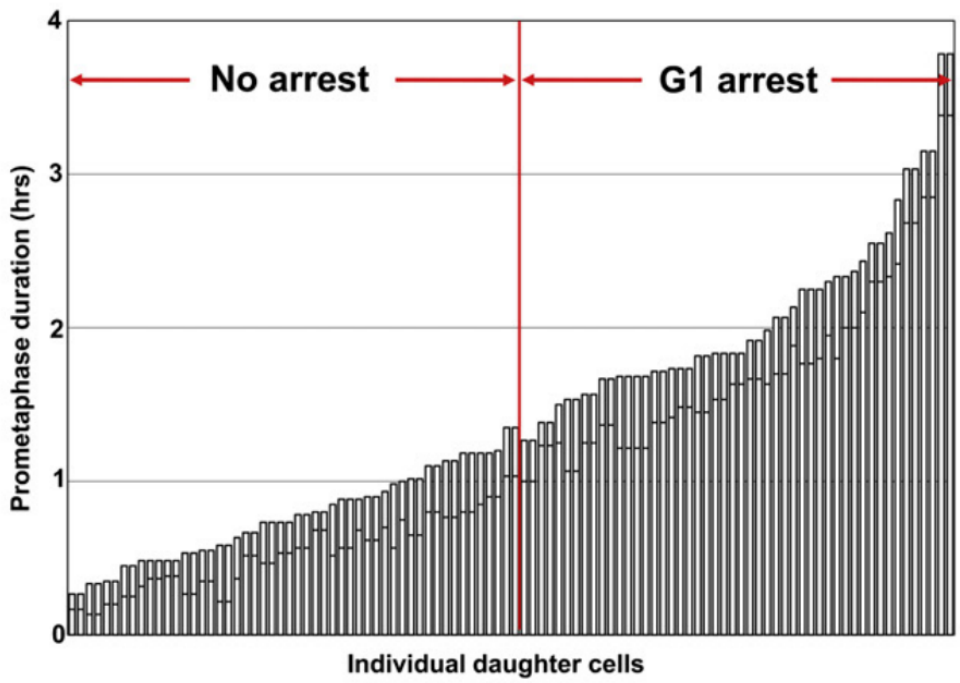

Figure 8. Link between prometaphase duration of the mother cell and the proliferative capacity of daughter cells. Each daughter cell is represented by a vertical bar while the bar's height corresponds to mother cell's prometaphase duration. The dark line across each bar indicates drug-induced prometaphase extension. Bars are ordered by prometaphase duration. Proliferating daughter cells appear left of the red line while those arrested in G_1 are on the right (Uetake & Sluder, 2010).

This was the first cue of a mechanism able to sense the prometaphase duration, although the precise trigger of this pathway was unknown. Surely, it was not dependent on DNA damage, p53 increased expression, or chromosome missegregation. Moreover, they also demonstrated that the arrest induced by MG132 was caused by a different mechanism. Although it was clearly accepted that cells were equipped with a p53-dependent sensor monitoring mitotic timing, the activating cue was still unknown. Some experimental works reported that p53 forms associations with centrosomes in mitotic cells and the presence of nocodazole disrupts this binding. Moreover, it was also shown that the induction of spindle damage, even if it's a temporary occurrence, abolishes the specific subcellular localization of p53 at distinct mitotic sites. This, in turn, influences cell cycle arrest in daughter cells (Ciciarello et al., 2001). Follow-up studies highlighted that this centrosomal localization depends on ATM-induced phosphorylation at serine 15 of p53 (p53Ser15P) on discrete foci

(Prodosmo et al., 2013). Later, it was also suggested that these foci are required for 53BP1 recruitment and for the activation of the mitotic surveillance pathway (Contadini et al., 2019). Nevertheless, the inability to reproduce the data on the centrosomal localization of p53, as indicated also by our unpublished research, suggests the potential for this localization to be an artifact caused by the antibodies used.

In a study involving *Sas4*$^{-/-}$ mouse embryos, a mutation leading to defective production of centrioles, and therefore centrosomes, it was suggested that the loss of centrosomes leads to a delay in mitosis and activates the sensor (Bazzi & Anderson, 2014). These embryos experienced an earlier developmental failure compared to mutants lacking cilia for example and this was coupled with widespread cell death and an increase in p53 expression. Surprisingly, genetical removal of p53 was able to rescue the phenotype. This was the first demonstration of this unidentified mechanism *in vivo*. Furthermore, it was also demonstrated that this pathway is preserved *in vivo* in mice, with 53BP1 and USP28 playing crucial roles in its activation upstream p53 (Xiao et al., 2021). Indeed, the model proposed showed that centrioles formed around E3 and progressively mature until approximately E7. At this point, they become capable of activate this p53-dependent response while in *Sas4* knockout embryos, this pathway may not activate until centrioles reach a more mature stage (Xiao et al., 2021).

Later, experimental work by Wong et al., further clarified this p53-dependent cell cycle arrest (Liang Wong et al., 2015). Indeed, by using centrinone, a reversible inhibitor of Polo-like-kinase 4 (PLK4), they found that centrosome loss irreversibly arrested normal cells in a senescence-like G1 state, confirming that depleting centrosomes as well as prolonging prometaphase lead to the activation of the same sensor. However, the molecular composition of this sensor and the precise mechanism of activation were again still not clear.

The Mitotic Surveillance Pathway (MSP)

All the studies previously described collectively seem to suggest the existence of a novel signalling pathway that activates p53 in response to signals associated with centrosome loss (Bazzi & Anderson,2014) (Liang Wong et al., 2015). While centrosomes are essential for the proliferation of non-transformed mammalian cells, a variety of tumour

cells can continue to divide even after losing their centrosomes (Liang Wong et al., 2015). However, cell division in the absence of centrosomes is error-prone (Lambrus et al., 2015) indicating that this centrosome surveillance pathway may serve to protect against genome instability. Nonetheless, the precise mechanisms and the molecular partners through which p53 is activated in response to centrosome loss in mammalian cells remain unclear.

In 2016 three different research groups performed a genome-wide, loss-of-function CRISPR/Cas9 screen to identify genes whose knockout can bypass cell cycle arrest after centrosome depletion (Lambrus et al., 2016) (Meitinger et al., 2016) (Fong et al., 2016). The best hits of the screen were p53 and p53 binding protein 1 (53BP1) along with Ubiquitin Specific Peptidase 28 (USP28). The proposed model for this centrosome loss sensor, the so-called Mitotic Surveillance Pathway (MSP) suggests that, upon centriole depletion, 53BP1 acts upstream of the pathway functioning as a scaffold for USP28 allowing p53 deubiquitination and stabilization **(Figure 9)**.

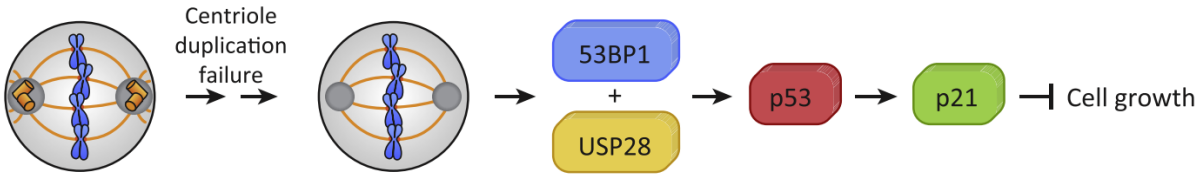

Figure 9. The Mitotic Surveillance Pathway (MSP). Schematic of MSP components. Upon centriole depletion, 53BP1 functions upstream in the pathway, acting as a scaffold for USP28. This facilitates the deubiquitination process, where USP28 contributes to the removal of ubiquitin molecules from p53. This deubiquitination event leads to the stabilization of p53 and the subsequent p21-dependent cell cycle arrest. Adapted from (Lambrus & Holland, 2017).

Moreover, as centrosome loss was demonstrated to cause an extension of mitotic timing, it was also evaluated whether the newly identified components of this surveillance pathway were essential for arresting cells after prolonged mitosis. By performing a mitotic timer assay, previously described by Uetake & Sluder, it was shown that the individual knockout of p53, 53BP1 and USP28 was able to destroy the ability of RPE1 cells to undergo cell cycle arrest after experiencing prolonged mitosis **(Figure 10)**. This suggests that both

centrosome loss and extended prometaphase induce stresses that converge on the same signalling components, leading to p53 stabilization and subsequent cell cycle arrest.

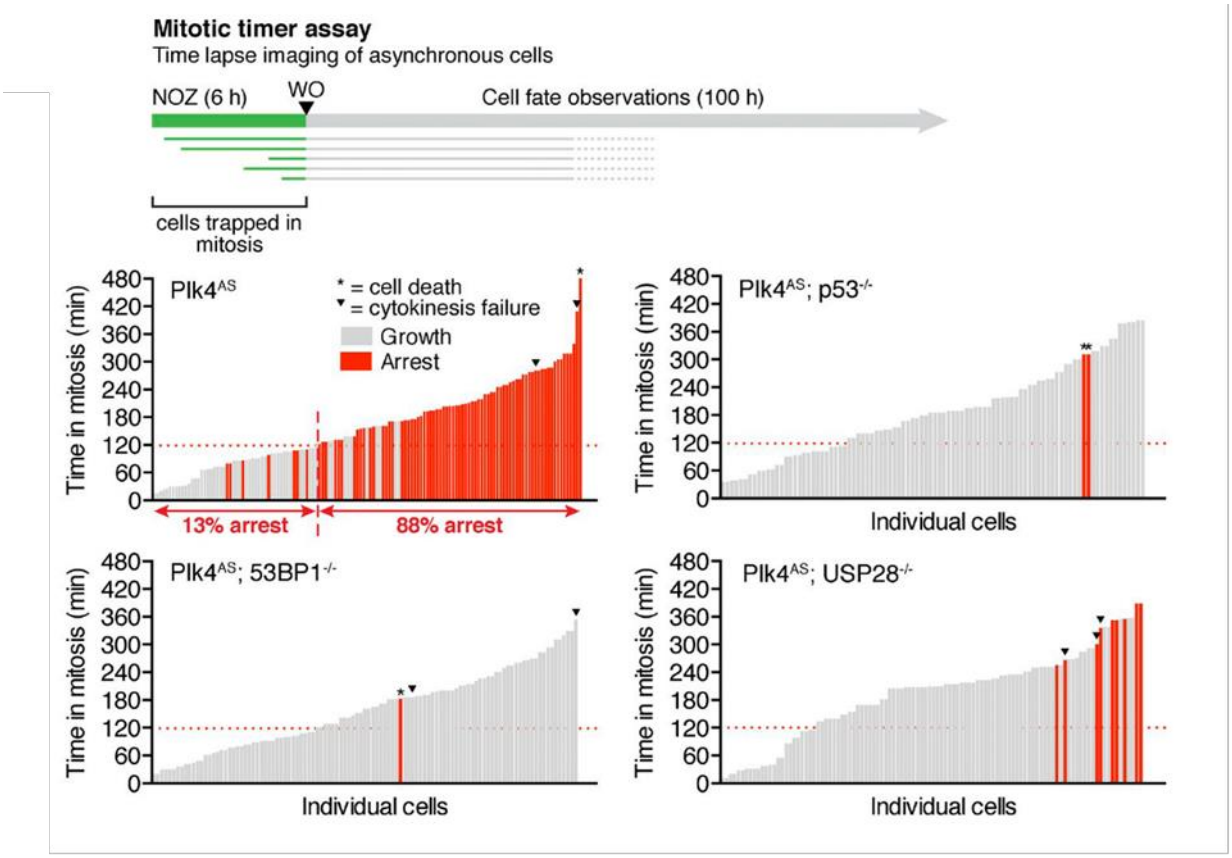

Figure 10. Knockout of individual MSP components impacts their ability to activate the pathway. The graph illustrates the prometaphase duration and proliferative capacity of cells undergoing prolonged mitosis. Each bar symbolizes a daughter cell, with its height indicating the mother cell's prometaphase duration and its colour denoting the fate of the daughter. The dashed red line represents the threshold prometaphase duration before over 85% of daughter cells undergo a cell cycle arrest. Image from (Lambrus et al., 2016).

Considering that p53 primarily responds to DNA damage, all studies assessed the interplay between centrosome loss and DNA damage, demonstrating that there is no increased DNA damage in cells experiencing centrosome loss and that the knockout of DNA damage components, such as Ataxia telangiectasia mutated (ATM), Checkpoint kinase 1 (CHK1), Checkpoint kinase 2 (CHK2), do not prevent cell cycle arrest. Regarding the relationship with the SAC instead, experiments, performed by the Tsou lab, demonstrated that the SAC and the 53BP1/USP28 axis are two mechanisms acting in parallel, with the

former monitoring the accuracy of chromosome segregation and the latter selecting against stressed/delayed mitosis (**Figure 11**) (Fong et al., 2016). Since the pathway was discovered, no mechanistic follow up studies clarifying the molecular nature of the timer were reported.

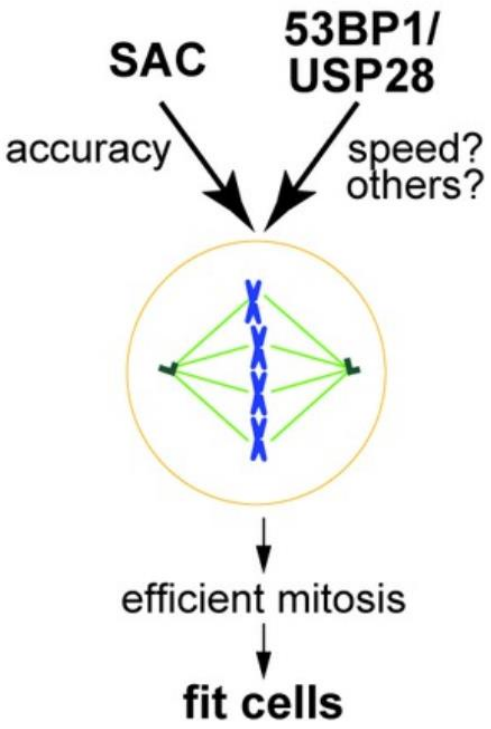

Figure 11. SAC activation and MSP are two independent mechanisms. Scheme from (Fong et al., 2016) describing how 53BP1/USP28 and SAC operate as parallel mitotic programs, wherein SAC prioritizes the fidelity of mitosis (even at the cost of speed), while 53BP1/USP28 acts as a selector against cells experiencing stress or prolonged mitosis.

Centrosome sensing vs measurement of mitotic timing

To date, while it remains possible that the mitotic surveillance pathway evolved to prevent divisions with an increased risk of mitotic errors, the specific sensor responsible for detecting centrosome loss remains elusive. Three hypothetical triggers for pathway activation have been proposed:

1. p53 is the Sensor: Research has shown that ATM plays a role in localizing p53 at centrosomes in mitotic RPE1 cells (Contadini et al., 2019). During mitosis, ATM phosphorylates p53, leading to its migration to the centrosome. At the centrosome, p53 undergoes dephosphorylation and disengages to facilitate mitotic progression. This ATM-p53-centrosome interaction may relate to the fact that in acentrosomal cells, p53 forms cytoplasmic foci, which can subsequently recruit 53BP1, resulting in p53 stabilization and cell cycle arrest (Oricchio et al., 2006) Indeed, p53 centrosomal localization depends on ATM-induced phosphorylation at serine 15 of p53 (Prodosmo et al., 2013). Moreover, later work showed that these foci can act as activating platform for 53BP1, suggesting that p53 contributes to preserve genome integrity by functioning as a sensor for the mitotic surveillance pathway (Contadini et al., 2019).
2. Microtubule-Kinetochore Interface Perturbations: 53BP1 has been observed to briefly localize at kinetochores during mitosis, even though the reason for this behaviour is unknown (Jullien D et al., 2001). This suggests that 53BP1, despite not being part of the conventional spindle assembly checkpoint, could have the capability to sense alterations at the microtubule-kinetochore interface and activate the MSP.
3. Time is of the essence (Phan & Holland, 2021): In this scenario, there is no centrosome counting mechanism involved. This theory appears to be the most plausible, as the mere extension of mitotic timing is sufficient to induce cell cycle arrest in daughter cells (Uetake & Sluder, 2010). This model may reconcile the findings associated with individual knockouts of 53BP1 and USP28, suggesting that they both play essential roles in orchestrating cell cycle arrest regardless of the trigger, whether it's prolonged prometaphase or centrosome depletion.

A recent pre-print from Oegema/Desai Lab showed that not only there is no counting mechanism but also that there is a sort of memory of mitotic duration transmitted to daughter cells, resulting in an increase of p21 levels (Meitinger et al.,2022). Moreover, p21 increase establishes a sharp threshold in mother cells without leading to arrest, by the way the sub-threshold extension is again transmitted to daughter cells creating a sort of cumulative mechanism.

To sum up, the Mitotic Surveillance (Stopwatch) Pathway acts as a fidelity mechanism identifying and transmitting to daughter cells also subtle extensions of mitotic timing. Indeed, a compromised stopwatch function likely plays a crucial role in enabling the

tolerance of problematic mitotic events, that can be both contributors to and consequences of the aneuploidy and genomic instability, all features of cancer.

The Mitotic Surveillance Pathway *in vivo*

Although *in vitro* experiments demonstrated the presence of the Mitotic Surveillance Pathway, it was completely unknown whether this mechanism functions *in vivo*. First of all, researchers discovered that mutations in centrosomal genes, such as Spindle assembly abnormal protein 4 (*Sas4*), in mouse radial glial progenitors (RGPs), led to a progressive loss of centrioles. This resulted in an increase in p53 levels and widespread apoptosis, impairing the composition of the superficial layer of neurons. Moreover, the removal of p53 fully rescued the defect, clarifying that the extensive cell death was p53- dependent (Bazzi & Anderson, 2014) (Insolera et al., 2014). However, how a centrosomal defect is able to activate p53 remained unclear.

Furthermore, cells *in vivo* experience mitotic delay surely after prolonged exposure to toxins. Moreover, in line with studies performed *in vitro*, the mutation of genes that encode proteins functioning at the centrosome or the spindle apparatus in the developing mouse brain resulted in prolonged mitosis in neural progenitor cells (NPCs) (Gruber R et al., 2011) (Insolera et al., 2014). Additionally, the extension of mitosis in NPCs, induced by pharmacological agents, led to increased cell death and/or premature differentiation of the progeny resulting from these divisions (Pilaz L J et al., 2016).

In mice, 53BP1 and USP28 are expressed during early embryogenesis (E5.5), with functional MSP signalling established around gastrulation (E7.5). The timing of MSP activation during development is believed to coincide with the centrosome's dominance as a microtubule-nucleating source, implying a close link between MSP signalling and centrosomal microtubule organizing center (MTOC) function (Xiao et al., 2021). Although 53BP1 has a vital role in DNA damage signalling, its knockout in mice leads to radiation sensitivity, immune deficiencies, and a cancer-prone phenotype. Conversely, USP28 knockout mice do not exhibit an apparent phenotype (Knobel et al., 2014) . Additionally, in the context of brain development, knocking out USP28 or 53BP1 does not result in an excess

of neurons, suggesting that the MSP does not universally suppress NPC proliferation (Phan et al., 2021).

Moreover, in patients with primary microcephaly, many mutations in centrosomal genes were found, demonstrating that cortical neurogenesis is sensitive to centrosome defects (Marthiens V & Basto R, 2020). Mice KO for centrosomal genes are well-established models for the study of microcephaly and helped revealing that centrosome defects impact neural cortex development by prolonging mitosis and pathologically activating the MSP. Indeed, it was also found that genetic ablation of the MSP was sufficient to revert the phenotype, restoring NPCs proliferation and rescuing microcephaly **(Figure 12)** (Phan et al., 2021).

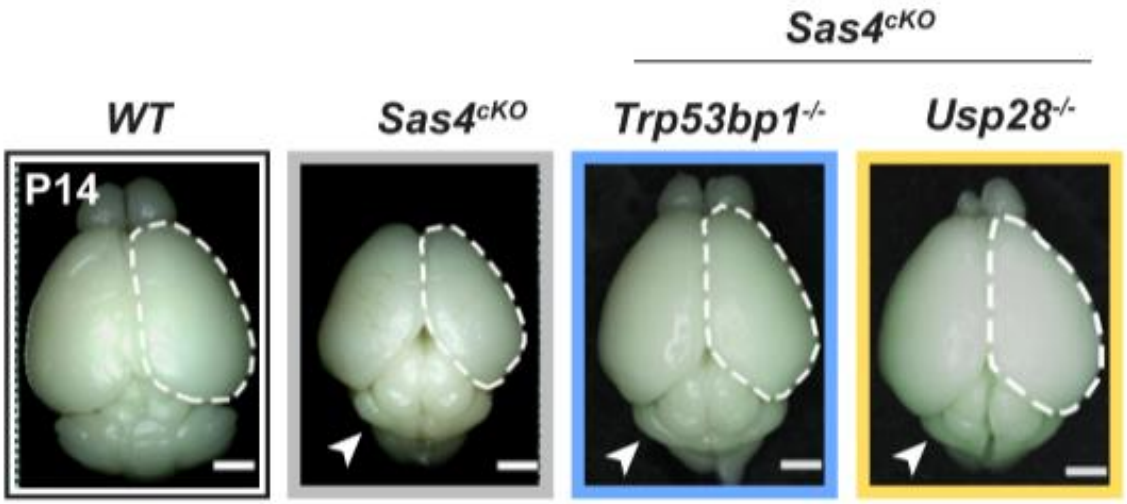

Figure 12. Centrosome defects impact brain size via the activation of the mitotic surveillance pathway. Sas4 deletion from neural progenitor cells (NPCs) resulted in a severe microcephaly phenotype characterized by a substantial 30% reduction in the telencephalic area and a 17% decrease in cortical thickness at P14. The additional knockout of MSP components largely restored the telencephalic area and cortical thickness, alleviating the microcephalic phenotype. Image adapted from (Phan et al., 2021).

Furthermore, it was also demonstrated that the main pathway responsible for the depletion of neural progenitor cells (NPCs) in *Sas4* KO animals is the MSP rather than DNA damage signalling. Although defects in various factors involved in DNA repair and DNA damage can result in microcephaly (**Figure 13**), in these cases, centrosome function and mitotic duration are unaffected and the activation of p53 relies on accumulated DNA lesions.

Regardless of the pathway that is activated, p53 leads to apoptosis, depleting the NPC pool and decreasing the number of mature neurons (Phan et al., 2021).

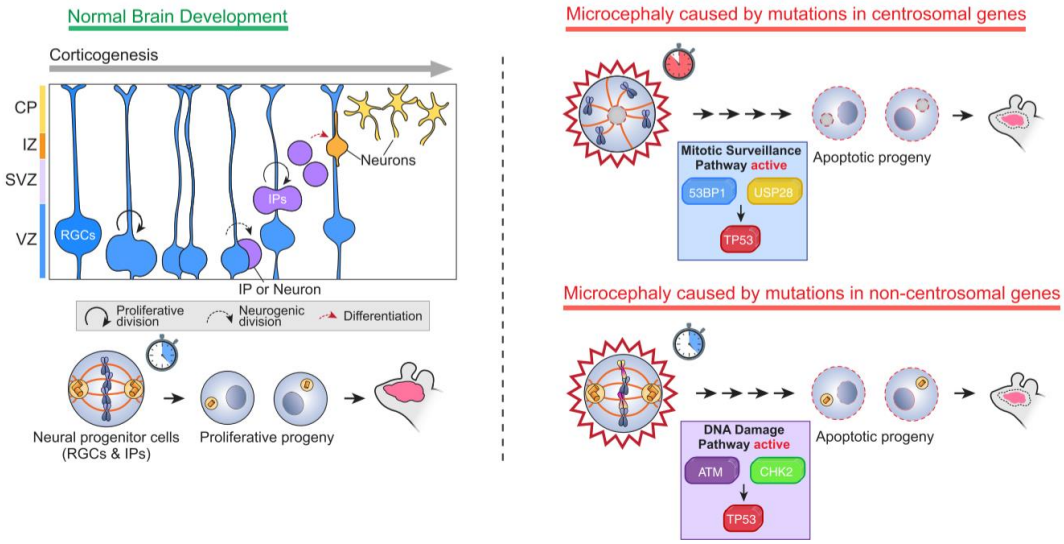

Figure 13. Model for microcephaly origin. In the first scenario (top right panel), NPCs carrying mutations in centrosome genes experience prolonged spindle assembly during mitosis, activating the mitotic surveillance pathway. This pathway, involving 53BP1 and USP28, subsequently activates TP53. Conversely, in microcephaly resulting from mutations in genes essential for DNA repair or genome stability (bottom right panel), centrosome function and mitotic duration remain unaffected. Instead, the accumulation of DNA lesions triggers DNA damage signalling in NPCs, activating TP53. In both models, heightened TP53 activity induces apoptosis, depleting the NPC pool and reducing the final number of neurons. Image from (Phan et al., 2021).

Although the MSP is an important pathway in the etiology of microcephaly, it is not the only one. The most challenging task could be to distinguish between microcephaly mutations that activate the MSP from those that trigger different pathogenic routes, shedding a light on brain development and microcephaly understanding.

AIMS OF THE THESIS

The Mitotic Surveillance Pathway is a mitotic failsafe mechanism triggered by prolonged prometaphase as well as centrosome depletion (Uetake & Sluder, 2010)(Bazzi & Anderson, 2014). The main actors of this pathway are: 53BP1, USP28 and p53. Once activated by an upstream trigger, 53BP1 acts as a scaffold to allow USP28-mediated deubiquitination of p53 thus stabilizing it. This leads to a p21-mediated cell cycle arrest (Shyang Fong et al., 2016) (Meitinger et al., 2016)(Lambrus et al., 2016). According to this, it has been speculated that this pathway could be rely on a centrosome counting mechanism able to impede the propagation of cells lacking centrosomes (Lambrus & Holland, 2017). However, the more plausible explanation is that centrosome defects generate a delay in mitosis, and this is the cue activating the pathway (Meitinger et al., 2022). Nevertheless, the precise mechanism activating the pathway remained elusive. Therefore, the open question on the MSP is: how a delay in mitosis can be translated in p53 activation?

Identification of 53BP1 kinetochore receptor

53BP1 has been reported to localize at kinetochores during mitosis (Jullien D et al., 2001). However, the reason for this behaviour remained unknown. The kinetochore is already important for SAC signalling and this dynamic association could lead to speculate that there is a regulatory reason for 53BP1 to be there during mitosis. Therefore, the study of 53BP1 mitotic partners enables to identify the kinetochore receptor of this protein allowing a precise dissection of this temporarily localization.

Study of the impact of 53BP1 displacement from kinetochores on the mitotic surveillance pathway

The first aim of this project was the investigation of 53BP1 mitotic partners. Once a kinetochore receptor for 53BP1 was identified, the subsequent step was to interfere with its binding to 53BP1 eventually preventing the recruitment of the protein to kinetochores. To do so, a mutant cell line lacking 53BP1 kinetochore localization was generated. Then, the impact of 53BP1 delocalization was tested by triggering the MSP activation and assessing whether a loss of function or an hyperactivation of the pathway occur.

Study of the effects of forcing 53BP1 at mitotic kinetochores on the mitotic surveillance pathway

The other way to perturb the system is to force 53BP1 at mitotic kinetochores and assess whether this could have an impact on the MSP. As mentioned before, 53BP1 displays maximal association with kinetochores during prophase and then gradually disappears. A key aspect was to investigate how 53BP1 dissociates from kinetochores assessing whether, as other corona localizing proteins, it is a dynein cargo or it is removed via a different mechanism. Moreover, 53BP1 is known to be hyperphosphorylated during mitosis (Jullien D et al., 2001) (Giunta et al., 2010) (Van Vugt et al., 2010) (Lee et al., 2014) and for this reason the last part of this project was aimed at investigating whether mitotic kinases play a role in modulating the affinity of 53BP1 for the kinetochore and whether they play a role in MSP regulation.

All the results presented in this thesis have been published in the paper: Burigotto M*, Vigorito V*, Gliech C, Mattivi A, Ghetti S, Bisio A, Lolli G, Holland AJ, Fava LL. PLK1 promotes the mitotic surveillance pathway by controlling cytosolic 53BP1 availability. EMBO Rep. 2023 Oct 27: e57234. Doi: 10.15252/embr.202357234. Epub ahead of print. PMID: 37888778.

*Contributed equally

MATERIALS AND METHODS

From (Burigotto, Vigorito et al., 2023)

Cell culture

hTERT-RPE1 cells (gift by Stephan Geley, Medical University of Innsbruck), hTERT-RPE1 PLK1AS cells (gift by Prasad Jallepalli, Memorial Sloan Kettering Cancer Center) and hTERT-RPE1 p21-EGFP cells (gift by Chris Bakal, Institute of Cancer Research) were cultured in DMEM/F12 1:1 (Gibco 21331-020). HEK 293T (gift by Ulrich Maurer, University of Freiburg) and HeLa S3 (gift by Erich Nigg) cells were maintained in DMEM (Gibco, 11960-044). All media were supplemented with 10% foetal bovine serum (Gibco, 10270-106), 2 mM L-glutamine (Corning, 25-005-CI), 100 IU/mL penicillin, and 100 µg/mL streptomycin solution (Corning, 30-002-CI). Cells were grown at 37°C with 5% CO2 and regularly tested for mycoplasma contamination.

Drug treatments, irradiation and synchronization protocol

The following compounds were used: 1 µM NU-7441 (Selleck Chemicals, S2638), 125 nM centrinone (MedChem Express, HY-18682), 2 mM thymidine (SigmaAldrich, TI895), 3.3 µM nocodazole (BioTrend, BN0389), 2 µM dimethylenastron (Selleck Chemicals, S0279), 100 nM BI-2536 (MedChem Express, HY-50698), 500 nM reversine (Enzo Life Sciences, BML-SC104), 10 µM KU-60019 (MedChem Express, HY-12061), 10 µM VE-822 (MedChem Express, HY-13902), 2 µM ZM-447439 (Selleck Chemicals, S1103), 10 µM BAY-524 (MedChem Express, HY-104001), 10 µM MG-132 (Selleck Chemicals, 133407-82-6), 10 µM 3-MB-PP1 (Cayman Chemical, 17860), 5 µM S-trityl-L-cysteine (STLC, Tocris Bioscience, 2191). Cells were irradiated using the XstrahI RS225 X-ray research Irradiator (West Midlands, UK) with 2 Gy (delivering at a dose rate of 1.6 Gy/min). After the irradiation cells were allowed to recover for 30 min and then fixed for immunofluorescence. Thymidine was solubilized in water while all the other drugs were dissolved in DMSO; to all the untreated controls only solvent was administered. Synchronization of RPE1 cells was performed by arresting cells with 2 mM thymidine for 24h, then cells were released in fresh medium containing nocodazole 3.3 µM. Mitotic cells were then directly fixed for immunofluorescence, or they were harvested by selective shake-off and either directly lysed or washed four times and released into fresh medium. For the

ATP depletion assay (Howell et al,2001), cells were washed in saline solution (140 mM NaCl, 5 mM KCl, 0.6 mM MgSO4, 0.1 mM CaCl2, 1 mM Na2HPO4, 1 mM KH2PO4, pH 7.3) and rinsed either in saline G (saline + 4.5 g/l D-glucose) or Az/DOG (saline + 5 mM sodium azide + 1 mM 2-deoxy-D-glucose) for 15 min at 37°C. Then cells were fixed to perform immunofluorescence.

siRNA -mediated gene knock-down

HeLa cells were transfected using Lipofectamine RNAiMAX Transfection Reagent (Life Technologies) according to the manufacturer's procedures with 40 nM CENP-F siRNA (5'-CAAAGACCGGUGUUACCAAG-3') or luciferase (GL2) siRNA (5'-CGUACGCGGAAUACUUCGA-3') whereas RPE1 cells where transfected with siRNA SMART pool targeting CENP-F (Dharmacon, L-003253-00-0005) or a non-targeting control (Dharmacon, D-001810-01-05). Cells were then either harvested for Western blot analysis or fixed for immunofluorescence 48h after the transfection.

Molecular cloning of phosphomutant 53BP1

To generate 53BP1 phosphomutant version, 13 PLK1 phosphorylation sites on 53BP1 were mapped using the following PLK1 consensus sequence: L(Φ) (E/N/D(Q)) X (S/T) L(Φ). Then, pcDNA5-FRT/TO-eGFP-53BP1 (Addgene plasmid #60813) was used as a template for site-directed mutagenesis. The primers used to generate the phosphomutant (13 S/T-A) are listed in Table 1.

AlphaFold molecular modelling

CENP-F models for WT and the E564P mutant were obtained through ColabFold v1.5.2 (Mirdita et al, 2022). Sequence boundaries (aa 546-780) were chosen to include all residues predicted in the AlphaFoldDB (Jumper et al, 2021) in the single α-helix comprising Glu564.

Nucleofection-based CRISPR/Cas9

RPE1 WT, RPE1 PLK1^{AS} and RPE1 p21-EGFP cell lines were electroporated using Lonza Nucleofector 4-D to introduce v5 tag and the CENP-F^{E564P} mutation (See Table 2). Briefly, according to Ghetti et al, 2021, 100 µM of crRNA (IDT) and 100 µM of tracRNA (IDT) were mixed to form gRNAs. Ribonocluoparticles (RNPs) were then obtained using 120 pmol of recombinant Cas9 and 150 pmol of gRNAs. Electroporation mix was prepared by resuspending 2x10^5 RPE1 cells in P3 Primary Cell Full Electroporation Buffer (Lonza) and adding RNPs, 4 µM Alt-R Cas9 Electroporation enhancer (IDT) and 4 µM single-strand DNA homology template (Ultramer DNA Oligonucleotide, Lonza). After the electroporation, cells were treated with 1 µM NU-7441 (Selleck Chemicals), a DNA-PK inhibitor, for 48h. Single-cell clones were obtained by limiting dilution. Genomic DNA was extracted using NucleoSpin Tissue columns (Macherey-Nagel, 740952) following the manufacturer's protocol. For each guide (Table 3), PCR reactions were performed using Phusion DNA polymerase (Thermo Scientific, F530-L), using a primer pair (see Table 4) designed to obtain amplicons spanning the cut site. PCR products were then purified on agarose gel and purified using NucleoSpin Gel and PCR Clean-up kit (Macherey-Nagel, 740609). Sanger sequencing of PCR products and Inference of CRISPR Edits (ICE) analysis confirmed the correct in-frame insertion of the V5 tag (TP53BP1 locus) or E564P mutation (*CENPF* locus) in homozygosis. The analysis of Sanger sequenced samples was performed takind advantage of a Synthego Bioinformatics tool (https://ice.synthego.com). RPE1 53BP1-V5 CENP-FE564P double knock-in cells were generated by two consecutive rounds of electroporation and single-cell cloning, starting from the V5-tagged cell line.

Lentitiviral-based CRISPR/Cas9

RPE1 T53BP1 KO cells were obtained using a lentiviral-based CRISPR/Cas9 strategy as previously described (Burigotto et al., 2021). Briefly, a gene-specific crRNA was cloned into the Lenti-CRISPR-V2 backbone (gift from Feng Zhang; Addgene plasmid #52961). This plasmid, along with pCMV-VSV-G (a gift from Bob Weinberg, Addgene plasmid #8454) and psPAX2 (a gift from Didier Trono, Addgene plasmid #12260), was used to co-transfect HEK 293T cells using calcium phosphate. After 48h, supernatants were harvested, filtered, mixed with 4 µg/mL hexadimethrine bromide (Sigma-Aldrich, H9268) and administered to

cells for 24 h. Transduced cells were enriched by 10 μg/mL puromycin selection (InvivoGen, ant-pr-1) for 72 h. RPE1 PLK1AS TP53BP1 KO cells were generated using an RNP-based CRISPR/Cas9 strategy (Ghetti et al, 2021), as described above (without the addition of a single-strand DNA homology template nor NU-7741 treatment). For both cell lines, isogenic clones were isolated by limiting dilution. The presence of gene disrupting INDELs in edited cells was confirmed by Sanger sequencing of PCR products spanning the crRNA recognition site, followed by Inference of CRISPR Edits (ICE) analysis (https://ice.synthego.com) (Hsiau et al, 2018).

Yeast two-hybrid screen

The yeast two-hybrid screen was performed by Hybrigenics Services, S.A.S., Evry, France. The KT binding domain sequence of 53BP1 (aa 1235-1616) was PCR-amplified from pcDNA5-FRT/TO-eGFP-53BP1 (Addgene plasmid #60813) and cloned into pB66 downstream to the Gal4 DNA-binding domain. This construct was used as bait to screen a human lung cancer cells cDNA library constructed into pP6. 70 million clones were screened using a mating approach with YHGX13 (Y187 ade2- 101:loxP-kanMX-loxP, matα) and CG1945 (mata) yeast strains as previously described (Fromont-Racine et al, 1997). 173 His+ colonies were selected on a medium lacking tryptophan, leucine, and histidine. Prey fragments of positive clones were amplified by PCR and sequenced at their 5' and 3' junctions. The resulting sequences were used to identify the corresponding interacting proteins in the GenBank database (NCBI) using a fully automated procedure. The sequences of 67 CENP-F fragments were overlapped and their positions calculated relative to the full-length protein sequence. The minimal region that overlaps represents the selected interacting domain.

Cell lysis and immunoblotting

Cells were harvested by trypsinization and lysed in 50 mM Tris pH 7.4, 150 mM NaCl, 0.5% v/v NP-40, 50 mM NaF, 1 mM Na3VO4, 1 mM PMSF, one tablet/50 mL cOmplete, EDTA-free Protease Inhibitor Cocktail (Roche, 11873580001), 2 mM MgCl2 and 0.2 mg/mL Dnase I (Thermo Fisher Scientific, 89836). Protein concentration was assessed by bicinchoninic acid assay (Pierce BCA Protein Assay Kit, Thermo Fisher Scientific, 23225) using a plate

reader. Equal amounts of total protein samples (40-50 µg) were resolved by polyacrylamide gels using self-made or pre-cast gels (Bio-Rad). Proteins were electroblotted on nitrocellulose membranes (Cytiva, 10600001) using a wet transfer system (Bio-Rad). Membranes were blocked in blocking solution (5% w/v non-fat milk in PBS-Tween 0.1% v/v), incubated overnight at 4°C with the relevant antibody diluted in blocking solution, washed several times with PBS-Tween 0.1% v/v and then incubated at room temperature for 50 min with HRP-conjugated secondary antibodies diluted in blocking solution. Protein detection was carried out using an Alliance LD2 Imaging System (UviTec Cambridge), after incubating membranes with Amersham ECL Select Western Blotting Detection Reagent (Cytiva, RPN2235). The following antibodies were used:

Primary antibody	Host	Dilution	Company	Reference
CENP-F	Rabbit	1:500	Cell Signalling Technology	58982
53BP1	Rabbit	1:500	Cell Signalling Technology	4937
CYCLIN-A2	Mouse	1:500	Abcam	ab38
VINCULIN	Mouse	1:2000	Sigma-Aldrich	V9264

Secondary antibody	Dilution	Company	Reference
Goat anti-rabbit IgG/HRP	1:5000	Dako	P0448
Rabbit anti-mouse IgG/HRP	1:5000	Dako	P0161

Clonogenic assay

$4x10^3$ RPE1 cells were seeded in 10-cm dishes and medium was refreshed every 5 days. When applied, centrinone was refreshed every 3 days. When subjected to synchronization protocol, cells were treated with thymidine for 24 h and released in medium containing nocodazole. Mitotic cells (M + 6 h) were selectively retrieved by shake-off, released from nocodazole and seeded for the clonogenic assay. In parallel, control cells were synchronized by a thymidine block, released in fresh medium for 16 h, detached by trypsinization and seeded for the assay. After 8 – 16 days, cells were washed in PBS and then stained for 30 min at 37°C with crystal violet (0.2% w/v, AcrosOrganics, 212120000) dissolved in 20% v/v

methanol. Cell plates were then washed several times with water and left to dry overnight. Images were acquired using a ChemiDoc Imaging System (Bio-Rad).

Immunoprecipitation and MS analysis

WT and 53BP1-V5 tagged RPE1 cells were grown in 15-cm dishes, arrested in thymidine and released in nocodazole for 10 h. Mitotic shake-off was performed, cells were washed with PBS and lysed as described above. 700 µg of each sample were incubated with 30 µL of slurry Affi-Prep protein A resin (Bio-Rad) and 1 µg of mouse anti-V5 tag antibody (Invitrogen, R96025) for 4 h at 4°C. The beads were collected by centrifugation and washed twice with lysis buffer. Dried bead complexes were eluted by boiling samples in Bolt™ LDS sample buffer with 10% v/v Bolt™ Sample Reducing Agent (Thermo Fisher Scientific) at 95°C for 10 min. Samples were separated in precast 10% Bolt Bis-Tris Plus gel (Thermo Fisher Scientific), run for ∼1 cm and stained with a Coomassie solution. For each sample, the entire stained area was excised and washed with 100 mM NH4HCO3 in 50% v/v acetonitrile (©) for 15 min. The colourless gel plugs were then dehydrated by adding 100% ACN. The dried gel pieces were reduced with 10 mM DTT for 1 h and alkylated with 55 mM iodoacetamide for 30 min. Gel fragments were then washed in water, dehydrated wi©ACN, and incubated in a digestion solution containing 12.5 ng/µL trypsin (Thermo Fisher Scientific) in 100 mM NH4HCO3 at 37°C overnight. Peptides were extracted by sequentially treating gel pieces with 3% trifluoroacetic acid (TFA) in 30©/v ACN, and 100% v/v ACN. Tryptic peptides were then dried in a speed-vac and acidified with TFA to a pH <2.5. After desalting on C18 stage tips, peptides were resuspended in 0.1% v/v formic acid (FA) for LC-MS/MS analysis.

Peptides were separated on an Easy-nLC 1200 HPLC system (Thermo Scientific) using a 25 cm reversed-phase column (inner diameter 75 µm packed in-house with ReproSil-Pur C18-AQ material: 3 µm particle size, Dr. Maisch, GmbH) with a two-component mobile phase (0.1% v/v FA in water and 0.1% v©FA in ACN). Peptides were then eluted using a gradient of 5% to 25% over 50 minutes, followed by 25% to 40% over 15 min and 40% to 98% over 10 min at a flow rate of 400 nL/min. Peptides were analysed in an Orbitrap Fusion Tribrid mass spectrometer (Thermo Fisher Scientific) in data-dependent mode, with a full-scan performed at 120.000 FWHM resolving power (mass range: 350–1100 m/z, AGC target value: 10e6 ions, maximum injection time: 50 ms), followed by a set of (HCD) MS/MS

scans over 3 sec cycle time at a collision energy of 30% (AGC target: 5 × 10e3 ions, maximum injection time: 150 ms). Dynamic exclusion was enabled and set at 30 sec, with a mass tolerance of 5 ppm. Data were acquired using Xcalibur 4.3 software and Tune 3.3 (Thermo Scientific). For all acquisitions, QCloud (Chiva et al, 2018) was used to control instrument longitudinal performance during the project using in-house quality control standards. Raw files were searched using Proteome Discoverer v.2.2.0 (Thermo Scientific). Peptide searches were performed against the in-silico digested UniProt Human database (downloaded April 2021), added with major known contaminants and the reversed versions of each sequence. Trypsin/P was chosen as the enzyme with 5 missed cleavages, and static modification of carb©domethyl (C) with variable modification of oxidation (M) and acetylation of protein N-terminus were incorporated in the search. The MASCOT search engine (v.2.6.2, MatrixScience) was used to identify proteins (precursor mass tolerance: 10 ppm, product mass tolerance: 0.6 Da). The FDR was set to < 0.01 at both the peptide and protein levels. Peak intensities of the peptides were log2 transformed and data were normalised on the average of the specific protein abundance within each sample (Aguilan et al, 2020). The fold change (FC) of each peptide was calculated. Then, the FC at protein level was calculated by averaging the FC of all peptides assigned to each protein. 53BP1-binding partners were identified by subtracting the log2-normalised intensities of the control sample (RPE1 WT mitotic cells) to the test sample (RPE1 53BP1-V5 mitotic cells). Statistical significance was assessed using Student's t-test (two-tailed, two-sample unequal variance).

Competition assay and FACS analysis

To generate cells constitutively expressing EGFP, the EGFP sequence was PCR amplified from pEGFP-N1 (Clontech) and cloned in the pAIB-CAG lentiviral vector between the PmeI and NotI sites, upstream of an IRES element and a blasticidin resistance gene under the CAG promoter. Lentiviral particles were produced as described above. After transduction, cells underwent antibiotic selection with 5 μg/mL blasticidin (InvivoGen, ant-bl-05) for 7 days. For competition growth assays, RPE1 WT cells stably expressing EGFP and non-fluorescent RPE1 cells of the desired genotype were mixed at a 1:1 ratio and seeded into duplicate wells. One well from each pair was treated with centrinone for 8 days. Cells were analysed on a Symphony A1 cytometer (BD Biosciences) to assess the percentage of EGFP+ cells. Live cells were gated through forward-scatter (FSC) and side scatter (SSC) parameters, and cell

doublets were excluded. For each sample, the fraction of EGFP- cells was divided by the fraction of EGFP+ cells. The value obtained from the centrinone-treated well was then divided by that obtained in the untreated well to determine the fold change in EGFP- cells. Analysis of flow cytometry data was performed using FlowJo software (FlowJo, LLC).

Immunofluorescence microscopy

Cells were grown on glass coverslips (Marienfeld-Superior, 0117580), washed in PBS and directly fixed and permeabilized with absolute ice-cold methanol for at least 20 min at −20°C. For NudE staining cells were pre-extracted for 2 min in PTEM buffer (0.2% v/v Triton X-100, 20 mM PIPES at pH 6.8, 1 mM MgCl2, 10 mM EGTA in ddH2O) and then fixed with 4% v/v formaldehyde (Sigma-Aldrich, F8775) in PTEM for 10 min at room temperature. Cells were rinsed with PBS, blocked with 3% w/v BSA in PBS for 20 min and stained for 1 h at room temperature with primary antibodies diluted in blocking solution. The following primary antibodies were used:

Primary antibody	Host	Dilution	Company	Reference
53BP1	Mouse	1:500	Millipore	MAB3802
V5	Mouse	1:1000	Invitrogen	R96025
V5	Rabbit	1:1000	Cell Signalling Technology	13202
CENP-F	Rabbit	1:500	Cell Signalling Technology	58982
Centromere/KT	Human	1:500	Antibodies Inc	15-234
NudE	Rabbit	1:250	ProteinTech	10233-1-AP
Phosphor-Histone H2A.X Ser139	Mouse	1:500	Millipore	05-636
γ-tubulin	Mouse	1:1000	Thermo Fisher Scientific	MAI-19421

Cells were washed with PBS and incubated with fluorescent secondary antibodies for 45 min at room temperature. DNA was stained with 1 µg/mL Hoechst 33342 (Invitrogen).

The following secondary antibodies were used:

Secondary antibody	Dilution	Company	Reference
AlexaFluor488 goat anti-mouse	1:1000	Invitrogen	A11029
AlexaFluor555 goat anti-mouse	1:1000	Invitrogen	A21424
AlexaFluor488 goat anti-rabbit	1:1000	Invitrogen	A11034
AlexaFluor555 goat anti-rabbit	1:1000	Invitrogen	A21429
AlexaFluore647 goat anti-human	1:1000	Invitrogen	A21445

After incubation, cells were rinsed with PBS and ddH2O, and mounted using ProLong Gold Antifade Reagent (Invitrogen). For Appendix Fig. S4B, a sheep anti-CENP-F antibody (kind gift of S. Taylor, University of Manchester, SCF.1, 1:1000) was used. Images in Fig. 1C, EV1B and EV2E were acquired on a spinning disc Eclipse Ti2 inverted microscope (Nikon Instruments Inc), equipped with Lumencor Spectra X Illuminator as LED light source, an X-Light V2 Confocal Imager and an Andor Zyla 4.2 PLUS sCMOS monochromatic camera using a plan apochromatic 100×/1.45 oil immersion objective. Images in Appendix Fig. S4B were collected using a Deltavision Elite system (GE Healthcare) controlling a Scientific CMOs camera (pco. edge 5.5). Acquisition parameters were controlled by SoftWoRx suite (GE Healthcare). Images were collected using an Olympus 100×/1.4 oil immersion objective. Images in Appendix Fig. S1A, S1C and S1E were acquired on a Nikon AX confocal microscope (Nikon Instruments Inc) equipped with a LUA-S4 laser unit using a plan apochromatic 100×/1.49 oil immersion objective. Images were deconvolved with Huygens Professional software (Scientific Volume Imaging, Hilversum, The Netherlands). All remaining images were acquired on a Leica TCS SP8 microscope using a 63x/1.4 oil objective with Lightening mode (adaptive as “Strategy” and ProLong Gold as “Mounting medium”) to generate deconvolved images. Images were processed using Fiji and displayed as maximum-intensity projections of deconvolved z-stacks. All displayed images were selected to represent the mean quantified data most closely.

Time-lapse video microscopy

Cells were seeded into Ibidi µ-Slide 8 Well dishes (Ibidi, 80826) in DMEM/F12 medium without phenol red the day before imaging. 1 h before imaging, fresh medium was added in

the presence of 1 μM SiR-DNA (Spirochrome, SC007) to visualize the DNA. To assess SAC proficiency, 1 h before imaging, the culture medium was replaced with a medium containing 3.3 μM nocodazole or DMSO. Movies were recorded every 3 min for 20 h (to measure mitotic timing) or every 5 min for 48 h (to test SAC proficiency). Cells were imaged on a spinning disc Eclipse Ti2 inverted microscope (Nikon Instruments Inc), equipped with Lumencor Spectra X Illuminator as LED light source, an X-Light V2 Confocal Imager and an Andor iXon Ultra 888 EMCCD camera using a plan apochromatic 20x/0.75 objective. The representative movies were deconvolved with Huygens Professional software (Scientific Volume Imaging, Hilversum, The Netherlands).

Image analysis

All images of similarly stained experiments were acquired with identical illumination settings. To quantify fluorescence intensity at KTs, maximum intensity projections of z-stacks were obtained using Fiji and circular regions of interest (ROIs) with a diameter of 5 pixels were drawn, centred on the KT (CREST signal). Measurements were performed on at least 10 independent images. For each cell, 3 background ROIs (placed in the cytoplasmic space, in proximity to the DNA staining) were drawn and their average value was subtracted from the intensity value of each KT. To quantify DNA damage foci, cell nuclei were segmented using Fiji, according to the Hoechst signal. The “find maxima” function was then applied to quantify the number of foci inside each nucleus. To quantify 53BP1 signal in the stripping assay, 2 binary masks for γ-tubulin signal (signal at poles and total signal) and a DNA mask were generated (Appendix Fig. S5). To the total γ-tubulin mask, the pole mask and the DNA mask were subtracted. The resulting ROI was used to measure 53BP1 fluorescence intensity in the region of the mitotic spindle external to the chromosome mass and not comprising the two centrosomes. To quantify the number of colonies in the clonogenic assay, plate scans were imported in Fiji, manually cropped to individual plates and median filtered. Colonies were equally segmented among different genotypes and treatments, and the “analyse particles” function was then used to count colonies.

In situ Proximity Ligation Assay (PLA)

RPE1 53BP1-V5 CENP-F^{WT}, RPE1 53BP1-V5 CENPF^{E564P} and RPE1 WT were grown on glass coverslips, washed in PBS and fixed with ice-cold methanol for 20 min at −20°C. Cells were rinsed with PBS, blocked with 3% w/v BSA in PBS (blocking buffer) for 20 min and then incubated for 1 h at room temperature with mouse anti-V5 tag antibody (Invitrogen, R96025) and rabbit anti-p53 antibody (Cell Signalling Technology, #9282), diluted 1:500 in blocking buffer. PLA ((Burigotto et al., 2021b; Ghetti et al., 2021; Howell et al., 2001; Jumper et al., 2021; Mirdita et al., 2022; Söderberg et al., 2008) was performed using the Duolink kit, according to the manufacturer's protocol. Briefly, samples were incubated with anti-mouse Minus probe (Sigma, DUO92004) and anti-rabbit Plus probe (DUO92002, Sigma) diluted in blocking buffer for 1 h at 37°C. Cells were rinsed twice with Wash Buffer A (Sigma, DUO82049), incubated with a ligation-ligase solution for 30 min at 37°C and then washed twice in Wash Buffer A. To each sample an amplification-polymerase solution (Sigma, DUO92007) was added, and they were incubated for 100 min at 37°C. Cells were rinsed with Wash Buffer B (Sigma, DUO82049) and coverslips were mounted using Duolink in Situ Mounting Medium with DAPI (Sigma, DUO82040). All incubation steps were performed in the dark inside a humidity chamber. To quantify PLA spots, cells were manually segmented using Fiji and the “find maxima” function was then applied to quantify the number of foci per cell.

Mitotic Surveillance Pathway threshold assay

RPE1 p21-EGFP CENP-FWT and CENP-FE564P cells were seeded into 4-well chamber slides (Ibidi, 80426) 24 hrs before imaging. For the experiment in Appendix Fig. S4, RPE1 p21-EGFP cells were treated with a siRNA SMART pool targeting CENP-F or a non-targeting control for 24 hr before seeding them in imaging chambers. Before imaging, standard media was replaced with CO2-independent base medium (Thermo Fisher) and cells maintained at 37 °C in an environmental control station. Once under the microscope, cells were blocked in mitosis with 2 μM dimethylenastron for 7 h. Fresh media was then replaced to allow cells to exit mitosis and cells were monitored for 2 additional days. Daughter cell fate (growth/arrest) was inferred using p21-EGFP expression (Appendix Fig. S4D) and related to time spent in mitosis (NEBD-anaphase onset). Long-term time-lapse imaging was

performed using a Deltavision Elite system (GE Healthcare) controlling a Scientific CMOS camera (pco.edge 5.5). Images were acquired with an Olympus 40× 1.4 NA oil objective. To assess the MSP threshold, cells were sorted by ascending mitotic duration, then scanned from short to long mitoses with a 10-cell window. Once identified a window containing >=50% arrested cells, the threshold was measured as the average of the two middle points.

Statistics

Data are presented either as dot plots or as bar charts and mean ± standard deviation (SD) are shown. Normality of datasets was determined by Shapiro–Wilk test. Statistical differences were calculated by unpaired two-tailed Student's t-test or Mann–Whitney test (between two groups) and by one-way ANOVA or Kruskal–Wallis test (between multiple groups), applying Tukey's or Dunn's multiple comparisons test, respectively. Statistical significance was annotated as: *P < 0.05; **P < 0.01; ***P < 0.001; ****P < 0.0001, or not significant (n.s.; P > 0.05. Statistical analyses and graphs were produced using GraphPad Prism 10 (GraphPad, San Diego, CA, USA) software.

Tables

Table 1 Primers for site-directed mutagenesis

Mutation	Primer	Sequence
T4A	FW	CCG ACC ATG GAC CCT GCA GGA AGT CAG TTG GAT TC
T4A	RV	GAATCCAACTGACTTCCTGCAGGGTCCATGGTCGG
T163A	FW	CTT GGT GCT GAA GAT GCT GCC TCA TCA CAG TTG
T163A	RV	CAACTGTGATGAGGCAGCATCTTCAGCACCAAG
S345A	FW	CAT CTC CTG CAG CTA GCT GGT CAG AGG TCC CTT G
S345A	RV	CAAGGGACCTCTGACCAGCTAGCTGCAGGAGATG
S349A	FW	CTA GCT GGT CAG AGA GCG CTT GTT CAG GAC AGT C
S349A	RV	GACTGTCCTGAACAAGCGCTCTCTGACCAGCTAG
S354A	FW	GCG CTT GTT CAG GAC GCT CTT TCC ACG AAT TCT TC
S354A	RV	GAAGAATTCGTGGAAAGAGCGTCCTGAACAAGCGC
S395A	FW	GAT AAG CCA ATG GAC ACT GCA GTG TTA TCT GAA GAA G
S395A	RV	CTTCTTCAGATAACACTGCAGTGTCCATTGGCTTATC
S721A	FW	CT ATG GAA GTT GAA ACT GCA GTG ATT AGT ATT GAT TC
S721A	RV	GAATCAATACTAATCACTGCAGTTTCAACTTCCATAG
T1082A	FW	TTG GAG GGT GAC CAT GCA ATC AGG CAG AGT CAA C
T1082A	RV	GTTGACTCTGCCTGATTGCATGGTCACCCTCCAA
S1160A	FW	CAA ACC ATG GAG TGT GCC TTG AGG GTC CCA GAA AC
S1160A	RV	GTTTCTGGGACCCTCAAGGCACACTCCATGGTTTG
S1618A	FW	CA AAG GCA GCA GAT ATA GCG CTA GAC AAT TTG GTG G
S1618A	RV	CCACCAAATTGTCTAGCGCTATATCTGCTGCCTTTG
T1709A	FW	GAG AGT GGA GAC AAC GCC GGT GAA CCC TCT GCC
T1709A	RV	GGCAGAGGGTTCACCGGCGTTGTCTCCACTCTC
S1713A	FW	C AAC GCC GGT GAA CCC GCG GCC CTG GAA GAG CAG
S1713A	RV	CTGCTCTTCCAGGGCCGCGGGTTCACCGGCGTTG
S1727A	FW	CT TTG CCT CTC AAC AAA GCT TTG TTT CTG GGC TAC
S1727A	RV	GTAGCCCAGAAACAAAGCTTTGTTGAGAGGCAAAG

Table 2 Ultramer DNA sequences for CRISPR/Cas9

Target gene	Application	Sequence 5'-3'
TP53BP1	V5-tag KI	G*A*ATTGGATTCAAGCAGCATCCAAAATATAAACACGATTATGTTTCTCACGGCAGCGGCAAGCCCATCCCCAACCCCCTGCTGGGCCTGGACAGCACCTAAAGATACTTGGTCTTACTGGTTTTATTCCCTGCTATCGTGGAGATT*G* T
CENP-F	E564P KI	C*T*TGACTTTAGAAAAACTGAAGCTTGCTGTGGCTGATCTGCCAAAGCAGCGAGATTGTTCTCAAGACCTTTTGAAGAAAAGAG*A*A

Table 3 sgRNAs for CRISPR/Cas9

Target gene	Application	Sequence 5'-3'	Target exon
TP53BP1KO	KO	CTGCTCAATGACCTGACTGA	4
TP53BP1	V5-tag KI	TGTTTCTCACTAAAGATACT	28
CENP-F	E564P KI	GAAGCTTGCTGTGGCTGATC	12

Table 4 PCR primers

Target gene	FW	RV
TP53BP1KO	TATCCTTGGGATGAGGCAACA	CGAGGAGACGGTAATAGTGGG
TP53BP1	GATGTGGTGGTGACGGACC	TGCAAGGAATCCAGTTACACAC
CENP-F	AGCGAAGAATACCTCTCAGGAA	TGCAAGTTTTCCTTTTCTGATTCCA

RESULTS

All the data presented in this thesis are the results of an equal contribution of Matteo Burigotto and myself, Vincenza Vigorito.

CENP-F is the 53BP1 kinetochore receptor

As previously reported, 53BP1 transiently localizes at mitotic kinetochores (KTs) without an associated function (Jullien D et al., 2001), so we decided to characterize the kinetochore receptor of 53BP1. To tackle this question, we employed CRISPR/Cas9 technology (Ghetti et al., 2021) to edit the endogenous *TP53BP1* locus in hTERT-RPE1 cells (referred to as RPE1). Specifically, we introduced a biallelic V5-epitope tag at the C-terminus of the 53BP1 protein (**Fig 14A**). Remarkably, the behaviour of the V5-tagged 53BP1 closely resembled that of the untagged protein with a pan-nuclear localization in interphase cells and being recruited at KTs upon mitotic entry (**Fig 14B**). The 53BP1-V5 fusion protein demonstrated similar dynamics to the untagged version, accumulating at γH2AX-positive foci in irradiated cells, indicating an intact role in DNA damage response and exhibiting mitotic phase-dependent dynamics at the KT, peaking in prophase and gradually diminishing during mitotic progression (**Fig 14C**). This indicated that the V5 tag did not interfere with the protein's dynamic localization or relevant protein–protein interactions.

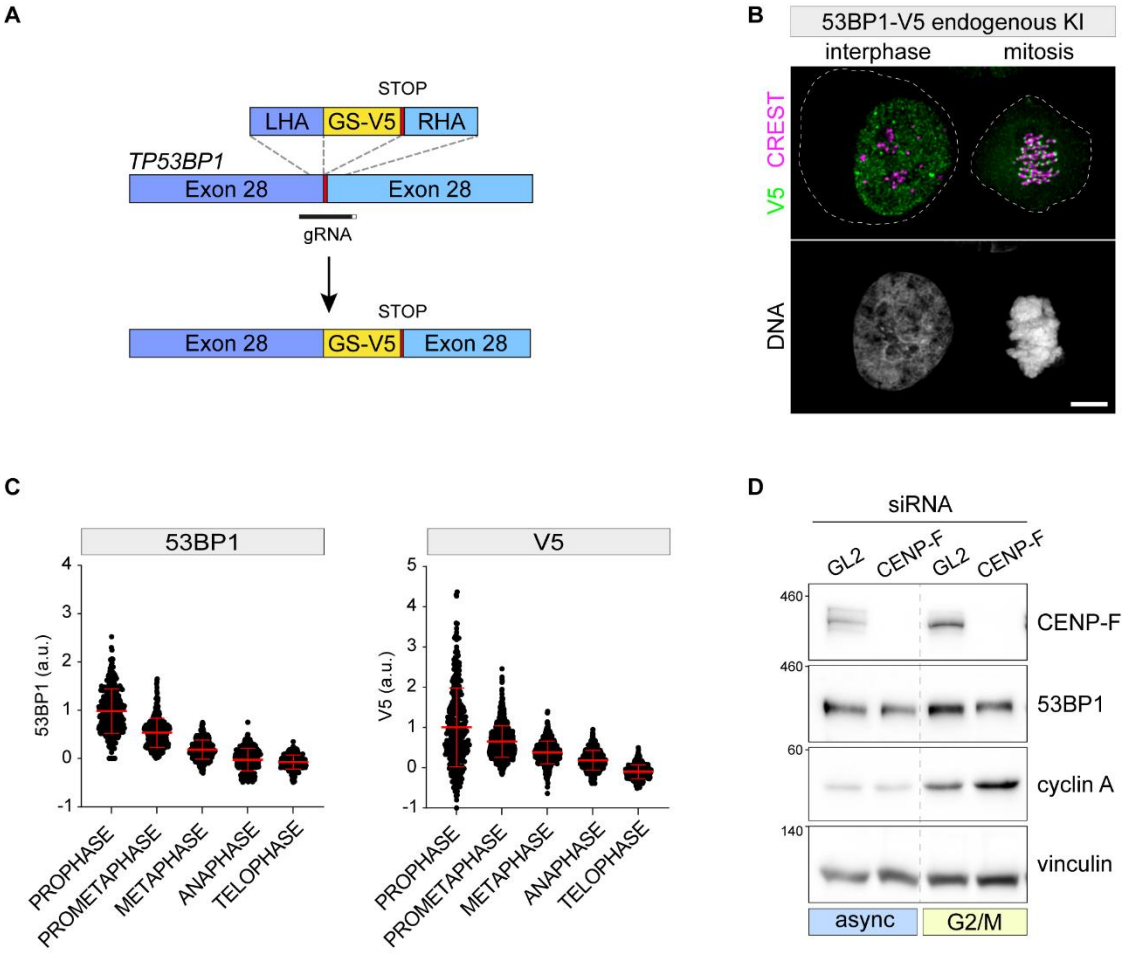

Figure 14. 53BP1-V5 endogenous knock-in does not impact 53BP1 localization and dynamics. (A) Diagram illustrating the knock-in strategy for editing the endogenous locus ofTP53BP1 with the insertion of a V5 tag sequence. LHA represents the left homology arm, RHA for the right homology arm, and GS-V5 denotes the Gly-Ser linker followed by the V5-epitope tag. (B) Representative fluorescence micrograph of 53BP1-V5 cells stained with the indicated antibodies. On the left is shown an interphase cell and, on the right, a mitotic one. (C) Dot plots displaying fluorescence intensity of 53BP1 (in RPE1 WT cells) or V5 (in RPE1 53BP1-V5 cells) at individual kinetochores throughout the cell cycle phases. Mean values (red lines) ± SD are reported, normalized on the prophase sample, with N ≥ 349 kinetochores assessed from 10 cells for each mitotic phase (a.u = arbitrary units). (D) HeLa S3 cells, were transfected with the indicated siRNAs and treated with thymidine or left untreated. Cells were analysed through immunoblotting using the specified antibodies.

To identify the mitotic interactors of 53BP1, we synchronized RPE1 53BP1-V5 knock-in cells in prometaphase with a single thymidine block followed by a release in nocodazole for 10h and performed immunoprecipitation against the V5-tag, followed by LC–MS. The MS analysis revealed 21 specific binding partners (Supplementary Table 1), including known 53BP1 interactors such as NUDT16L1/TIRR, DYNLL2, USP28, and PLK1 (**Fig 15A**). Notably, the KT fibrous corona protein CENP-F emerged as one of the top enriched hits, suggesting a potential role in 53BP1 localization at the KT. In an orthogonal approach to define the KT-binding partner(s) of 53BP1, we performed a yeast two-hybrid screen using the KT-binding domain of 53BP1, previously described in (Jullien D et al., 2001), as bait against a human cDNA library. This identified 67 CENP-F clones at a high confidence level, confirming a direct interaction between CENP-F and 53BP1 (**Fig 15B**).

Further investigations were carried out to explore the impact of CENP-F on 53BP1 recruitment to the KT. siRNA-mediated depletion of CENP-F in HeLa S3 cells disrupted 53BP1 localization at mitotic KTs without affecting 53BP1 protein levels (**Fig 15C and D**). This highlights the essential role of CENP-F in recruiting 53BP1 to the KT.

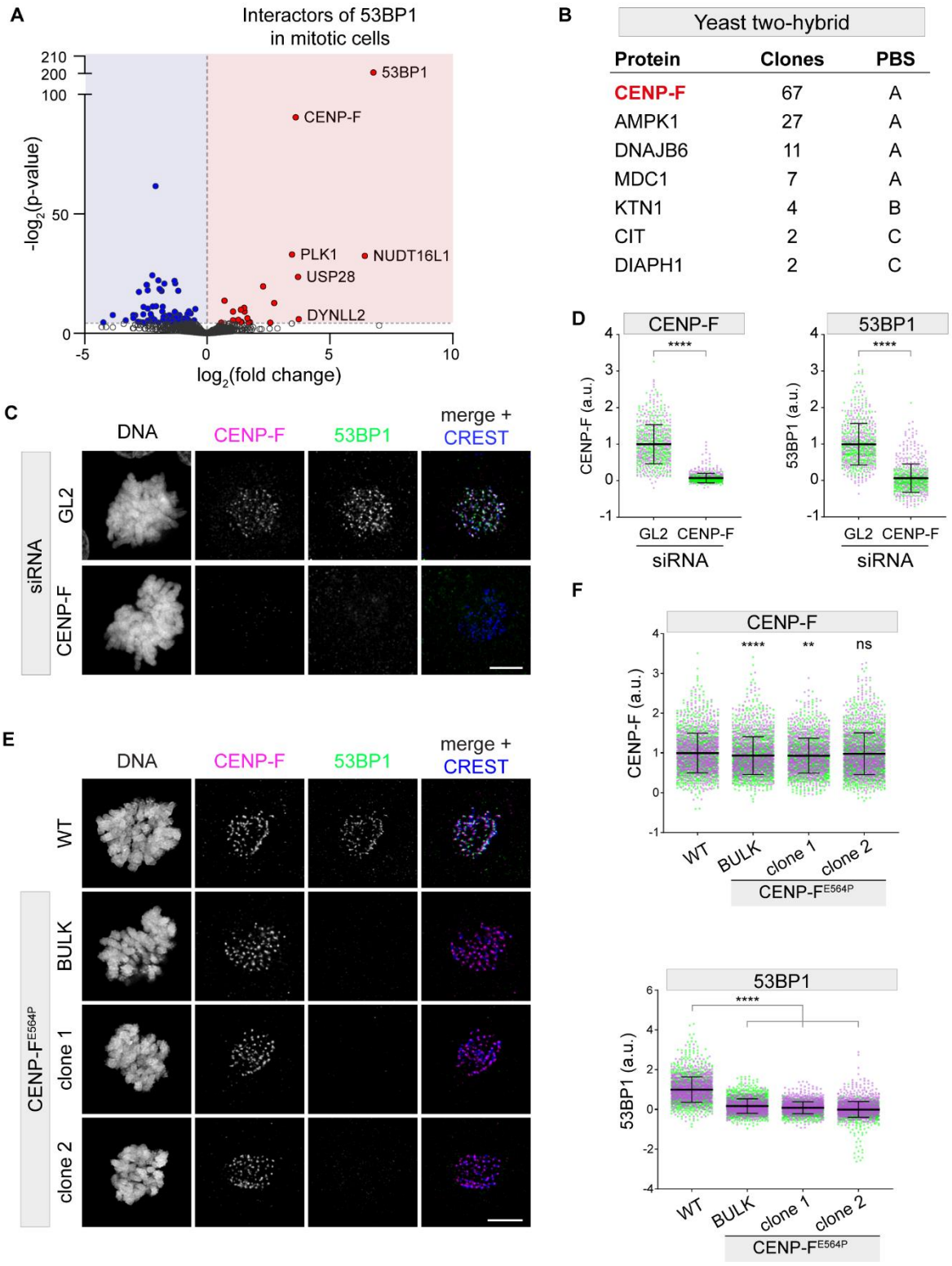

Figure 15. CENP-F is the 53BP1 kinetochore receptor. (A) Volcano plot showing proteins interacting with 53BP1 during mitosis, as identified through mass spectrometry. Each dot on the plot represents an individual protein, with the x-axis indicating the log2(fold change) compared to the untagged control, and the y-axis expressing significance as -log10(P-value). (B) List of the prey fragments retrieved from a yeast two-hybrid screen. The information includes the name of the protein, the number of clones, and the specific protein binding

score (PBS), offering insights into the outcomes of the screen. (C) HeLa S3 cells, following transfection with specific siRNA, underwent immunofluorescence using indicated antibodies. A scale bar of 5 μm is provided for reference. (D) Dot plots illustrating the intensity of specified proteins at individual kinetochores, derived from images obtained in (C). Each dot represents a distinct kinetochore, with mean values and standard deviations reported. Data is normalized to the GL2 sample, and statistical significance was determined using an unpaired Mann–Whitney test (****P < 0.0001). (E) Representative fluorescent micrographs of RPE1 cells of the specified genotypes, co-stained with designated antibodies. A scale bar of 5 μm is included. (F) Dot plots showing the intensity of indicated proteins at individual kinetochores, derived from images obtained in (E). Each dot corresponds to a specific kinetochore, with mean values and standard deviations reported. Data is normalized to the WT sample, and statistical significance was assessed using a Kruskal–Wallis test (****P < 0.0001; **P = 0.0019; n.s.=non-significant).

CENP-F is known to play a crucial role in facilitating the attachment of kinetochores (KTs) to microtubules and safeguarding corona cargoes from dynein-mediated "stripping" (Bomont et al., 2005) (Auckland et al., 2020). Supporting this function, the median Chronos gene score (Dempster et al., 2021) for *CENPF* knockout in 1,078 diverse cell lines analysed in DepMap was −0.23, with the gene deemed essential in 113 of them, indicating that complete *CENPF* knockout results in a loss of fitness (**Fig 16A**). To avoid problems linked to *CENPF* knockout, we decided to search for a targeted approach to impede CENP-F binding to 53BP1. The yeast two-hybrid screen pinpointed a specific domain of CENP-F crucial for interaction with 53BP1, spanning residues 564–588 (**Fig 16B**). This region, predicted to be part of a coiled-coil motif (Ciossani et al., 2018), led us to explore a strategy involving the substitution of glutamic acid (E) at position 564 with proline (P), known to destabilize the α-helical fold (**Fig 16C**). Employing CRISPR/Cas9, we introduced the E564P substitution into the endogenous *CENPF* locus of RPE1 cells (**Fig 16D**) (Ghetti et al., 2021). Sequencing of the electroporated polyclonal population (hereafter termed bulk) confirmed the successful introduction of the desired mutation with a high editing rate at 5 days post-electroporation (i.e., > 80%, **Appendix Fig S2**). Bulk analysis on day 15 demonstrated that the penetrance of the desired edit did not diminish over time (**Appendix Fig S2**). Furthermore, we derived homozygous monoclonal CENP-F^{E564P} RPE1 cells from the polyclonal population (**Appendix Fig S2**).

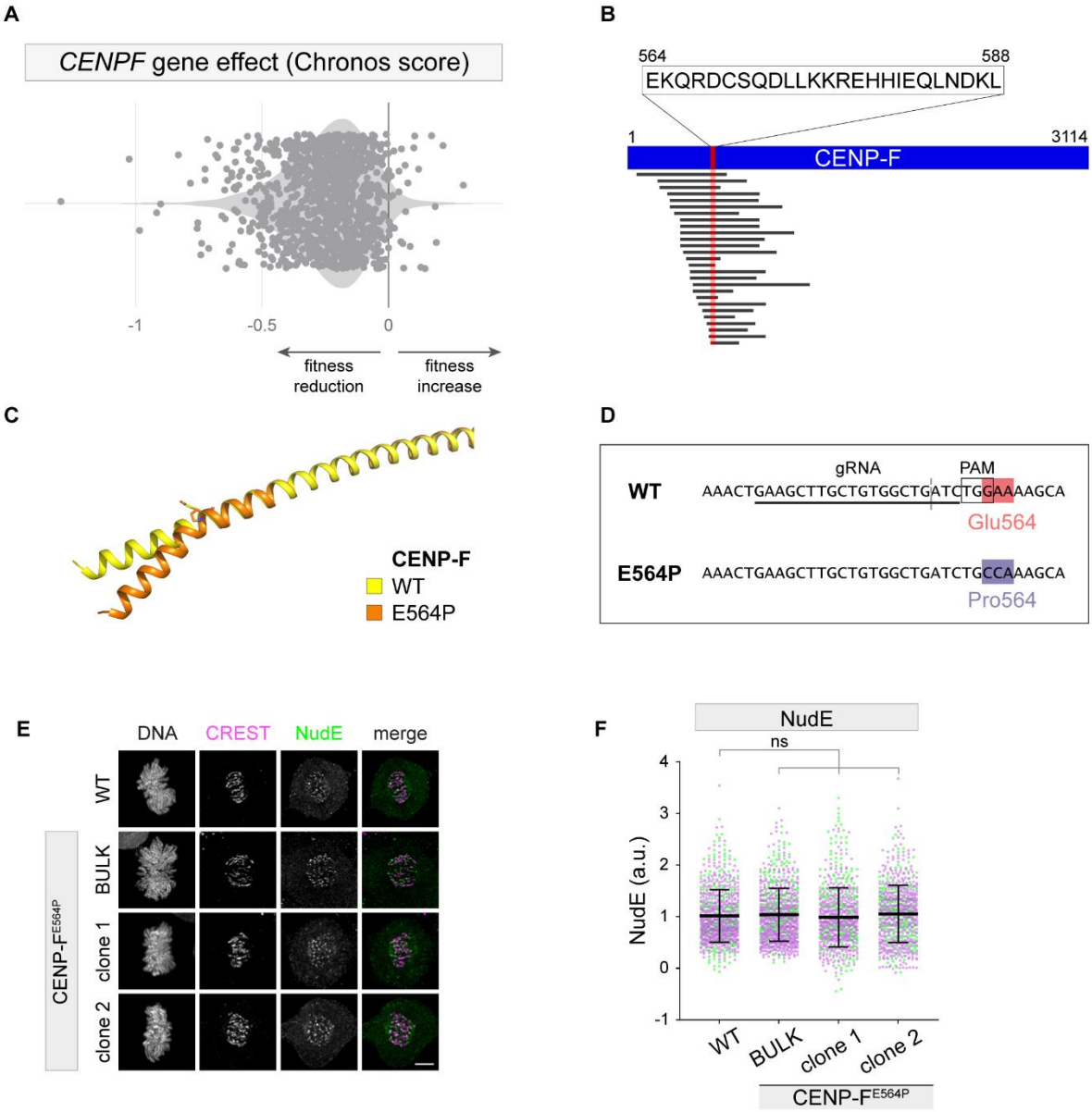

Figure 16. Knock-in strategy to interfere with 53BP1 and CENP-F binding avoiding 53BP1 recruitment to kinetochores. (A) Chronos gene dependency scores for *CENPF* across 1,078 cell lines were extracted from the DepMap database (CRISPR DepMap 22Q4), with the x-axis representing the Chronos score. (B) Schematic of CENP-F prey fragment identified by yeast two-hybrid screen and their relative positions to the CENP-F sequence. The overlap of various clones identified a 25-amino-acid region as a putative binding domain between the kinetochore-binding domain of 53BP1 (bait) and CENP-F. (C) AlphaFold modelling of the putative 53BP1 binding domain of CENP-F indicated that the introduction of a proline at position 564 is expected to create a kink in this coiled coil region. (D) Knock-in strategy to introduce the E564P mutation in *CENPF*. (E) Representative fluorescence micrographs of RPE1 cells of the indicated genotype, co-stained with specific antibodies. The scale bar is 5 µm. (F) Dot plots showing the intensity of NudE protein at individual kinetochores from images as in (E). Each dot represented a particular kinetochore, with mean values (black lines) ± SD reported and normalized on the WT sample. The arbitrary units (a.u.) were used, and N = 2

biological replicates were shown in green and magenta. Significance was assessed using a Kruskal–Wallis test, where n.s. indicated non-significant results.

CENP-F^{E564P} mutant cells demonstrated a complete absence of 53BP1 recruitment to mitotic kinetochores (KTs), closely resembling the phenotype observed upon CENP-F depletion (**Fig 15E and F)**. Crucially, this point mutation did not eliminate the recruitment of CENP-F to the corona (**Fig 15F**). Furthermore, the CENP-F^{E564P} mutation resulted in a statistically significant reduction in the CENP-F signal at KTs in some edited cells ($6.3 \pm 3.5\%$ for the bulk and $6.9 \pm 3.9\%$ in clone 1), however this is unlikely to be functionally relevant. Notably, neither the ability of CENP-F to recruit its downstream effector protein NudE (**Fig 16E and F**) nor its mitotic proficiency was compromised by this edit (**Appendix Fig S3**). Therefore, we precisely identified the minimal domain of CENP-F required for 53BP1 recruitment to the KT, and the introduction of a single amino acid substitution in the CENP-F sequence allowed the generation of a separation-of-function mutant. This mutant selectively interferes with 53BP1 binding while leaving other essential functions of CENP-F, such as NudE KT recruitment, unaffected.

53BP1 kinetochore localization is dispensable for mitotic surveillance pathway functionality

The establishment of CENP-F^{E564P} mutant cell lines has provided a valuable tool for precisely dissecting the functional implications of 53BP1 kinetochore localization. We initially hypothesized that the recruitment of 53BP1 at the fibrous corona might represent a priming state for the Mitotic Surveillance Pathway (MSP), similar to the recruitment pattern observed for Spindle Assembly Checkpoint (SAC) proteins. However, our findings strongly refute this hypothesis.

Upon activation of the MSP with centrinone, a specific PLK4 kinase inhibitor causing centriole depletion overtime, wild-type (WT) RPE1 cells exhibited a significant reduction in clonogenic potential as assessed with a clonogenic assay (**Fig 17A and B**). As anticipated, MSP deficiency, achieved through TP53BP1 knockout, substantially increased clonogenic potential in the presence of centrinone. Remarkably, this response was not observed in CENP-F^{E564P} cells, both in the bulk population and the homozygote clonal

derivatives (**Fig 17A and B**). This pattern was consistently observed in a competition-based growth assay, where only TP53BP1 knockout weakened the cell cycle arrest induced by centrinone, while CENP-F^{E564P} mutant cells exhibited an arrest comparable to that in WT cells (**Fig 17E**).

Furthermore, we evaluated MSP functionality in CENP-F^{E564P} cells using an alternative MSP trigger that is SAC activation induced by transient exposure to nocodazole, a drug able to interfere with microtubule polymerization and spindle formation, leading to a prolonged mitosis. In these conditions, TP53BP1 knockout was the only genotype retaining high clonogenic potential, whereas the extension of mitotic duration in CENP-F^{E564P} knock-in cell lines resulted in a reduction of clonogenic potential stronger at least as the one observed in WT cells (**Fig 17C and D**)

To ascertain the MSP time threshold of CENP-F^{WT} and CENP-F^{E564P} cells, we employed live cell imaging to monitor p21 expression relative to the time spent in mitosis. The results revealed no discernible contribution of 53BP1 KT localization to the mitotic timer. Similar outcomes were observed upon CENP-F knockdown (**Appendix Fig S4**). In summary, our data conclusively demonstrate that 53BP1 recruitment at the KT is not a prerequisite for MSP function.

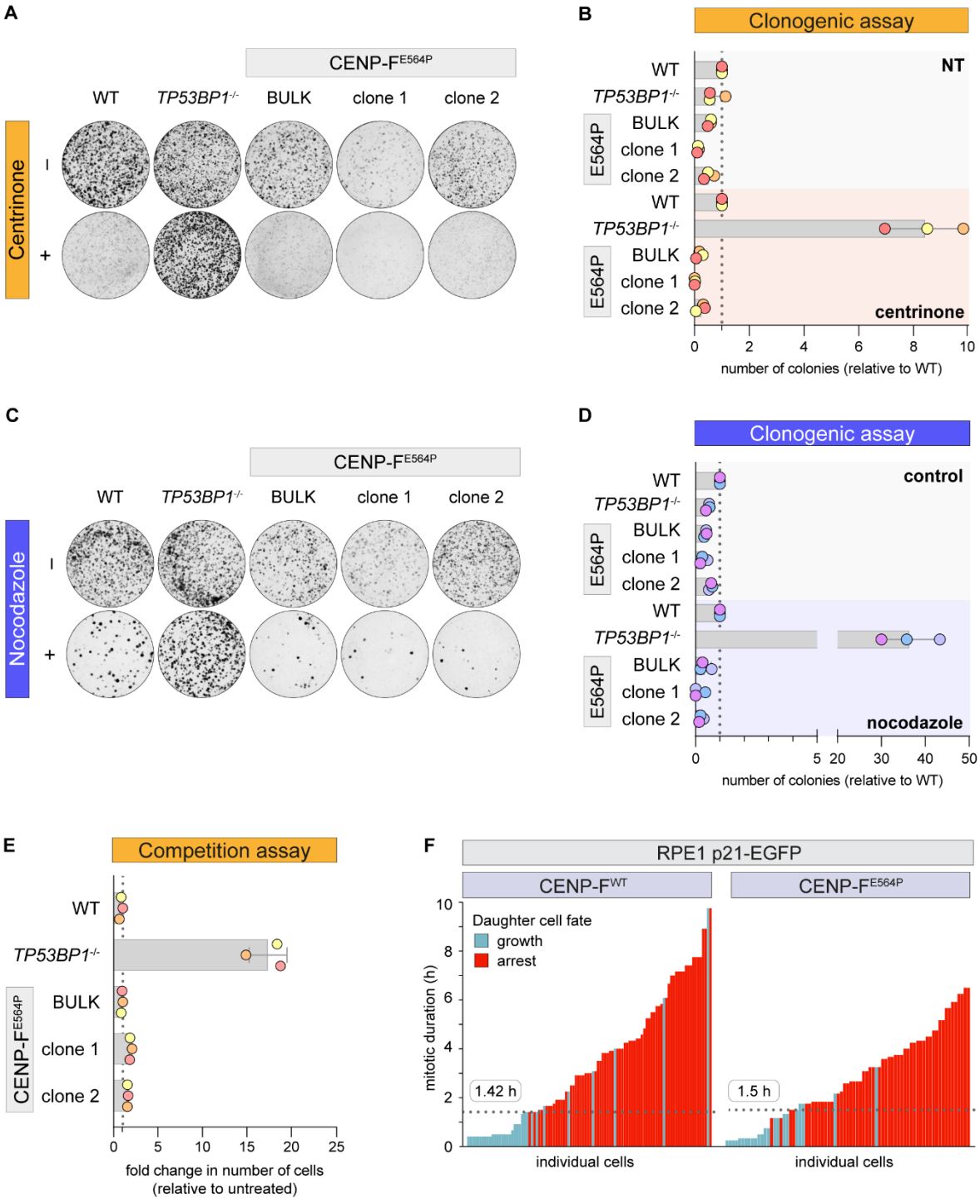

Figure 17. 53BP1 kinetochore localization is dispensable for MSP functionality. (A) Cells of the indicated genotypes were exposed to centrinone for 12 days or left untreated (for 8 days) and subsequently stained with crystal violet. Representative images are shown, reflecting N=3 biological replicates. (B) Quantification of the experiment as described in (A). The data is presented as the number of colonies relative to WT cells (depicted by the dotted line). The bars indicate the mean ± SD (N=3 biological replicates). (C) Pre-synchronized cells of the indicated genotypes were subjected to prometaphase arrest (+ nocodazole) or left untreated (- nocodazole), harvested, seeded for the clonogenic assay, and stained with crystal violet after 12 and 8 days, respectively.

Representative images are presented for N=3 biologically independent experiments. (D) Quantification of three independent experiments as detailed in (C). The data is presented as the number of colonies relative to WT cells (depicted by the dotted line). The bars indicate the mean ± SD (N=s3 biological replicates). (E) Cells of the specified genotypes were mixed 1:1 with EGFP-expressing WT cells and cultured either in the presence or absence of centrinone. After 8 days, the relative growth of each genotype was assessed by flow cytometry. The bars represent the mean ± SD (N=3 biological replicates), and values are expressed relative to the WT sample (dotted line). (F) RPE1 CENP-F^{WT} and RPE1 CENP-F^{E564P} cells were treated with dimethylenastron under the microscope, released from the drug, and imaged for 2 days. The graph illustrates the fate of daughter cells in relation to the time spent in mitosis by the mother cell. Each daughter cell is represented by a vertical bar, with its height indicating the mitotic duration of its mother, and the colour indicating the fate of the daughter (growth or arrest). The dotted lines indicate the Mitotic Surveillance Pathway (MSP) threshold. N=100 CENP-F^{WT} and N=77 CENP-F^{E564P} cells were analysed. Experiment performed by Colin Gliech (Johns Hopkins University).

PLK1 promotes 53BP1 loss of kinetochore affinity

While our CENP-F mutant cell lines provided a means to displace 53BP1 from the kinetochore (KT), it was not clear whether the system could be disrupted in the opposite direction that is forcing 53BP1 to persist at the KT. To gain deeper insights into this aspect, we conducted a more detailed characterization of 53BP1 behaviour during mitosis.

Consistent with prior research (Jullien D et al., 2001), 53BP1 exhibited maximal association with mitotic KTs during prophase, gradually dissociating in subsequent phases (**Fig 14C**). This pattern mirrored the behaviour of other corona-localizing proteins. Under normal mitotic conditions, the outermost fibrous corona layers undergo disassembly via dynein-motor protein activity upon microtubule-KT attachment, a process known as stripping (Auckland et al., 2020). In a stripping hyperactivation assay (Howell et al., 2001), 53BP1 was removed from the KT and accumulated on the mitotic spindle (**Fig 18A and B**; **Appendix Fig S5**), suggesting that, like CENP-F, 53BP1 is a dynein cargo during mitosis. However, in the context of delayed mitosis induced by the microtubule-poison nocodazole, the 53BP1 signal was still gradually lost over time, completely disappearing from KTs around 6 hours after mitotic entry (**Fig 18C and D**). This indicates that, in addition to stripping, 53BP1 undergoes a time-dependent loss of affinity for the KT.

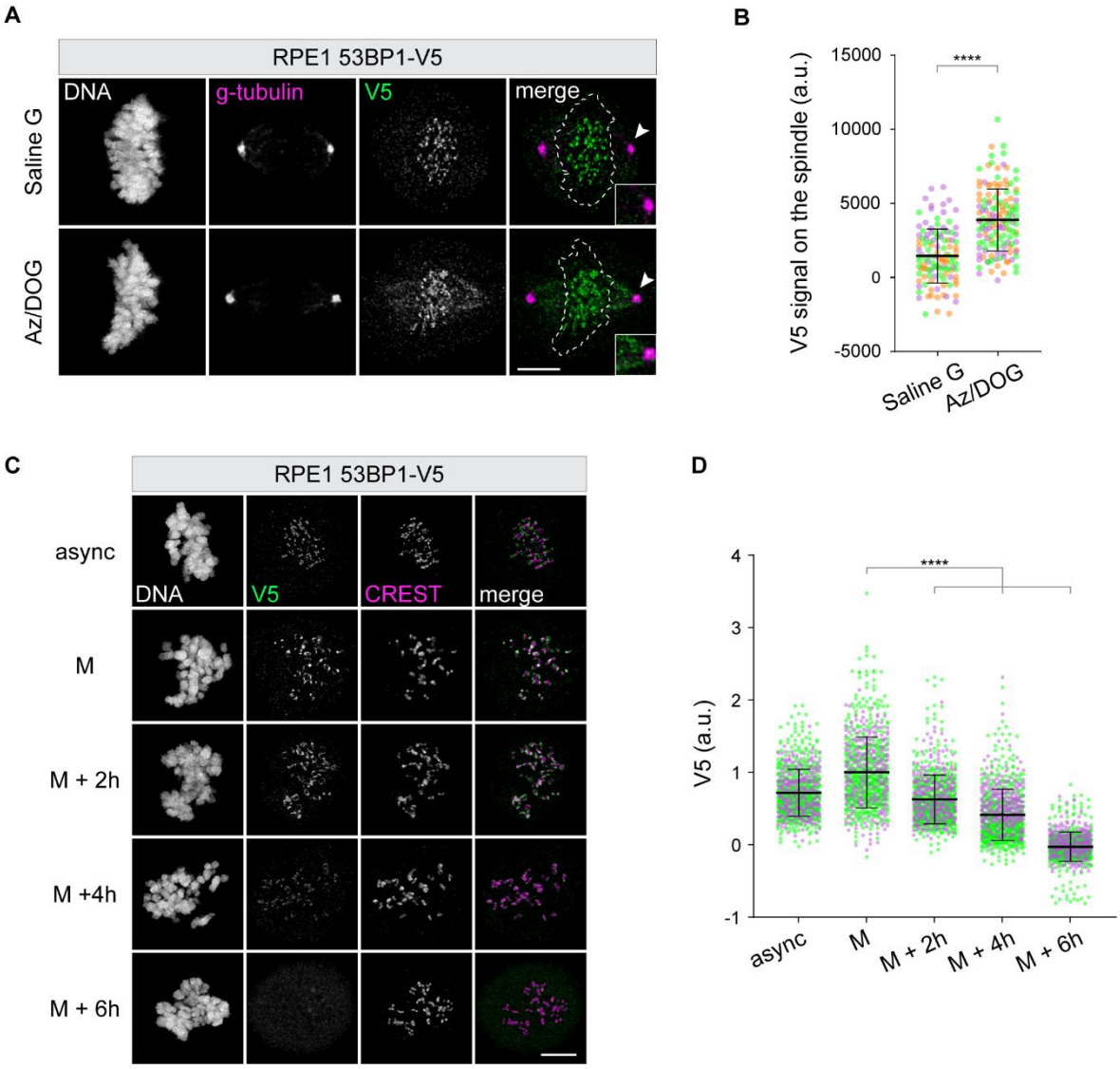

Figure 18. 53BP1 detachment from kinetochores relies on both stripping and time-dependent loss of affinity. (A) Representative fluorescence micrographs of RPE1 53BP1-V5 cells incubated for 15 min in isotonic salt solution in the presence of either glucose (Saline G) or sodium azide/2-deoxy-D-glucose (AZ/DOG) and co-stained with the indicated antibodies. The blow-up shows a portion of the mitotic spindle in proximity to one of the spindle poles (arrowhead). Scale bar: 5 µm. (B) Dot plots showing V5 fluorescence intensity on the spindle obtained from images as in (A). Each dot represents a specific spindle. Mean values (black lines) ± SD (calculated on the entire dataset) are reported; a.u.= arbitrary units. N=3 biological replicates are shown, one replicate in green, one in magenta, one in orange. Significance was tested using an unpaired t-test (****$P < 0.0001$). (C) RPE1 53BP1-V5 cells were either left untreated (async = asynchronous) or synchronized in prometaphase in medium containing nocodazole, fixed immediately (M = mitosis) or after 2, 4, or 6 h and co-stained with the indicated antibodies. Scale bar: 5 µm. (D) Dot plots showing V5 fluorescence intensity at individual KTs from images as in (C). Each dot represents a particular KT. Mean values (black lines) ± SD (calculated on the entire dataset) are reported, normalized on the mitotic (M) sample; a.u.= arbitrary

units. N=2 biological replicates are shown, one replicate in green, one in magenta. Significance was tested using a Kruskal–Wallis test (****P < 0.0001).

Phosphorylation events play crucial roles in mitotic KT assembly, dynamics, and remodelling (Musacchio & Desai, 2017) (Saurin, 2018). Furthermore, 53BP1 is known to be hyperphosphorylated during mitosis (Jullien D et al., 2001) (Giunta et al., 2010) (Van Vugt et al., 2010) (Lee et al., 2014). Therefore, we investigated whether major known kinases targeting 53BP1 (ATM, ATR, PLK1, and Aurora B) and master regulator kinases acting at the KT (MPS1 and BUB1) contribute to modulating the affinity of 53BP1 for the KT. Our mini kinases screen showed that inhibition of none of the tested kinases abolished 53BP1 loading to KTs, although ATM, ATR, BUB1, and MPS1 inhibition caused a measurable loading reduction (**Fig 19A**; **Appendix Fig S6**). In a complementary setting, we also assessed the contribution of these kinases to 53BP1's loss of affinity for the KT. This analysis revealed a significant contribution from PLK1, as its inhibition prevented the loss of affinity for the KT (**Figs 19B and 20A**).

To eliminate potential off-target effects of the PLK1 inhibitor used in our screen, we utilized RPE1 cells with endogenous PLK1 deletion, relying on the constitutive expression of a genetically modified allele ($PLK1^{AS}$) that can be chemically inactivated taking advantage of the so-called Shokat approach (Peter J Alaimo et al., 2001). In this context, inhibition of PLK1 under MSP-activating conditions retained 53BP1 KT localization in WT cells but did not restore the impaired localization of the protein in our CENP-F^{E564P} mutant (**Fig 19C**; **Appendix Fig S7**).

To overcome problems related to the absence of microtubules achieved using nocodazole, we performed the same experiment prolonging mitosis by inhibiting Eg5, a condition where dynein-mediated stripping is not prevented. Crucially, this approach yielded results consistent with those obtained with nocodazole (**Fig 20B**; **Appendix Fig S8**). Surprisingly, 53BP1 did not seem to be the relevant PLK1 substrate in this process, as 53BP1 carrying the simultaneous mutation of 13 Ser/Thr to Ala in all theoretical PLK1 consensus sites retained the ability to undergo PLK1-dependent KT loss of affinity (**Fig 21A**; **Appendix Fig S9**).

In summary, while dynein-mediated stripping might be a crucial component in an unperturbed cell division, in the presence of delayed anaphase, 53BP1 requires PLK1 activity to exhibit time-dependent loss of KT affinity.

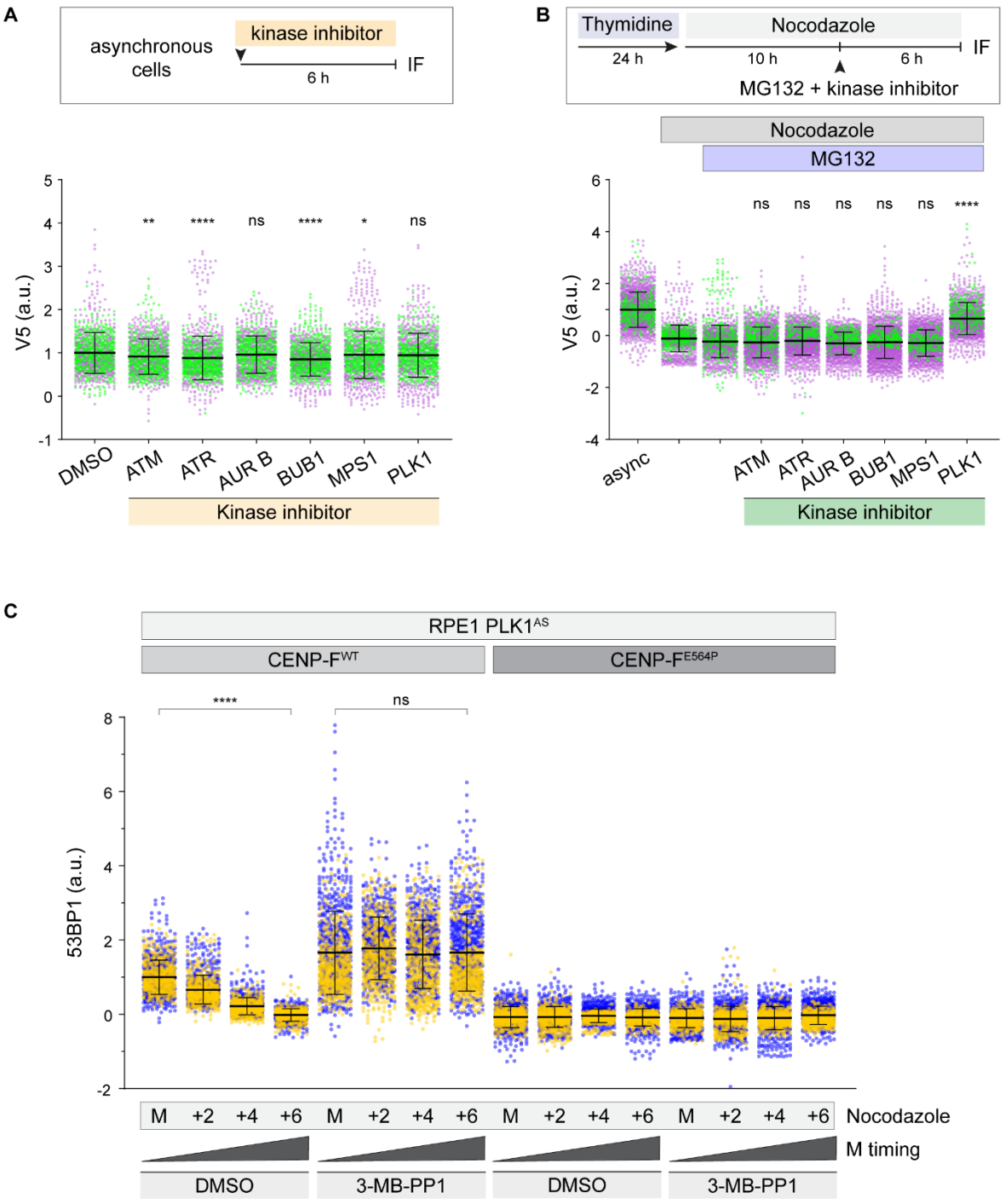

Figure 19. PLK1 activity induces 53BP1 loss of kinetochore affinity. (A)Top: Asynchronous RPE1 53BP1-V5 cells were treated with kinase inhibitors for 6 hours (AUR B = Aurora B). The bottom panel displays dot plots illustrating V5 fluorescence intensity at individual KTs. Each dot represents a specific KT, with mean values (black lines) and standard deviations (calculated on the entire dataset) reported and normalized against the DMSO sample. Immunofluorescence (IF) and arbitrary units (a.u.) are denoted. Two biological replicates are shown in green and magenta. Significance was assessed using a Kruskal–Wallis test: ****P < 0.0001; **P = 0.0074; *P = 0.0333; n.s.=non-significant. (B) Top: RPE1 53BP1-V5 cells were either untreated or treated with thymidine for 24 hours, released in medium containing nocodazole, and, after 10 hours, MG-132 and the

indicated kinase inhibitor were added. The bottom panel features dot plots depicting V5 fluorescence intensity at individual KTs. Each dot represents a particular KT. Asynchronous cell (Async) and Aurora B (AUR B) are labeled. Mean values (black lines) and standard deviations (calculated on the entire dataset) are reported, normalized against the asynchronous sample; a.u. = arbitrary units. Two biological replicates are shown in green and magenta. Significance was assessed using a Kruskal–Wallis test: ****P < 0.0001, n.s.=non-significant. (C) Cells of the indicated genotypes were synchronized in prometaphase in medium containing nocodazole, in the presence or absence of PLK1 inhibition (3-MB-PP1), and fixed immediately (M = mitosis) or after 2, 4, or 6 hours. Dot plots show 53BP1 fluorescence intensity at individual KTs. Each dot represents a specific KT. Mean values (black lines) and standard deviations (calculated on the entire dataset) are reported, normalized on the WT early mitotic sample; a.u. = arbitrary units. Two biological replicates are shown in blue and yellow. Significance was assessed using a Kruskal-Wallis test: ****P < 0.0001; n.s.=non-significant.

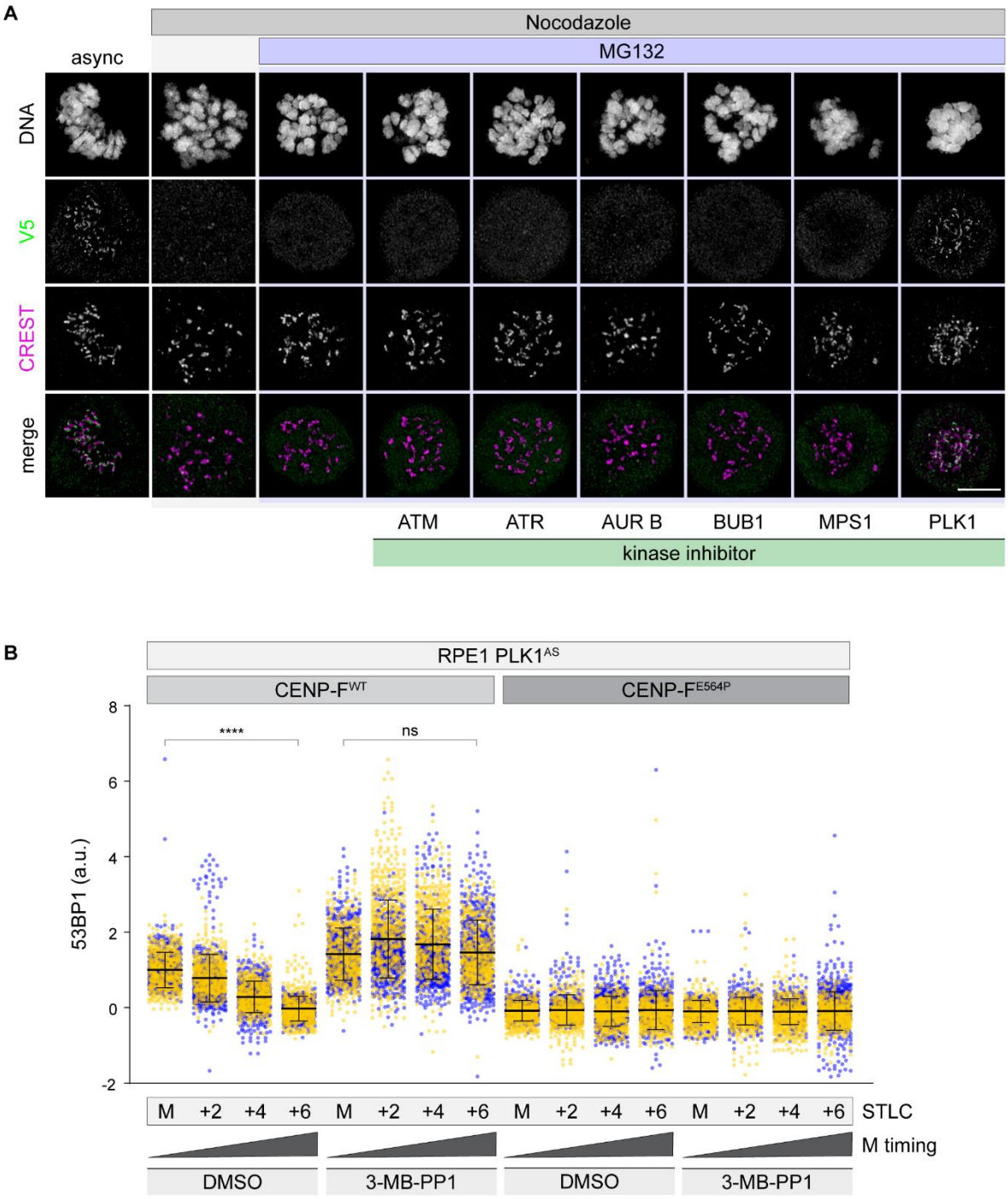

Figure 20. PLK1 regulates 53BP1 dynamics regardless microtubules status. (A) Fluorescence micrographs representative of RPE1 53BP1-V5 cells treated as described in Fig 16B, co-stained with the specified antibodies. Asynchronous cells are denoted as "Async," and Aurora B is labelled as "AUR B." The scale bar is 5 µm. (B) Cells of designated genotypes were synchronized in prometaphase in medium containing STLC, with or without PLK1 inhibition (3-MB-PP1), and immediately fixed (M = mitosis) or after 2, 4, or 6 h. Dot plots illustrate 53BP1 fluorescence intensity at individual kinetochores, with each dot representing a specific kinetochore. Mean values (black lines) ± SD (calculated on the entire dataset) are presented, normalized to the

WT early mitotic sample, using arbitrary units (a.u.). Two biological replicates are displayed in blue and yellow, with significance assessed via a Kruskal-Wallis test: ****P < 0.0001; n.s. = non-significant

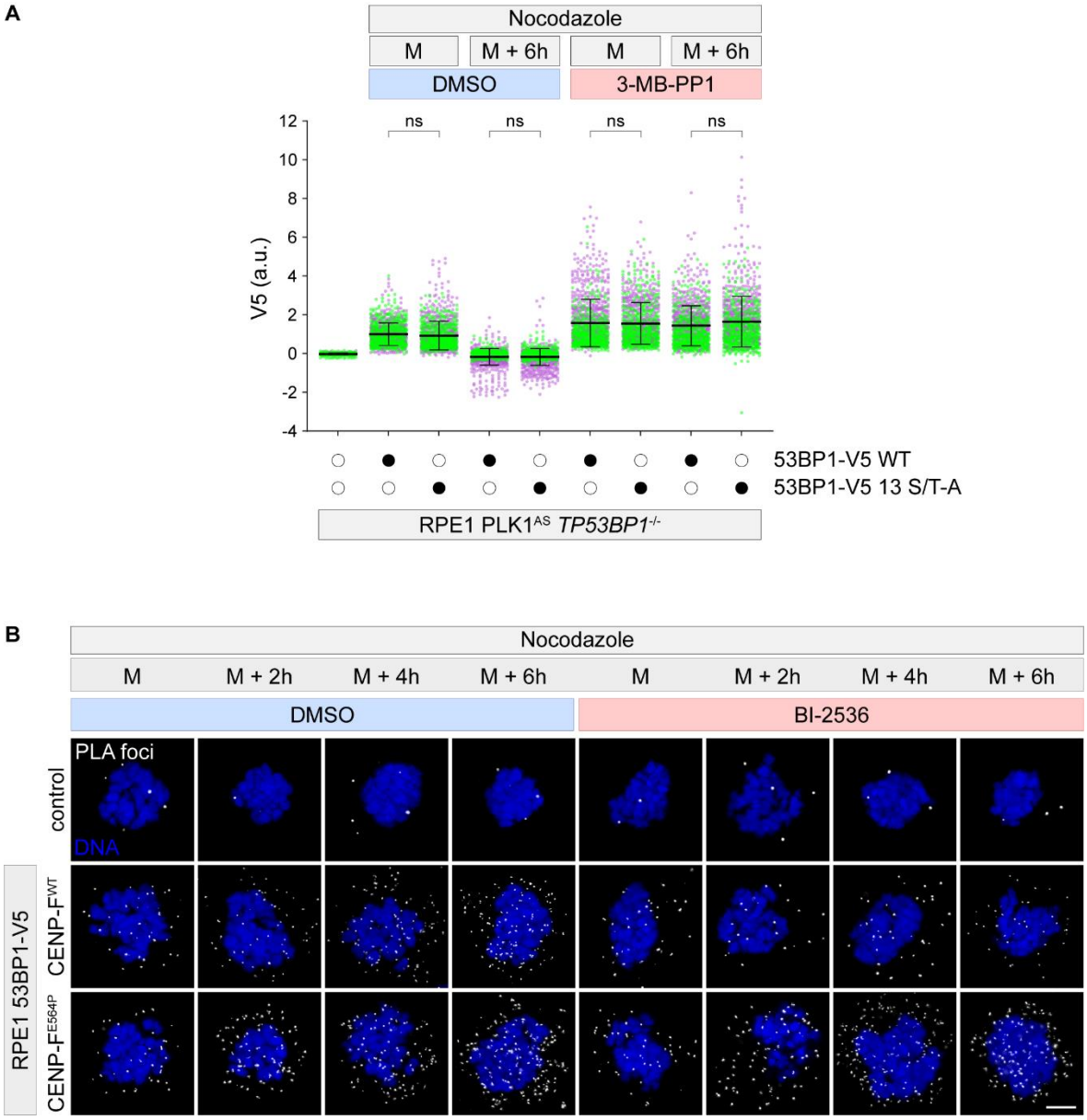

Figure 21. A Phosphomutant of 53BP1 exhibits unaltered kinetochore dynamics regulated by PLK1. (A) RPE1 PLK1^{AS} TP53BP1 KO cells were transduced with the indicated lentiviral vector, followed by synchronization in prometaphase in the presence or absence of PLK1 inhibition (3-MB-PP1). Cells were fixed either immediately (M = mitosis) or after 6 h (M + 6 h). Dot plots illustrate V5 fluorescence intensity at individual kinetochores (KTs), with each dot representing a specific KT. Mean values (black lines) ± SD (calculated on the entire dataset) are presented, normalized to the earliest timepoint of 53BP1 WT expression; a.u. = arbitrary units. Two biological replicates are depicted in green and magenta, with significance determined

using a Kruskal-Wallis test (n.s. = non-significant). (B) Representative fluorescence micrographs of RPE1 cells of the designated genotype, treated as outlined in Fig 22A, are included. M = mitosis. The scale bar is 5 μm.

PLK1 promotes 53BP1-p53 association and mitotic surveillance pathway activation

The observed contribution of PLK1 in the loss of 53BP1 KT affinity led us to investigate whether enforcing 53BP1 localization at the KT through PLK1 inhibition impacts the Mitotic Surveillance Pathway (MSP) functionality. Initially, we focused on monitoring the time-dependent assembly of 53BP1-p53 complexes in mitotically arrested cells. Utilizing our V5-tagged 53BP1 cell line, a proximity ligation assay (PLA) revealed a specific and time-dependent accumulation of PLA signals in cells experiencing mitotic delay. Interestingly, PLK1 inhibition prevented this phenomenon reducing 53BP1-p53 association (**Figs 22A and 21B**). Intriguingly, CENP-F^{E564P} cells exhibited a time-dependent accumulation of PLA signals both in the presence or absence of PLK1 inhibition. However, unlike CENP-F^{WT} cells, they appeared insensitive to PLK1 inhibition, suggesting that PLK1 contributes to the formation of 53BP1-p53 protein complexes by promoting 53BP1 loss of KT affinity.

In a subsequent analysis, $PLK1^{AS}$ CENP-F^{WT} and CENP-F^{E564P} cells were subjected to prometaphase delay in the presence or absence of the ATP analogue (3-MB-PP1). Following release, long-term proliferative capabilities were assessed by evaluating clonogenic potential in the absence of any drug. PLK1 inhibition during prometaphase arrest enhanced the clonogenic potential of CENP-F^{WT} cells upon drug wash-out (**Fig 22B and C**). Strikingly, when PLK1 inhibition was applied to CENP-F^{E564P} cells, the clonogenic potential was no longer increased. These findings collectively indicate that PLK1 regulates both the ability of 53BP1 to form complexes with p53 in the mitotic cytosol and the extended proliferative potential of cells exposed to prometaphase delay. As both these phenotypes are absent in CENP-F^{E564P} cells, we propose that the contribution of PLK1 lies in promoting time-dependent loss of KT affinity by 53BP1.

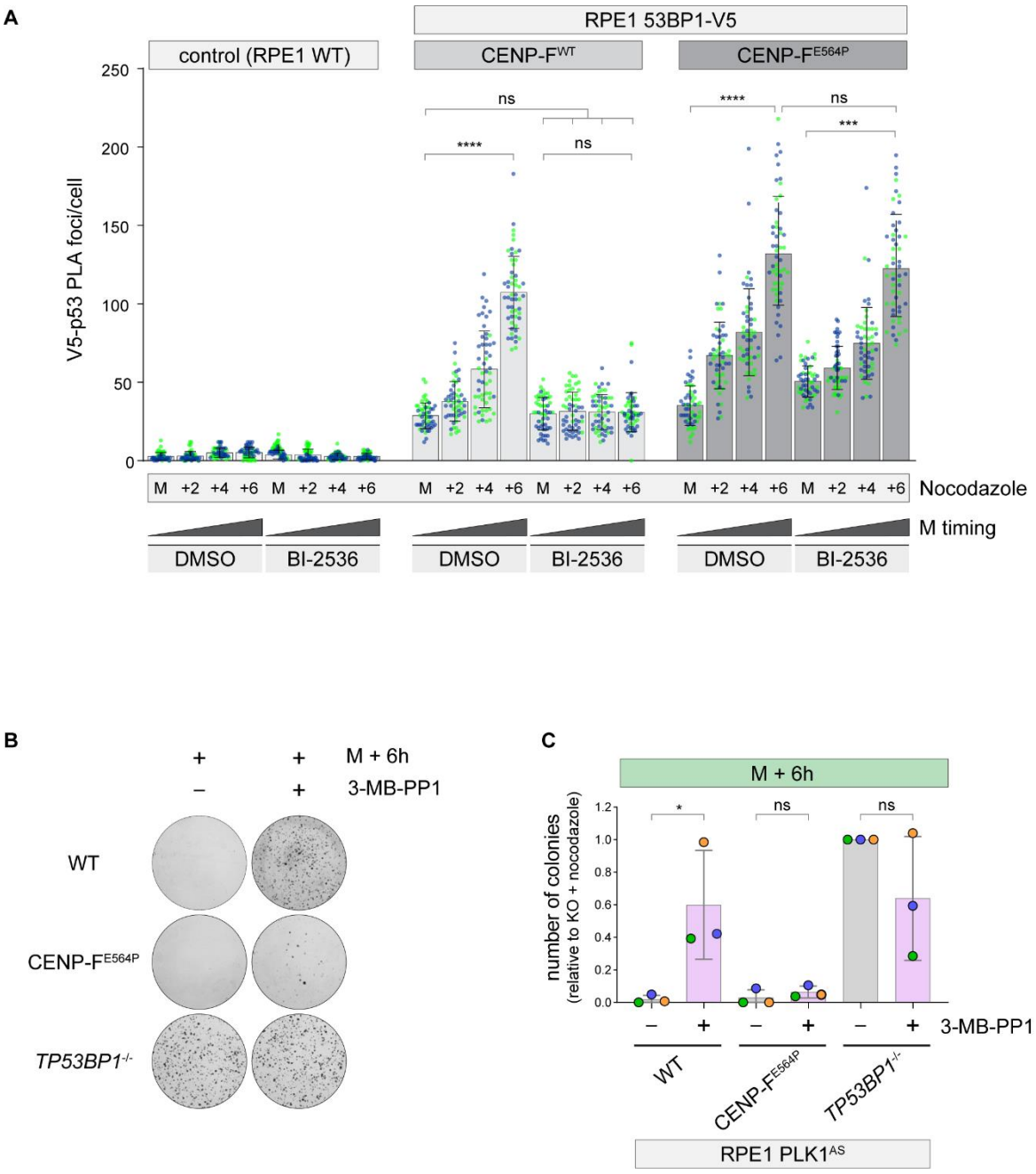

Figure 22. PLK1 activity is required for the MSP. (A) Cells of the indicated genotypes were synchronized in prometaphase in medium containing nocodazole, with or without PLK1 inhibition (BI-2536), and immediately fixed (M=mitosis) or after 2, 4, or 6 hours. Dot plots representing the number of V5-p53 PLA foci per cell. Mean values (black lines) ± SD (calculated on the entire dataset) are reported. N=2 biological replicates are shown, one replicate in blue, one in green. Significance was tested using a Kruskal-Wallis test: ****P < 0.0001; ***P = 0.0009; n.s. = non-significant. (B) RPE1 PLK1^{AS} cells of the indicated genotypes were treated with thymidine for 24 h and released into medium containing nocodazole for 16 h (M + 6 h, M = mitosis), in the presence or absence of PLK1 inhibition (3-MB-PP1). Mitotic cells were selectively retrieved by shake-off, washed out from the drugs, seeded for the clonogenic assay, and stained with crystal violet after 16 days. Images are representative of N=3 biologically independent experiments. (C) Quantification of 3

independent experiments as in (B). Data are presented as the number of colonies relative to the TP53BP1$^{-/-}$- 3-MB-PP1 condition. The bars indicate the mean ± SD (N=3 biological replicates). One-way ANOVA test: *P = 0.0455; n.s.=non-significant.

DISCUSSION

Mitosis is a tightly regulated process leading to the generation of two identical daughter cells. The key factors governing the duration of mitosis are the activation of Cyclin B/CDK1, crucial for initiating mitosis, and the activation of the anaphase-promoting complex/cyclosome (APC/C), responsible for triggering mitotic exit (Murray & Kirschner, 1989) (Pines, 2011). Different control mechanisms contribute to ensuring mitotic fidelity, among them, the spindle assembly checkpoint (SAC), which delays the anaphase onset until all chromosomes are correctly attached to spindle microtubules. However, this arrest cannot last infinitely, and the activity of SAC alone may not be adequate to preserve mitotic fidelity (Brito & Rieder, 2006) (Doménech et al., 2015).

Work by Uetake and Sluder identified a new pathway activated in response to prolonged prometaphase (Uetake & Sluder, 2010). Indeed, they demonstrated that mother cells whose mitosis exceeds a threshold (90 minutes) generate daughter cells that become arrested in the next G_1. This arrest has been demonstrated to be p53-dependent. Moreover, both prolonged prometaphase and pharmacological depletion of centrosomes lead to the activation of this p53-p21 axis. Later, three independent research groups performed a genome wide CRISPR/Cas9 screen searching for genes able to overcome cell cycle arrest when knocked-out upon centrosome depletion (Shyang Fong et al., 2016), (Lambrus et al., 2016), (Meitinger et al., 2016). The top hits were 53BP1 along with p53 and USP28. The proposed model for this mechanism, called the mitotic surveillance pathway (MSP), suggests that 53BP1 acts as a scaffold allowing p53 deubiquitination by USP28. This leads to p53 stabilization and p21-mediated cell cycle arrest.

Moreover, in mouse models of microcephaly, where the deletion of centrosomal proteins induces mitotic delay in neural progenitor cells, the aberrant activation of MSP appears crucial to the etiology of the microcephalic phenotype (Phan & Holland, 2021) (Phan et al., 2021). Despite these insights, the specific mechanism governing MSP complex assembly and the precise cue activating the pathway remained unclear.

Importantly, neither 53BP1 nor USP28 localize at centrosomes whereas 53BP1 has been reported to transiently localize at kinetochores during mitosis (Jullien D et al., 2001). This association seems to be dependent on mitotic duration and independent from SAC activation (Shyang Fong et al., 2016).

Here, searching for 53BP1 mitotic interactors, we performed an IP-MS detecting known and unknown 53BP1 partners. The fibrous corona protein CENP-F ranked among the top hits (**Fig 15A**). This was also confirmed by yeast-two hybrid screen performed using the KT-binding domain of 53BP1 (Jullien D et al., 2001) as a bait (**Fig 15B**). Taken together, these data highlighted that CENP-F and 53BP1 are direct *bona fide* interactors. Silencing of CENP-F in HeLa S3 cells disrupted the recruitment of 53BP1 to kinetochores (**Figure 15C**) suggesting a role of CENP-F in 53BP1 localization. Furthermore, we defined the CENP-F fragment interacting with 53BP1: aa 564-588 (**Figure 16B**). This portion of the protein is predicted to be part of a coiled-coil motif (Ciossani et al., 2018) (**Figure 16C**). Therefore, we took advantage of CRISPR/Cas9 to substitute the glutamic acid (E) at position 564 with a proline (P) thus destabilizing the proper folding of this region with the ultimate aim of interfering with the interaction between 53BP1 and CENP-F (**Figure 16D**). Once generated and tested this mutant, we assessed the impact of 53BP1 KT localization on MSP activation. Here, we expected two possible scenarios: first of all, assuming that the KT is an inhibitory state for the MSP, the delocalization could lead to an hyperactivation of the pathway; secondly, a loss of function of the MSP also could occur. The first possibility was soon tested as we observed no proliferative defects at any stage of the generation of the CENP-F^{E564P} cells; whereas, to test the second option, we activated the MSP with experimental triggers finding out that the KT localization was dispensable for MSP functionality as the edited cells were proficient at least as WT cells (**Figure 17 A and C**).

Importantly, better investigating 53BP1 dynamics during mitosis, we demonstrated that 53BP1 displays a loss of affinity from kinetochores during prolonged prometaphase that is PLK1-dependent (**Figure 20A**). Moreover, this loss of affinity seems to be independent of direct phosphorylation of 53BP1 (**Figure 21A**), suggesting that it might be dependent on the phosphorylation of other proteins, for example the KT receptor, CENP-F. Moreover, we demonstrated that the role of PLK1 is broader than a simple regulation of the KT loss of affinity of 53BP1. Indeed, PLK1 inhibition has an impact on 53BP1-p53 complex formation in the cytosol (**Figure 21B**). PLK1 activity reduces the clonogenic potential of cells experiencing prolonged mitosis (**Figure 22B**). However, in our mutant cell line both phenotypes are reverted highlighting that the contribution of PLK1 is visible only if 53BP1 KT localization is intact. Indeed, CENP-F^{E564P} cells showed no dependency on PLK1 activity. To sum up, the role of PLK1 in cells undergoing prolonged prometaphase is to promote the association of MSP proteins and reduce their clonogenic potential.

The model proposed in this study is the following: in a normal mitosis, 53BP1 is recruited to the KT via direct interaction with CENP-F. This association is transient as, going on with mitosis, 53BP1 is released from KT until the next mitosis. Moreover, in the context of prolonged prometaphase, 53BP1 is normally recruited at kinetochores via CENP-F, then PLK1 promotes the loss of affinity of 53BP1 for the KT (first priming step) and the formation of cytosolic complexes. However, an additional cytosolic trigger (second priming step) able to induce the association of MSP components is still missing (**Figure 23**). One might speculate that there is a threshold of non-KT bound 53BP1 in the cytosol able to trigger the formation of complexes or that additional adaptor proteins or kinases play a role in pathway initiation.

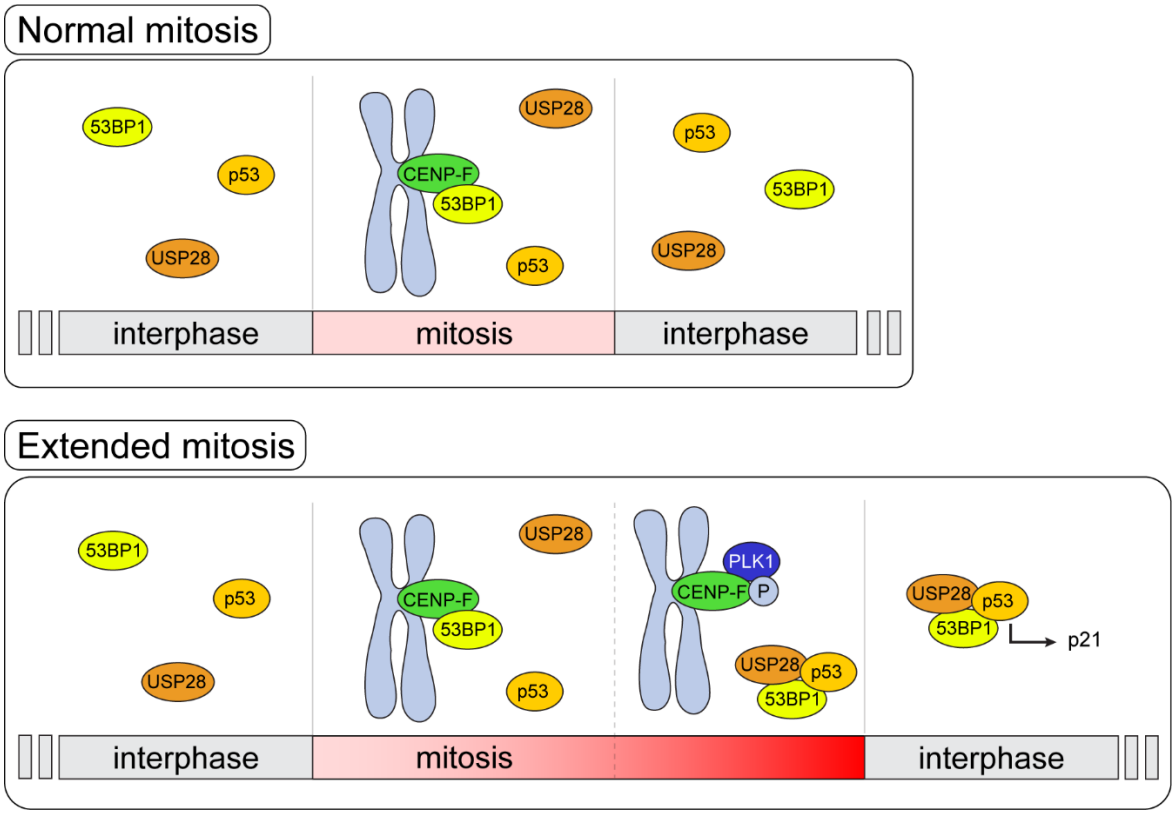

Figure 23. The mitotic surveillance pathway relies on a cytosolic clock. In a normal mitosis (upper panel), 53BP1 is recruited to the KT via a direct interaction with CENP-F. In the context of prolonged mitosis (lower panel), PLK1 activity promotes the loss of affinity of 53BP1 for the KT (first priming step). Cytosolic 53BP1 needs an additional yet unidentified trigger to induce the formation of MSP complexes and USP28-dependent deubiquitination of p53, which leads to cell cycle arrest (second priming step).

Moreover, 53BP1 forms dynamic repair compartments with droplet-like behaviour and p53 is found to be enriched within these 53BP1 optoDroplets (Kilic et al., 2019). Therefore, by performing immunofluorescence analysis, we found that upon an MSP activating stimulus (extending mitotic timing with nocodazole, for example), 53BP1 forms droplet-like foci in the cytosol colocalizing with p53 and PLK1 (data not shown). This suggests that also in the context of MSP activation 53BP1 might undergo phase separation. Surprisingly, these foci are more present in our mutant and by forcing mitotic exit in the context of an extended mitosis, we found that they persist in the next G_1. Curiously, these foci disappear in the presence of PLK1 inhibition (data not shown). Considering these evidence, we hypothesize that the cytosolic localization of 53BP1 could serve as a priming platform for the pathway, promoting its activation. The potential mechanism could be as follows: several distinct foci of 53BP1 accumulate independently and, over time, merge together. As they fuse, these foci grow in size including also p53 and PLK1. In essence, the aggregation and fusion of these individual 53BP1 foci create a larger, consolidated structure that plays a key role in triggering and supporting the pathway activation process. To investigate whether these foci are cause or consequence of MSP activation, it could be interesting to take advantage of Optogenetics. By inducing foci in a normal mitosis in a system in which we can follow the MSP activation (p21-EGFP reporter cells) we can assess whether these foci are sufficient to trigger pathway activation.

This study provides new insights into MSP understanding, highlighting that the time measurement is a cytosolic process not involving the KT. Indeed, the assembly of cytosolic MSP complexes, here assessed by PLA, has been investigated also by Meitinger et al., 2022. Performing co-immunoprecipitation experiments, they confirmed that PLK1 inhibition impacts the formation of p53-53BP1 complexes. Importantly, they speculated that a memory of mitotic timing is transmitted to daughter cells. Therefore, PLK1 promotes the formation of MSP complexes that persist through G_1. Depending on their abundance, these complexes can either induce a cell cycle arrest or retain a memory of prolonged mitosis for the next cell cycle. This memory is able to register also subtle extension of mitosis and transmit them throughout consecutive cell cycles to regulate cell fate.

Moreover, it is well documented how frequently this mechanism is inactivated in cancers. Compromised MSP functionality can lead to an increased tolerance of problematic mitosis. As demonstrated by Metinger et al. in their unpublished pre-print, the status of MSP

can influence the efficacy of therapeutic agents targeting mitotic processes. Thus, a complete understanding of how this pathway works and how it is regulated could help achieving the development of drugs or combining different treatments.

Taken together, we speculate that the dynamic 53BP1 KT localization could represent an additional layer of regulation, contributing to the tight control of mitotic timing. The most relevant conclusion of this study is that the measurement of mitotic timing is a cytosolic process finally excluding the contribution of KT and again highlighting how SAC and MSP are completely separated pathways.

Additional work is needed to investigate the physiological relevance of 53BP1 KT localization during normal mitosis but also to answer to the open question on the cytosolic still unknown mechanism able to regulate the formation and the activation of MSP complexes. To do so, our mutant could be a unique tool as it allows for the precise dissection of a physiological mitosis in which 53BP1 localizes at kinetochores or not. In this perspective, our future goal on this project is to perform a genome wide CRISPR screen. We identified two different screens that can be carried out:

A. Cells treated with DMSO: this should be a drop-out screen in which guides of selected genes will disappear in our mutant.
B. Cells treated with centrinone (MSP activating condition): this should be an enrichment screen and we expect that guides of selected genes will be enriched in the edited genotype.

The screen will be carried out as follows. RPE1 CENP-F^{WT} cells and RPE1 CENP-F^{E564P} are transduced with the Brunello sgRNA knockout library and selected for 3 days using puromycin. Then cells are left to recover after the antibiotic selection, pooled and seeded for treatment. Centrinone treated cells are treated with 125 nM centrinone. Cells are either passaged or fresh media is be added every 3-4 days. After 30 days, cells are harvested and genomic DNA is isolated for unbiased barcode amplification by PCR. Last step is Illumina Sequencing (**Figure 24**).

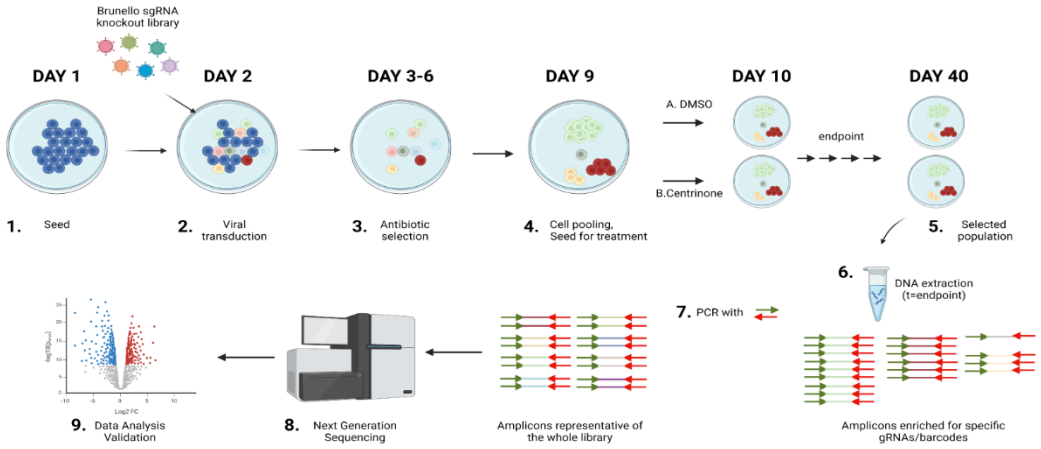

Figure 24. Schematic of CRISPR screen on RPE1 CENP-F^{WT} and RPE1 CENP-F^{E564P}. Cells are transduced using a human CRISPR Brunello lentiviral pooled library, selected with Puromycin for almost 72 hours. Then after three days of recovery post-selection cells are seeded for treatment with DMSO or 125 nM centrinone. After 30 days cells are harvested, and samples processed for the sequencing steps.

Our results demonstrated that the 53BP1 kinetochore localization is an additional layer of regulation of the MSP and that PLK1 plays a role on the detachment of 53BP1 from kinetochores and in the formation of cytosolic complexes with p53. Although this is clear, we failed to reveal a contribution of 53BP1 KT localization in MSP time threshold. In this perspective, the DMSO screen can help us to investigate whether the absence of 53BP1 at KTs can have an impact on pathway activation. This screen should be a drop-out screen in which guides of selected genes will disappear in our mutant compared to the WT condition. Indeed, we can expect that these disappeared guides could represent pathway inhibitors, in particular we can imagine that over time an inhibitory activity taking place downstream of KTs disappears in our mutant while it is still working in the WT cells. This is due to the fact that the absence of KT localization plus this/these gene/s (pathway inhibitor) work together activating the pathway so the guide will disappear in the mutant. So, the expectation is to find a drop-out of inhibitors working downstream of kinetochores in the CENP-F ^{E564P}.

Moving to the centrinone screen, this should be an enrichment screen in which guides of selected genes will be more represented in our mutant. The idea is that being in mitosis is an activating state for the MSP. In this case, we can assume that a build-up of enzymatic activity overtime (for example phosphorylation) could have a greater impact on the mutant compared to the WT. So, we expect to find an enrichment of positive regulators of the MSP (kinases

as mentioned before) but also proteins able to regulate the propensity of 53BP1 to oligomerize in the cytosol. Indeed, the fact that in RPE1 CENP-F^{E564P} the inhibition of PLK1 is not able to prevent the formation of 53BP1-p53 complexes measured by PLA demonstrated that PLK1 contribution is visible only when 53BP1 localizes at KTs. For this reason, this screen can help us to investigate whether there are other proteins in the mutant with a redundant role with PLK1, able to promote the formation of p53-53BP1 complexes also in the absence of KT localization. Surely, in this screen we will find common hits such as 53BP1, USP28, p53, p21 in both WT and mutant cells, but hopefully we will find in CENP-F^{E564P} other pathway activators such as foci regulators or kinases or enzymes able to perform modifications needed for pathway activation.

Moreover, by comparing the results of all the screens, we aim to better investigate the physiological relevance of 53BP1 KT localization but also to find differences among the two genotypes in an MSP activating condition, hopefully finding out regulators of the pathway or regulators of 53BP1 propensity to form cytosolic aggregates.

APPENDIX

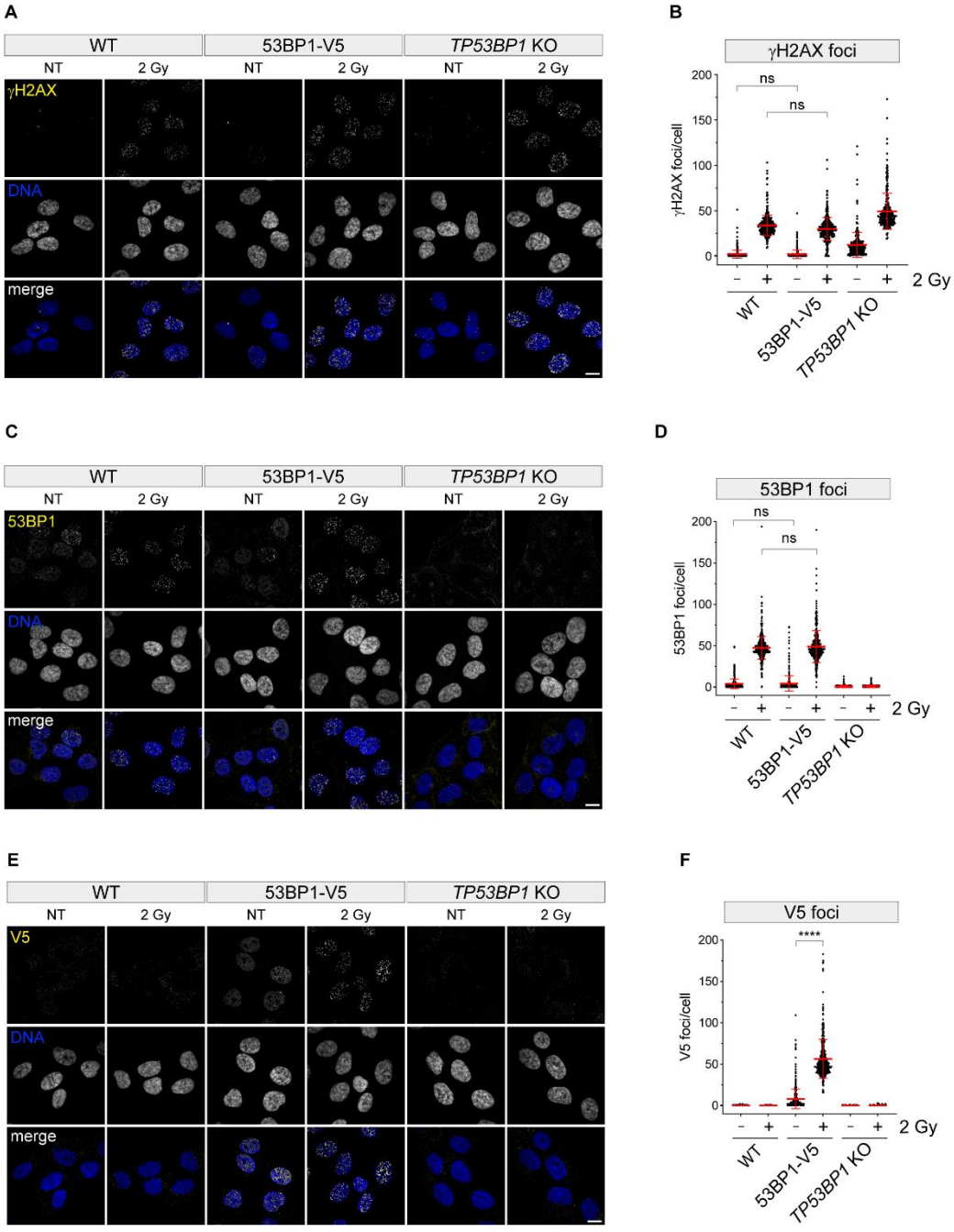

Appendix Figure S1. (A) Representative fluorescence micrographs of cells of the indicated genotypes irradiated (2 Gy) or left untreated and stained with γH2AX antibody. The scale bar is 10 µm. (B) Dot plots illustrate the number of γH2AX foci in cells treated as described in (A). Mean values (red lines) ± SD are presented, with quantification based on N ≥ 280 cells for each condition. The Kruskal-Wallis test resulted in non-significance (n.s.). (C) Representative fluorescence micrographs of cells, subjected to irradiation (2 Gy) or left untreated, and probed against the 53BP1 protein. The scale bar is 10 µm. (D) Dot plots show the number

of 53BP1 foci in cells treated as in (A). Mean values (red lines) ± SD are reported, with quantification based on N ≥ 352 cells for each condition. The Kruskal-Wallis test indicated non-significance (n.s.). (E) Cells treated as in (A) were stained with the antibody against the V5-tag. The scale bar is 10 µm. (F) Dot plots illustrate the number of V5 foci in cells treated as in (A). Mean values (red lines) ± SD are presented, with quantification based on N ≥ 349 cells for each condition. The Kruskal-Wallis test resulted in a significant difference (****P < 0.0001).

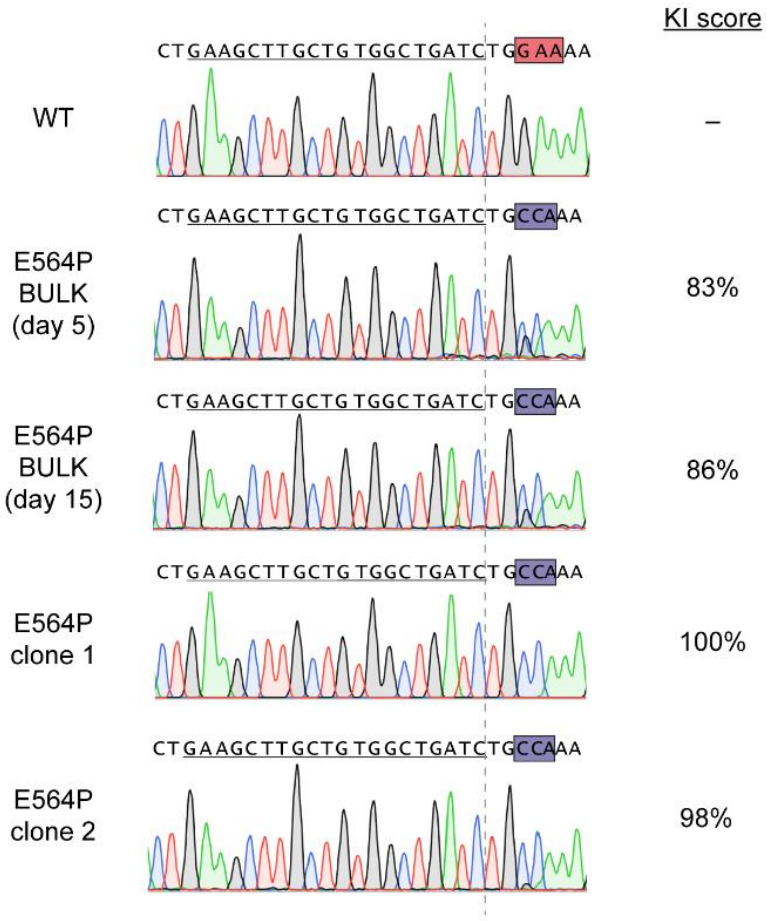

Appendix Figure S2. The genomic DNA of the indicated cells was PCR amplified and sequenced to analyse the CENPF region targeted by the gRNA (depicted by the black solid line). Electropherograms, along with the knock-in score calculated by ICE, are provided. The vertical dashed line represents the Cas9 cut site, the red box indicates the wild-type (WT) codon (E564), and the blue box represents the mutant codon (P564).

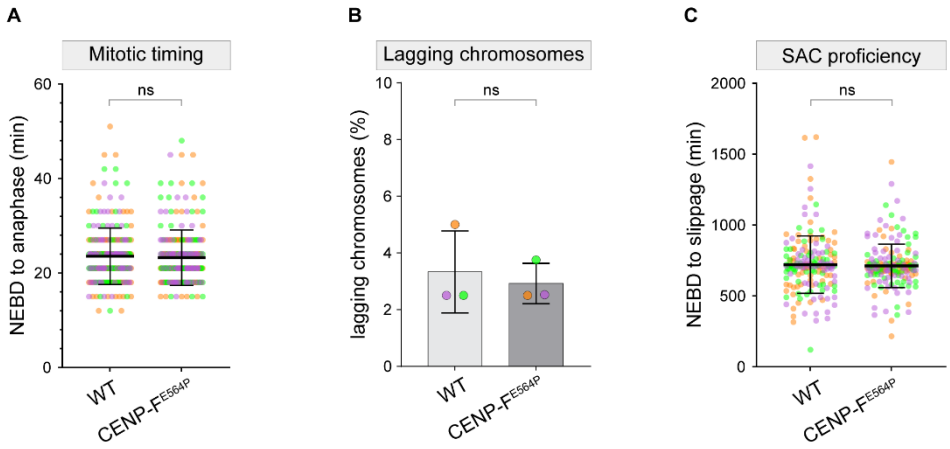

Appendix Figure S3. (A) Asynchronous RPE1 cells of the indicated genotypes were subjected to live-imaging as they progressed through mitosis. Mitotic duration, measured from nuclear envelope breakdown (NEBD) to anaphase onset, is presented in dot plots, where each dot represents a single cell. Mean values (black lines) ± SD (calculated on the entire dataset) are included for N=3 biological replicates, depicted in green, magenta, and orange. Significance was assessed using a Mann-Whitney test, and n.s. indicates non-significance. (B) The percentage of lagging chromosomes was determined from cells filmed as described in (A). Mean values (black lines) ± SD are reported for N=3 biological replicates, and the Mann-Whitney test indicated non-significance (n.s.). (C) To evaluate spindle assembly checkpoint (SAC) proficiency, RPE1 cells of the indicated genotype underwent pre-treatment with nocodazole for 1 h, followed by imaging (in the presence of nocodazole) for 48 h. Dot plots illustrate the time between NEBD and mitotic slippage for each cell. Mean values (black lines) ± SD (calculated on the entire dataset) are shown for N=3 biological replicates in green, magenta, and orange. Significance was determined using a Mann-Whitney test, and n.s. denotes non-significance.

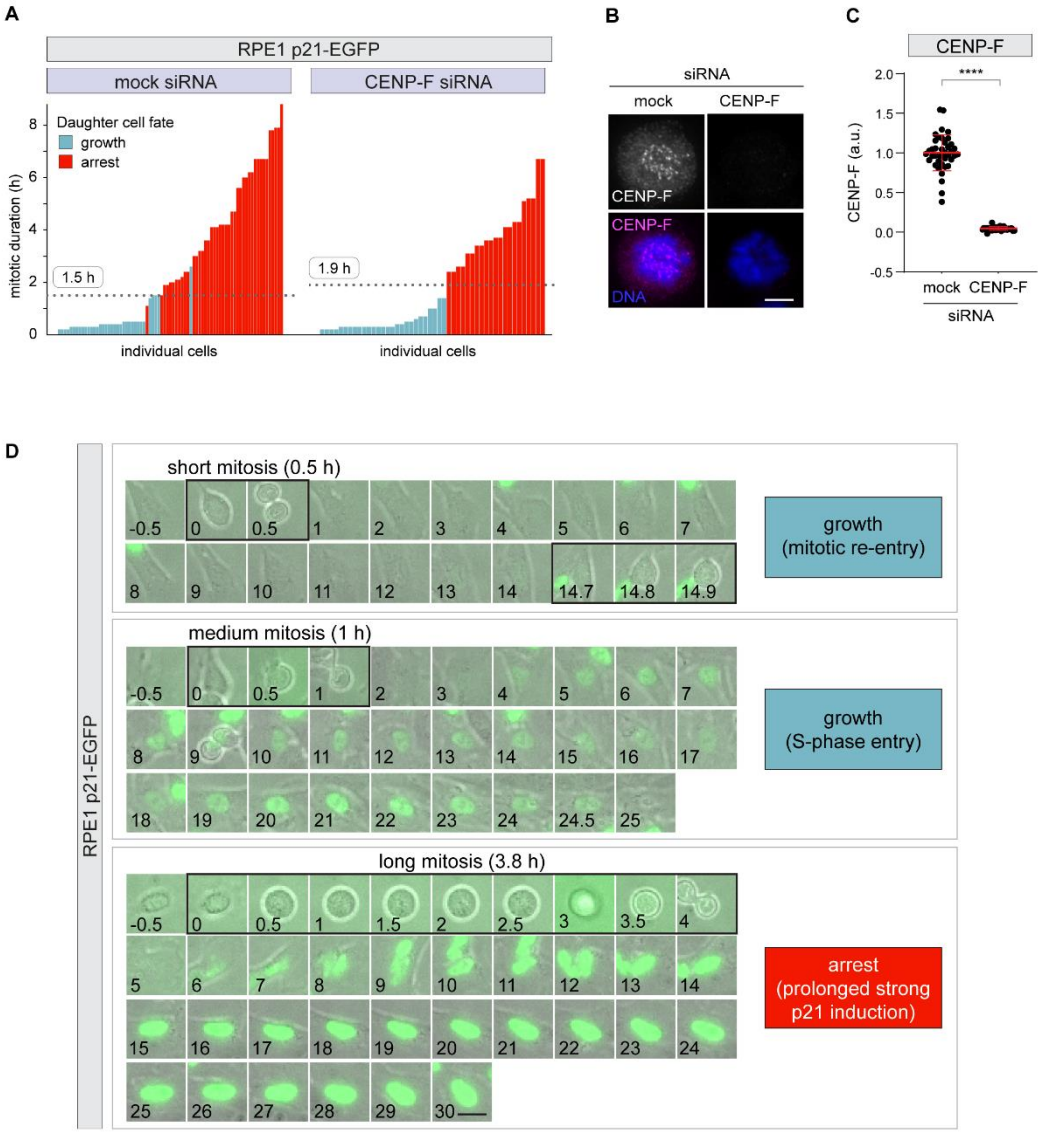

Appendix Figure S4. (A) RPE1 p21-EGFP cells were transfected with the indicated siRNA, briefly treated with dimethylenastron, and monitored for 2 days. The graph illustrates the daughter cell's fate relative to the mother cell's mitotic duration. Each daughter cell is depicted by a vertical bar, where the height represents the mother's mitotic duration, and the colour stands for the daughter's fate (growth or arrest). Dotted lines indicate the MSP threshold. Data are from N=77 control cells and 48 CENP-F depleted cells. (B) Representative images of RPE1 p21-EGFP cells transfected with the indicated siRNA and subjected to immunofluorescence using specified antibodies. Scale bar: 5 µm. (C) Dot plots exhibit nuclear CENP-F intensity from images as in (B). Mean values (red lines) ± SD are reported, normalized on the mock sample; a.u.=arbitrary units. Data are from N=40 cells per condition. Unpaired t-test (****$P < 0.0001$). (D) Movie stills of representative RPE1 p21-EGFP cells in the timer assay as described in Fig. 17F. Mitotic timing was measured from cell rounding to anaphase onset, based on the phase contrast signal (grey). Daughter cell fate was categorized as "growth" with mitotic re-entry (upper panel), abrupt decrease in p21 signal indicative of S-phase entry (middle panel), or "arrest"

with prolonged strong p21 induction (lower panel). Time is expressed in hours; scale bar: 20 µm. Experiments performed by Colin Gliech (Johns Hopkins University).

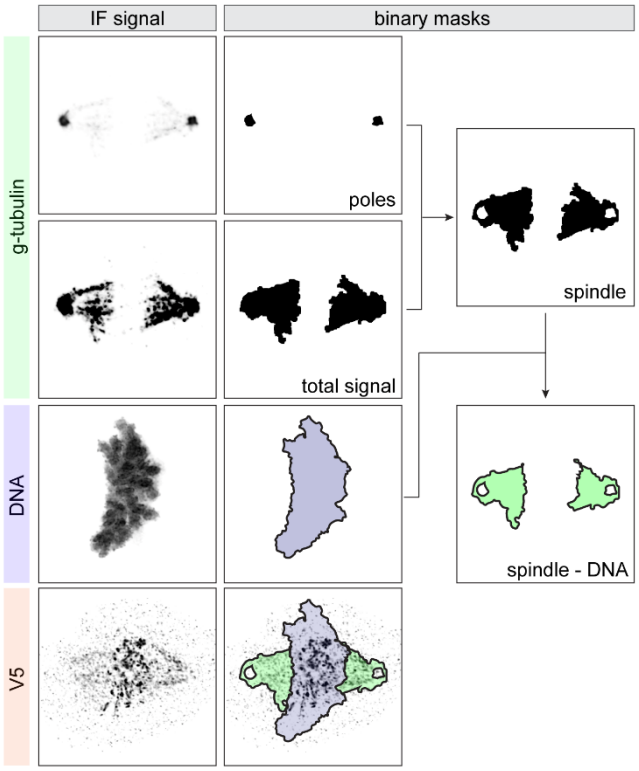

Appendix Figure S5. Scheme of the strategy used to quantify 53BP1 immunofluorescence signal in the stripping assay as in Fig 18A. The mitotic spindle binary mask (in green) resulted from the subtraction of a mask for spindle poles (black dots) and a mask for DNA signal (blue) to the total γ-tubulin signal. The final mask was used to measure 53BP1 fluorescence intensity in a region of the spindle not comprising DNA and the two centrosomes.

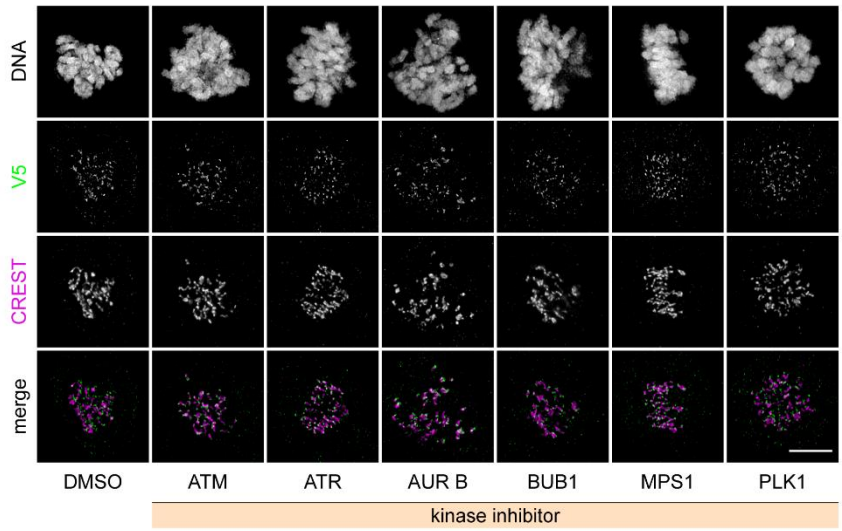

Appendix Figure S6. Representative fluorescence micrographs of RPE1 53BP1-V5 cells treated as in Fig 18A. Cells were co-stained with the indicated antibodies. Async=asynchronous cells: AUR B =Aurora B kinase. Scale bar: 5 μm.

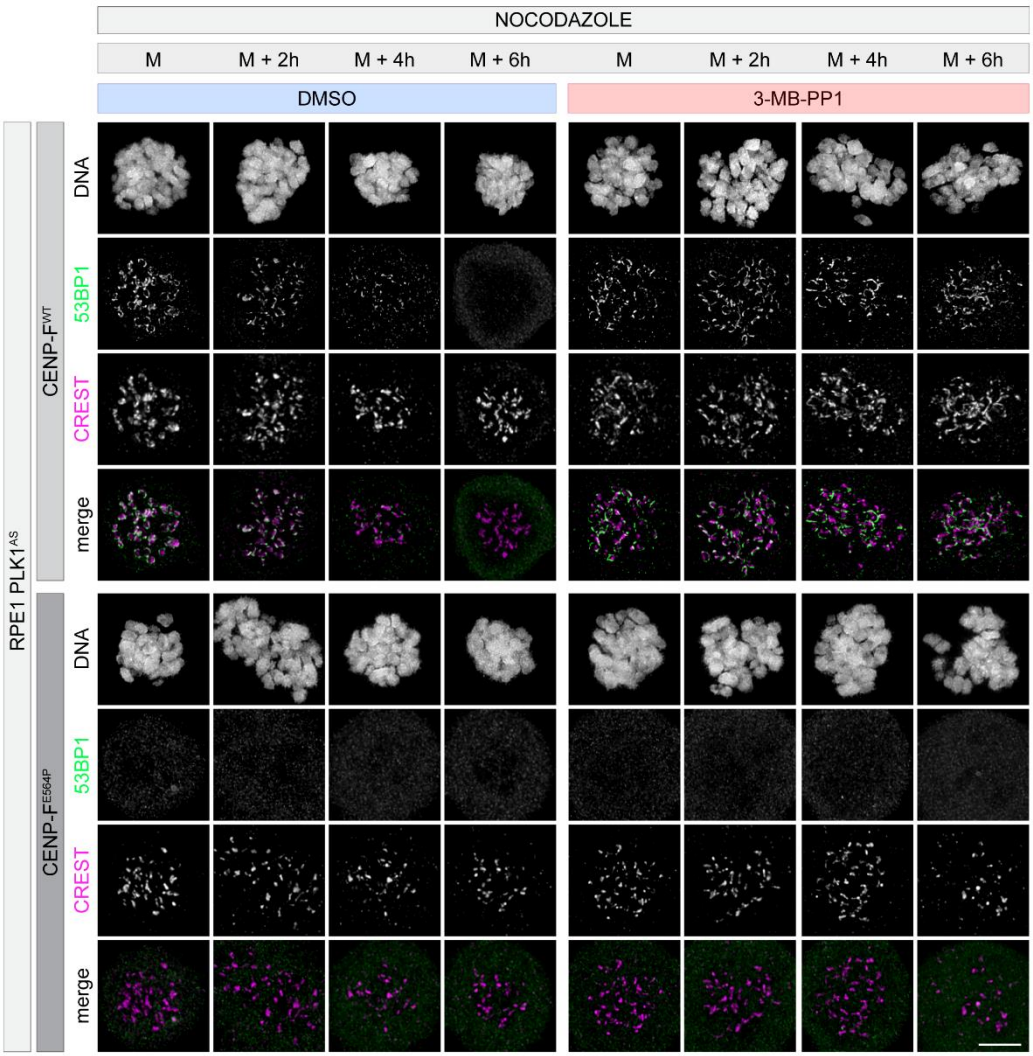

Appendix Figure S7. Representative fluorescence micrographs of RPE1 cells of the indicated genotypes, treated as in Fig 18C and co-stained with 53BP1 antibody. M=mitosis. Scale bar: 5 µm.

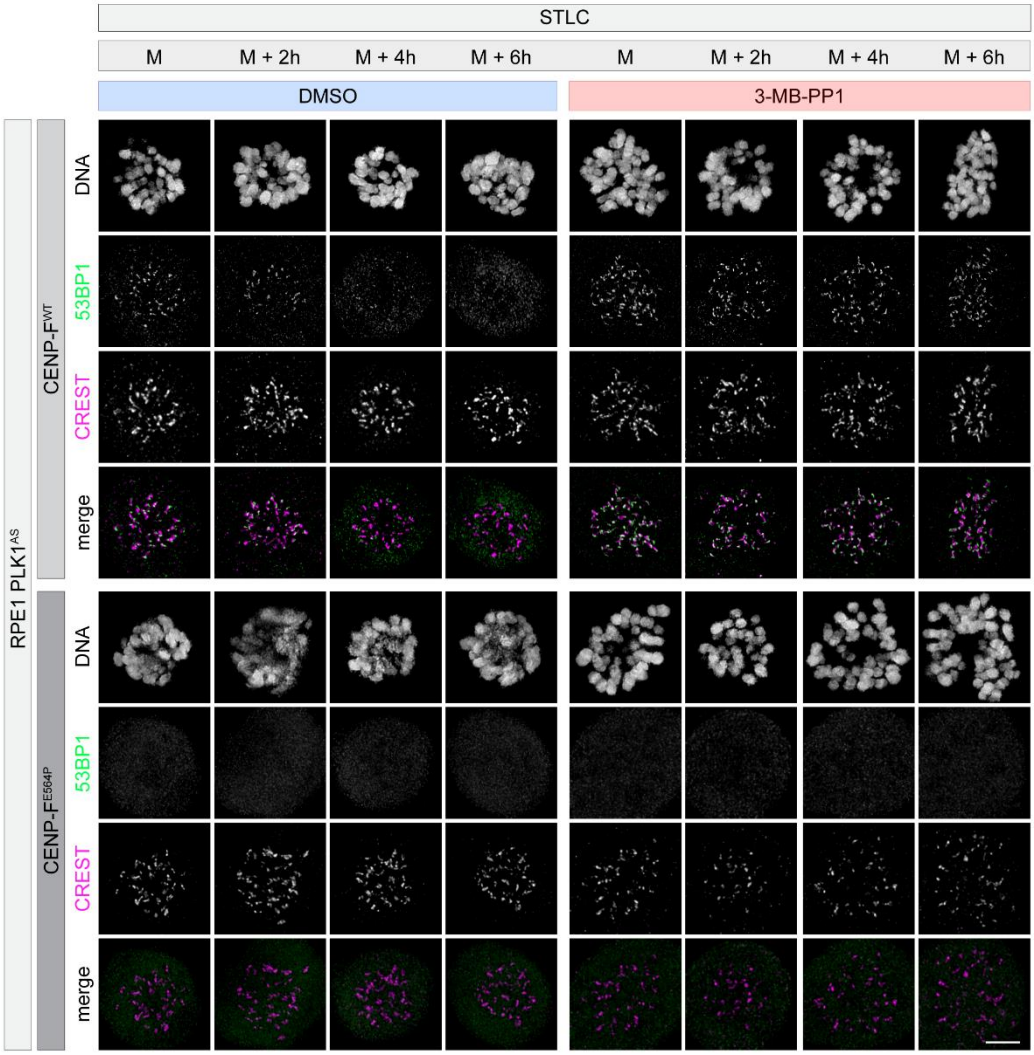

Appendix Figure S8. Representative fluorescence micrographs of RPE1 cells of the indicated genotypes, treated as in Fig 20B and co-stained with 53BP1 antibody. M=mitosis. Scale bar: 5 µm.

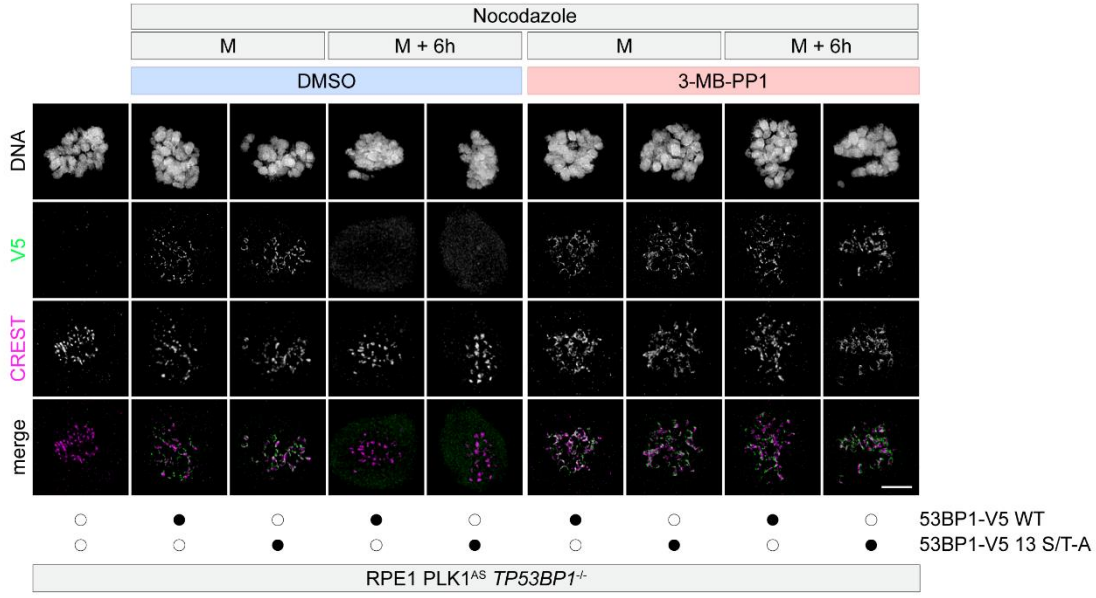

Appendix Figure S9. Representative fluorescence micrographs of RPE1 PLK1^{AS} TP53BP1 KO cells treated as in Fig 21A. M=mitosis. Scale bar: 5 µm.

SUPPLEMENTARY TABLE

Protein Identifier	Description	Gene	Fold change (log2)	P-value (-log10)
Q12888	TP53-binding protein 1 OS=Homo sapiens OX=9606 GN=TP53BP1 PE=1 SV=2	TP53BP1	6,77	60,39
P49454	Centromere protein F OS=Homo sapiens OX=9606 GN=CENPF PE=1 SV=3	CENPF	3,60	27,22
P21333	Filamin-A OS=Homo sapiens OX=9606 GN=FLNA PE=1 SV=4	FLNA	-2,10	18,54
P53350	Serine/threonine-protein kinase PLK1 OS=Homo sapiens OX=9606 GN=PLK1 PE=1 SV=1	PLK1	3,45	9,94
Q9BRJ7	Tudor-interacting repair regulator protein OS=Homo sapiens OX=9606 GN=NUDT16L1 PE=1 SV=1	NUDT16L1	6,42	9,75
P14618	Pyruvate kinase PKM OS=Homo sapiens OX=9606 GN=PKM PE=1 SV=4	PKM	-2,23	7,31
Q96RU2	Ubiquitin carboxyl-terminal hydrolase 28 OS=Homo sapiens OX=9606 GN=USP28 PE=1 SV=1	USP28	3,70	7,11
Q00610	Clathrin heavy chain 1 OS=Homo sapiens OX=9606 GN=CLTC PE=1 SV=5	CLTC	-1,99	6,67
Q9Y490	Talin-1 OS=Homo sapiens OX=9606 GN=TLN1 PE=1 SV=3	TLN1	-1,33	6,62
P35580	Myosin-10 OS=Homo sapiens OX=9606 GN=MYH10 PE=1 SV=3	MYH10	-1,30	6,28
Q14315	Filamin-C OS=Homo sapiens OX=9606 GN=FLNC PE=1 SV=3	FLNC	-1,74	6,26
P04406	Glyceraldehyde-3-phosphate dehydrogenase OS=Homo sapiens OX=9606 GN=GAPDH PE=1 SV=3	GAPDH	-2,47	6,12
P12814	Alpha-actinin-1 OS=Homo sapiens OX=9606 GN=ACTN1 PE=1 SV=2	ACTN1	-2,45	6,08
Q9NUQ6	SPATS2-like protein OS=Homo sapiens OX=9606 GN=SPATS2L PE=1 SV=2	SPATS2L	2,28	5,92
P10809	60 kDa heat shock protein, mitochondrial OS=Homo sapiens OX=9606 GN=HSPD1 PE=1 SV=2	HSPD1	-1,94	5,60
Q14204	Cytoplasmic dynein 1 heavy chain 1 OS=Homo sapiens OX=9606 GN=DYNC1H1 PE=1 SV=5	DYNC1H1	-1,91	5,52
P06733	Alpha-enolase OS=Homo sapiens OX=9606 GN=ENO1 PE=1 SV=2	ENO1	-2,42	5,43
P13639	Elongation factor 2 OS=Homo sapiens OX=9606 GN=EEF2 PE=1 SV=4	EEF2	-1,18	5,38
P78527	DNA-dependent protein kinase catalytic subunit OS=Homo sapiens OX=9606 GN=PRKDC PE=1 SV=3	PRKDC	-1,85	5,32
P00338	L-lactate dehydrogenase A chain OS=Homo sapiens OX=9606 GN=LDHA PE=1 SV=2	LDHA	-2,78	5,23
O15027	Protein transport protein Sec16A OS=Homo sapiens OX=9606 GN=SEC16A PE=1 SV=4	SEC16A	0,71	4,11
Q04446	1,4-alpha-glucan-branching enzyme OS=Homo sapiens OX=9606 GN=GBE1 PE=1 SV=3	GBE1	2,73	3,84
P04075	Fructose-bisphosphate aldolase A OS=Homo sapiens OX=9606 GN=ALDOA PE=1 SV=2	ALDOA	-2,08	3,43
P13010	X-ray repair cross-complementing protein 5 OS=Homo sapiens OX=9606 GN=XRCC5 PE=1 SV=3	XRCC5	-2,21	3,40

Table 1. Mitotic interactors of 53BP1. The table lists the first 24 mitotic interactors of 53BP1 that are enriched in the V5 pull-downs from RPE1 53BP1-V5 cells in comparison to RPE1 WT cells.

REFERENCES

Ariyoshi, M., & Fukagawa, T. (2023). An updated view of the kinetochore architecture. In *Trends in Genetics*. Elsevier Ltd. https://doi.org/10.1016/j.tig.2023.09.003

Auckland, P., Roscioli, E., Coker, H. L. E., & McAinsh, A. D. (2020). CENP-F stabilizes kinetochore-microtubule attachments and limits dynein stripping of corona cargoes. *Journal of Cell Biology*, *219*(5). https://doi.org/10.1083/jcb.201905018

Barnum, K. J., & O'Connell, M. J. (2014). Cell cycle regulation by checkpoints. *Methods in Molecular Biology*, *1170*, 29–40. https://doi.org/10.1007/978-1-4939-0888-2_2

Basu, S., Greenwood, J., Jones, A. W., & Nurse, P. (2022). Core control principles of the eukaryotic cell cycle. *Nature*, *607*(7918), 381–386. https://doi.org/10.1038/s41586-022-04798-8

Bazzi, H., & Anderson, K. V. (2014). Acentriolar mitosis activates a p53-dependent apoptosis pathway in the mouse embryo. *Proceedings of the National Academy of Sciences of the United States of America*, *111*(15). https://doi.org/10.1073/pnas.1400568111

Blower M D, & Karpen G H. (2001). The role of Drosophila CID in kinetochore formation, cell-cycle progression and heterochromatin interactions. *Nat Cell Biol,*.

Bomont, P., Maddox, P., Shah, J. V., Desai, A. B., & Cleveland, D. W. (2005). Unstable microtubule capture at kinetochores depleted of the centromere-associated protein CENP-F. *EMBO Journal*, *24*(22), 3927–3939. https://doi.org/10.1038/sj.emboj.7600848

Brito, D. A., & Rieder, C. L. (2006). Mitotic Checkpoint Slippage in Humans Occurs via Cyclin B Destruction in the Presence of an Active Checkpoint. *Current Biology*, *16*(12), 1194–1200. https://doi.org/10.1016/j.cub.2006.04.043

Burigotto, M., Vigorito, V., Gliech, C., Mattivi, A., Ghetti, S., Bisio, A., Lolli, G., Holland, A. J., & Fava, L. L. (2023). PLK1 promotes the mitotic surveillance pathway by controlling cytosolic 53BP1 availability. *EMBO Reports*. https://doi.org/10.15252/embr.202357234

Cheeseman I A, & Desai A. (2008). Molecular architecture of the kinetochore–microtubule interface. *Nat Rev Mol Cell Biol*.

Cheeseman, I. M. (2014). The Kinetochore. *Cold Spring Harbor Perspectives in Biology*, *6*(7). https://doi.org/10.1101/cshperspect.a015826

Cheeseman, I. M., Niessen, S., Anderson, S., Hyndman, F., Yates, J. R., Oegema, K., & Desai, A. (2004). A conserved protein network controls assembly of the outer kinetochore and its ability to sustain tension. *Genes and Development*, *18*(18), 2255–2268. https://doi.org/10.1101/gad.1234104

Chen RH, Waters JC, Salmon ED, & Murray AW. (1996). Association of spindle assembly checkpoint component XMAD2 with unattached kinetochores. *Science*.

Ciciarello, M., Mangiacasale, R., Casenghi, M., Limongi, M. Z., D'Angelo, M., Soddu, S., Lavia, P., & Cundari, E. (2001). p53 Displacement from Centrosomes and p53-mediated G1 Arrest following Transient Inhibition of the Mitotic Spindle. *Journal of Biological Chemistry*, *276*(22), 19205–19213. https://doi.org/10.1074/jbc.M009528200

Ciossani, G., Overlack, K., Petrovic, A., Huis In 'T Veld, P. J., Koerner, C., Wohlgemuth, S., Maffini, S., & Musacchio, A. (2018). The kinetochore proteins CENP-E and CENP-F directly and specifically interact with distinct BUB mitotic checkpoint Ser/Thr kinases. *Journal of Biological Chemistry*, *293*(26), 10084–10101. https://doi.org/10.1074/jbc.RA118.003154

Contadini, C., Monteonofrio, L., Virdia, I., Prodosmo, A., Valente, D., Chessa, L., Musio, A., Fava, L. L., Rinaldo, C., Di Rocco, G., & Soddu, S. (2019). p53 mitotic centrosome localization preserves centrosome integrity and works as sensor for the mitotic surveillance pathway. *Cell Death and Disease*, *10*(11). https://doi.org/10.1038/s41419-019-2076-1

D. Killander, & A. Zetterberg. (1965). A quantitative cytochemical investigation of the relationship between cell mass and initiation of DNA synthesis in mouse fibroblasts *in vitro*. In *Experimental Cell Research: Vol. Volume 40, Issue 1,*.

DeLuca, J. G., & Musacchio, A. (2012). Structural organization of the kinetochore-microtubule interface. In *Current Opinion in Cell Biology* (Vol. 24, Issue 1, pp. 48–56). https://doi.org/10.1016/j.ceb.2011.11.003

Dempster, J. M., Boyle, I., Vazquez, F., Root, D. E., Boehm, J. S., Hahn, W. C., Tsherniak, A., & McFarland, J. M. (2021). Chronos: a cell population dynamics model of CRISPR experiments that improves inference of gene fitness effects. *Genome Biology*, *22*(1). https://doi.org/10.1186/s13059-021-02540-7

Doménech, E., Maestre, C., Esteban-Martínez, L., Partida, D., Pascual, R., Fernández-Miranda, G., Seco, E., Campos-Olivas, R., Pérez, M., Megias, D., Allen, K., López, M., Saha, A. K., Velasco, G., Rial, E., Méndez, R., Boya, P., Salazar-Roa, M., & Malumbres, M. (2015). AMPK and PFKFB3 mediate glycolysis and survival in response to mitophagy during mitotic arrest. *Nature Cell Biology*, *17*(10), 1304–1316. https://doi.org/10.1038/ncb3231

Domingo-Sananes, M. R., Kapuy, O., Hunt, T., & Novak, B. (2011). Switches and latches: A biochemical tug-of-war between the kinases and phosphatases that control mitosis. In *Philosophical Transactions of the Royal Society B: Biological Sciences* (Vol. 366, Issue 1584, pp. 3584–3594). Royal Society. https://doi.org/10.1098/rstb.2011.0087

Fava, L. L., Kaulich, M., Nigg, E. A., & Santamaria, A. (2011). Probing the *in vivo* function of Mad1:C-Mad2 in the spindle assembly checkpoint. *EMBO Journal*, *30*(16), 3322–3336. https://doi.org/10.1038/emboj.2011.239

Foley, E. A., & Kapoor, T. M. (2013). Microtubule attachment and spindle assembly checkpoint signalling at the kinetochore. In *Nature Reviews Molecular Cell Biology* (Vol. 14, Issue 1, pp. 25–37). https://doi.org/10.1038/nrm3494

Ghetti, S., Burigotto, M., Mattivi, A., Magnani, G., Casini, A., Bianchi, A., Cereseto, A., & Fava, L. L. (2021). CRISPR/Cas9 ribonucleoprotein-mediated knockin generation in hTERT-RPE1 cells. *STAR Protocols*, *2*(2). https://doi.org/10.1016/j.xpro.2021.100407

Giunta, S., Belotserkovskaya, R., & Jackson, S. P. (2010). DNA damage signaling in response to double-strand breaks during mitosis. *Journal of Cell Biology*, *190*(2), 197–207. https://doi.org/10.1083/jcb.200911156

Grana, X., & Reddy, E. P. (1995). Cell cycle control in mammalian cells: Role of cyclins, cyclin dependent kinases (CDKs), growth suppressor genes and cyclin-dependent kinase inhibitors (CKIs). *Oncogene*. https://www.researchgate.net/publication/15575285

Gruber R, Zhou Z, Sukchev M, Joerss T, Frappart P O, & Wang Z Q. (2011). MCPH1 regulates the neuroprogenitor division mode by coupling the centrosomal cycle with mitotic entry through the Chk1-Cdc25 pathway. *Nat Cell Biol*.

Hara, M., & Fukagawa, T. (2018). Kinetochore assembly and disassembly during mitotic entry and exit. In *Current Opinion in Cell Biology* (Vol. 52, pp. 73–81). Elsevier Ltd. https://doi.org/10.1016/j.ceb.2018.02.005

Harper, J. V, & Brooks, G. (2010). The Mammalian Cell Cycle An Overview. In *Cell Cycle Control: Mechanisms and Protocols* (Vol. 296).

Howell, B. J., McEwen, B. F., Canman, J. C., Hoffman, D. B., Farrar, E. M., Rieder, C. L., & Salmon, E. D. (2001). Cytoplasmic dynein/dynactin drives kinetochore protein transport to the spindle poles and has a role in mitotic spindle checkpoint inactivation. *Journal of Cell Biology*, *155*(7), 1159–1172. https://doi.org/10.1083/jcb.200105093

Hoyt, M. A., Totis, L., & Roberts, B. T. (1991). S. cerevisiae Genes Required for Cell Cycle Arrest in Response to Loss of Microtubule Function. In *Cell* (Vol. 66).

Insolera, R., Bazzi, H., Shao, W., Anderson, K. V., & Shi, S. H. (2014). Cortical neurogenesis in the absence of centrioles. *Nature Neuroscience*, *17*(11), 1528–1535. https://doi.org/10.1038/nn.3831

Jullien D, Vagnarelli P, Earnshaw W C, & Adachi Y. (2001). Kinetochore localisation of the DNA damage response component 53BP1 during mitosis. *Journal Of Cell Science*.

Jumper, J., Evans, R., Pritzel, A., Green, T., Figurnov, M., Ronneberger, O., Tunyasuvunakool, K., Bates, R., Žídek, A., Potapenko, A., Bridgland, A., Meyer, C., Kohl, S. A. A., Ballard, A. J., Cowie, A., Romera-Paredes, B., Nikolov, S., Jain, R., Adler, J., … Hassabis, D. (2021). Highly accurate protein structure prediction with AlphaFold. *Nature*, *596*(7873), 583–589. https://doi.org/10.1038/s41586-021-03819-2

Kilic, S., Lezaja, A., Gatti, M., Bianco, E., Michelena, J., Imhof, R., & Altmeyer, M. (2019). Phase separation of 53BP1 determines liquid-like behavior of DNA repair compartments. The *EMBO journal*, 38(16), e101379. https://doi.org/10.15252/embj.2018101379

Knobel, P. A., Belotserkovskaya, R., Galanty, Y., Schmidt, C. K., Jackson, S. P., & Stracker, T. H. (2014). USP28 Is Recruited to Sites of DNA Damage by the Tandem BRCT Domains of 53BP1 but Plays a Minor Role in Double-Strand Break Metabolism.

Molecular and Cellular Biology, *34*(11), 2062–2074. https://doi.org/10.1128/mcb.00197-14

Lambrus, B. G., Daggubati, V., Uetake, Y., Scott, P. M., Clutario, K. M., Sluder, G., & Holland, A. J. (2016). A USP28-53BP1-p53-p21 signaling axis arrests growth after centrosome loss or prolonged mitosis. *Journal of Cell Biology*, *214*(2), 143–153. https://doi.org/10.1083/jcb.201604054

Lambrus, B. G., & Holland, A. J. (2017). A New Mode of Mitotic Surveillance. In *Trends in Cell Biology* (Vol. 27, Issue 5, pp. 314–321). Elsevier Ltd. https://doi.org/10.1016/j.tcb.2017.01.004

Lambrus, B. G., Uetake, Y., Clutario, K. M., Daggubati, V., Snyder, M., Sluder, G., & Holland, A. J. (2015). P53 protects against genome instability following centriole duplication failure. *Journal of Cell Biology*, *210*(1), 63–77. https://doi.org/10.1083/jcb.201502089

Lara-Gonzalez, P., Kim, T., Oegema, K., Corbett, K., & Desai, A. (2021). A tripartite mechanism catalyzes Mad2-CDC20 assembly at unattached kinetochores. *Science*. https://www.science.org

Lara-Gonzalez, P., Westhorpe, F. G., & Taylor, S. S. (2012). The spindle assembly checkpoint. In *Current Biology* (Vol. 22, Issue 22). https://doi.org/10.1016/j.cub.2012.10.006

Lee, D. H., Acharya, S. S., Kwon, M., Drane, P., Guan, Y., Adelmant, G., Kalev, P., Shah, J., Pellman, D., Marto, J. A., & Chowdhury, D. (2014). Dephosphorylation Enables the Recruitment of 53BP1 to Double-Strand DNA Breaks. *Molecular Cell*, *54*(3), 512–525. https://doi.org/10.1016/j.molcel.2014.03.020

Levine, M. S., & Holland, A. J. (2018). The impact of mitotic errors on cell proliferation and tumorigenesis. *Genes Dev*. https://doi.org/10.1101/gad.314351

Li, R., & Murray, A. W. (1991). Feedback control of mitosis in budding yeast. *Cell*, *Volume 66*(Issue 3).

Li, X., & Nicklas, R. (1995). Mitotic forces control a cell-cycle checkpoint. *Nature*.

Liang Wong, Y., Anzola, J. V, Davis, R. L., Yoon, M., Motamedi, A., Kroll, A., Seo, C. P., Hsia, J. E., Kim, S. K., Mitchell, J. W., Mitchell, B. J., Desai, A., Gahman, T. C., Shiau, A. K., & Oegema, K. (2015). *CELL BIOLOGY Reversible centriole depletion with an inhibitor of Polo-like kinase 4*. https://www.science.org

Mapelli, M., Massimiliano, L., Santaguida, S., & Musacchio, A. (2007). The Mad2 Conformational Dimer: Structure and Implications for the Spindle Assembly Checkpoint. *Cell*, *131*(4), 730–743. https://doi.org/10.1016/j.cell.2007.08.049

Marthiens V, & Basto R. (2020). Centrosomes: The good and the bad for brain development. In *Biology of the Cell* (Vol. 112).

Matthews, H. K., Bertoli, C., & de Bruin, R. A. M. (2022). Cell cycle control in cancer. In *Nature Reviews Molecular Cell Biology* (Vol. 23, Issue 1, pp. 74–88). Nature Research. https://doi.org/10.1038/s41580-021-00404-3

McKinley, K. L., & Cheeseman, I. M. (2016). The molecular basis for centromere identity and function. In *Nature Reviews Molecular Cell Biology* (Vol. 17, Issue 1, pp. 16–29). Nature Publishing Group. https://doi.org/10.1038/nrm.2015.5

Meitinger, F., Anzola, J. V., Kaulich, M., Richardson, A., Stender, J. D., Benner, C., Glass, C. K., Dowdy, S. F., Desai, A., Shiau, A. K., & Oegema, K. (2016). 53BP1 and USP28 mediate p53 activation and G1 arrest after centrosome loss or extended mitotic duration. *Journal of Cell Biology*, *214*(2), 155–166. https://doi.org/10.1083/jcb.201604081

Meitinger, F., Davis, R. L., Martinez, M. B., Shiau, A. K., Oegema, K., & Desai, A. (2022). Control of cell proliferation by memories of mitosis. *BioRxiv*. https://doi.org/10.1101/2022.11.14.515741

Mirdita, M., Schütze, K., Moriwaki, Y., Heo, L., Ovchinnikov, S., & Steinegger, M. (2022). ColabFold: making protein folding accessible to all. *Nature Methods*, *19*(6), 679–682. https://doi.org/10.1038/s41592-022-01488-1

Mitchison, T. J., & Salmon, E. D. (2001). Mitosis: a history of division. In *NATURE CELL BIOLOGY* (Vol. 3). http://cellbio.nature.com

Molinari, M. (2000). Cell cycle checkpoints and their inactivation in human cancer. In *Cell Prolif* (Vol. 33).

Murray, A. W., & Kirschner, M. W. (1989). Dominoes and Clocks: The Union of Two Views of the Cell Cycle. In *Philos. Tranis. R. Soc. Lotndon Ser. B* (Vol. 58). www.sciencemag.org

Musacchio, A., & Desai, A. (2017). A molecular view of kinetochore assembly and function. In *Biology* (Vol. 6, Issue 1). MDPI AG. https://doi.org/10.3390/biology6010005

Musacchio, A., & Salmon, E. D. (2007). The spindle-assembly checkpoint in space and time. In *Nature Reviews Molecular Cell Biology* (Vol. 8, Issue 5, pp. 379–393). https://doi.org/10.1038/nrm2163

Nagpal, H., & Fukagawa, T. (2016). Kinetochore assembly and function through the cell cycle. In *Chromosoma* (Vol. 125, Issue 4, pp. 645–659). Springer Science and Business Media Deutschland GmbH. https://doi.org/10.1007/s00412-016-0608-3

Navarro, A. P., & Cheeseman, I. M. (2021). Kinetochore assembly throughout the cell cycle. *Seminars in Cell and Developmental Biology*, *117*, 62–74. https://doi.org/10.1016/j.semcdb.2021.03.008

Nigg, E. A., & Holland, A. J. (2018). Once and only once: Mechanisms of centriole duplication and their deregulation in diseases. In *Nature Reviews Molecular Cell Biology* (Vol. 19, Issue 5, pp. 297–312). Nature Publishing Group. https://doi.org/10.1038/nrm.2017.127

Novais, P., Silva, P. M. A., Amorim, I., & Bousbaa, H. (2021). Second-generation antimitotics in cancer clinical trials. *Pharmaceutics*, *13*(7). https://doi.org/10.3390/pharmaceutics13071011

Oegema K, Desai A, Rybina S, Kirkham M, & Hyman A A. (2001). Functional analysis of kinetochore assembly in Caenorhabditis elegans. *J Cell Biol*.

Oliferenko, S., Chew, T. G., & Balasubramanian, M. K. (2009). Positioning cytokinesis. In *Genes and Development* (Vol. 23, Issue 6, pp. 660–674). https://doi.org/10.1101/gad.1772009

Oricchio, E., Saladino, C., Iacovelli, S., Soddu, S., & Cundari, E. (2006). ATM is activated by default in mitosis, localizes at centrosomes and monitors mitotic spindle integrity. *Cell Cycle*, *5*(1), 88–92. https://doi.org/10.4161/cc.5.1.2269

Orr, B., De Sousa, F., Gomes, A. M., Afonso, O., Ferreira, L. T., Figueiredo, A. C., & Maiato, H. (2021). An anaphase surveillance mechanism prevents micronuclei formation from frequent chromosome segregation errors. *Cell Reports*, *37*(6). https://doi.org/10.1016/j.celrep.2021.109783

Panagopoulos, A., & Altmeyer, M. (2021). The Hammer and the Dance of Cell Cycle Control. In *Trends in Biochemical Sciences* (Vol. 46, Issue 4, pp. 301–314). Elsevier Ltd. https://doi.org/10.1016/j.tibs.2020.11.002

Pesenti, M. E., Weir, J. R., & Musacchio, A. (2016). Progress in the structural and functional characterization of kinetochores. In *Current Opinion in Structural Biology* (Vol. 37, pp. 152–163). Elsevier Ltd. https://doi.org/10.1016/j.sbi.2016.03.003

Peter J Alaimo, Michael A Shogren-Knaak, & Kevan M Shokat. (2001). *Chemical genetic approaches for the elucidation of signaling pathways Alaimo, Shogren-Knaak and Shokat 361*.

Phan, T. P., & Holland, A. J. (2021). Time is of the essence: the molecular mechanisms of primary microcephaly. *Genes Dev*. https://doi.org/10.1101/gad.348866

Phan, T. P., Maryniak, A. L., Boatwright, C. A., Lee, J., Atkins, A., Tijhuis, A., Spierings, D. C., Bazzi, H., Foijer, F., Jordan, P. W., Stracker, T. H., & Holland, A. J. (2021). Centrosome defects cause microcephaly by activating the 53BP1-USP28-TP53 mitotic surveillance pathway. *The EMBO Journal*, *40*(1). https://doi.org/10.15252/embj.2020106118

Pilaz L J, McMahon J J, Miller E E, Lennox A L, Suzuki A, Salmon E, & Silver D L. (2016). Prolonged Mitosis of Neural Progenitors Alters Cell Fate in the Developing Brain. *Neuron*.

Pines, J. (2011). Cubism and the cell cycle: The many faces of the APC/C. In *Nature Reviews Molecular Cell Biology* (Vol. 12, Issue 7, pp. 427–438). https://doi.org/10.1038/nrm3132

Prodosmo, A., De Amicis, A., Nisticò, C., Gabriele, M., Di Rocco, G., Monteonofrio, L., Piane, M., Cundari, E., Chessa, L., & Soddu, S. (2013). P53 centrosomal localization diagnoses ataxia-telangiectasia homozygotes and heterozygotes. *Journal of Clinical Investigation*, *123*(3), 1335–1342. https://doi.org/10.1172/JCI67289

Régnier V, Vagnarelli P, Fukagawa T, Zerjal T, Burns E, Trouche D, Earnshaw W, & Brown W. (2005). CENP-A is required for accurate chromosome segregation and sustained kinetochore association of BubR1. *Mol Cell Biol*.

Richard Mcintosh, J. (2016). Mitosis. *Cold Spring Harbor Perspectives in Biology*, *8*(9). https://doi.org/10.1101/cshperspect.a023218

Rieder, C. L. (2011). Mitosis in vertebrates: The G2/M and M/A transitions and their associated checkpoints. In *Chromosome Research* (Vol. 19, Issue 3, pp. 291–306). https://doi.org/10.1007/s10577-010-9178-z

Rieder, C. L., Cole, R. W., Khodjakov, A., & Sluder, G. (1995). The Checkpoint Delaying Anaphase in Response to Chromosome Monoorientation Is Mediated by an Inhibitory Signal Produced by Unattached Kinetochores. *J Cell Biol*. http://rupress.org/jcb/article-pdf/130/4/941/1479135/941.pdf

Rieder, C. L., & Maiato, H. (2004). Stuck in Division or Passing through. *Developmental Cell*.

Salaun P, Rannou Y, & Prigent C. (2008). Cdk1, Plks, Auroras, and Neks: the mitotic bodyguards. *Adv Exp Med Biol*.

Santaguida, S., & Musacchio, A. (2009). The life and miracles of kinetochores. In *EMBO Journal* (Vol. 28, Issue 17, pp. 2511–2531). https://doi.org/10.1038/emboj.2009.173

Santamaría, D., Barrière, C., Cerqueira, A., Hunt, S., Tardy, C., Newton, K., Cáceres, J. F., Dubus, P., Malumbres, M., & Barbacid, M. (2007). Cdk1 is sufficient to drive the mammalian cell cycle. *Nature*, *448*(7155), 811–815. https://doi.org/10.1038/nature06046

Saurin, A. T. (2018). Kinase and phosphatase cross-talk at the kinetochore. In *Frontiers in Cell and Developmental Biology* (Vol. 6, Issue JUN). Frontiers Media S.A. https://doi.org/10.3389/fcell.2018.00062

Shyang Fong, C., Mazo, G., Das, T., Goodman, J., Kim, M., O, B. P., Izquierdo, D., & Bryan Tsou, M.-F. (2016). 53BP1 and USP28 mediate p53-dependent cell cycle arrest in response to centrosome loss and prolonged mitosis. *eLife*. https://doi.org/10.7554/eLife.16270.001

Sironi Lucia, Mapelli Marina, Knapp Stefan, De Antoni Anna, Jeang Kuan-Teh, & Musacchio Andrea. (2002). Crystal structure of the tetrameric Mad-Mad2 core complex: implications of a `safety belt' binding mechanism for the spindle checkpoint. *The EMBO Journal*, *21*(10).

Söderberg, O., Leuchowius, K. J., Gullberg, M., Jarvius, M., Weibrecht, I., Larsson, L. G., & Landegren, U. (2008). Characterizing proteins and their interactions in cells and tissues using the *in situ* proximity ligation assay. *Methods*, *45*(3), 227–232. https://doi.org/10.1016/j.ymeth.2008.06.014

Strohacker LK, Mackay DR, Whitney MA, Couldwell GC, Sundquist WI, & Ullman KS. (2021). Identification of abscission checkpoint bodies as structures that regulate ESCRT factors to control abscission timing. *ELife*.

Tanaka, T. U. (2010). Kinetochore-microtubule interactions: Steps towards bi-orientation. *EMBO Journal*, *29*(24), 4070–4082. https://doi.org/10.1038/emboj.2010.294

Taylor SS, & McKeon F. (1997). Kinetochore localization of murine Bub1 is required for normal mitotic timing and checkpoint response to spindle damage. *Cell*.

Uetake, Y., & Sluder, G. (2010). Prolonged prometaphase blocks daughter cell proliferation despite normal completion of mitosis. *Current Biology*, *20*(18), 1666–1671. https://doi.org/10.1016/j.cub.2010.08.018

Uzbekov, R., & Prigent, C. (2022). A Journey through Time on the Discovery of Cell Cycle Regulation. *Cells*, *11*(4). https://doi.org/10.3390/cells11040704

Van Vugt, M. A. T. M., Gardino, A. K., Linding, R., Ostheimer, G. J., Reinhardt, H. C., Ong, S. E., Tan, C. S., Miao, H., Keezer, S. M., Li, J., Pawson, T., Lewis, T. A., Carr, S. A., Smerdon, S. J., Brummelkamp, T. R., Yaffe, M. B., & Lichten, M. (2010). A mitotic phosphorylation feedback network connects Cdk1, Plk1, 53BP1, and Chk2 to inactivate the G2/M DNA damage checkpoint. *PLoS Biology*, *8*(1). https://doi.org/10.1371/journal.pbio.1000287

Weiss, E., & Winey, M. (1996). The Saccharomyces cerevisiae spindle pole body duplication gene MPS1 is part of a mitotic checkpoint. *J. Cell Biol*.

Xiao, C., Grzonka, M., Meyer-Gerards, C., Mack, M., Figge, R., & Bazzi, H. (2021). Gradual centriole maturation associates with the mitotic surveillance pathway in mouse development. *EMBO Reports*, *22*(2). https://doi.org/10.15252/embr.202051127

ACKNOWLEDGMENTS

I would like to express my sincere gratitude to my advisor, Luca Fava, for his support, guidance, and mentorship throughout my PhD. His expertise, encouragement, and constructive feedbacks have been crucial in shaping my research and academic growth. Surely, his mentorship involves more than just knowledge transmission giving me a lot of chances to collaborate with other teams, sharing my work in conferences and growing not only scientifically but also personally. Altogether, I am really grateful to Luca for helping me to show my potential in his lab.

I would like to thank Matteo Burigotto for teaching me almost everything. Thank you for being such an example for me: we shared a lot of good times also in bad moments such as shaking-off hundreds of 15cm dishes. I won't forget our late-night conversation washing out drugs. Matteo's patient explanations, and willingness to share his knowledge have significantly contributed to my intellectual growth. I am truly thankful for the privilege of being mentored by him.

Thank you to all the current and former members of the Fava laboratory for sharing with me this long journey. In particular, thanks to Alessia for the constant support all along my PhD. Thanks for the good time spent together, for the conversations, for the coffee breaks in all the long days of work. I would also thank the so-called "il 38esimo", Daniele, Giorgia and Gian Mario, for being by my side during this hard period. Thank you for the shared enthusiasm, encouragement, and teamwork that have made this journey both rewarding and memorable. Thanks for support me and put up with me.

I would also like to thank the Advanced Imaging Facility, thanks to Michela and Giorgina for helping me in achieving a very good quality for the images and for training me.

I would also like to express my gratitude to Angelo. Thank you for standing by me through the long hours of research, the moments of self-doubt, and the joys of breakthroughs. Your belief in me has been a source of inspiration, motivating me to persevere in my journey. I am truly fortunate to have you by my side. Your patience, encouragement, and understanding have been invaluable to me.

Finally, I am profoundly grateful to my parents, for their endless love, support, and sacrifices during all these years. I am indebted to you for instilling in me the values of resilience and

hard work, which have shaped me into the person I am today. Thank you for always being there for me.

ANNEXES

Burigotto, M., Vigorito, V., Gliech, C., Mattivi, A., Ghetti, S., Bisio, A., Lolli, G., Holland, A. J., & Fava, L. L. (2023). PLK1 promotes the mitotic surveillance pathway by controlling cytosolic 53BP1 availability. *EMBO reports*, e57234. Advance online publication. https://doi.org/10.15252/embr.202357234